

University of Nebraska - Lincoln

DigitalCommons@University of Nebraska - Lincoln

---

Student Research Projects, Dissertations, and  
Theses - Chemistry Department

Chemistry, Department of

---

Spring 5-2011

## Characterization of Novel Macrocyclic Polyether Modified Pseudostationary Phases for use in Micellar Electrokinetic Chromatography and Development of a Chemiluminescence Presumptive Assay for Peroxide-based Explosives

Raychelle Burks

St. Edwards University, rburks@stedwards.edu

Follow this and additional works at: <https://digitalcommons.unl.edu/chemistrydiss>

 Part of the [Analytical Chemistry Commons](#)

---

Burks, Raychelle, "Characterization of Novel Macrocyclic Polyether Modified Pseudostationary Phases for use in Micellar Electrokinetic Chromatography and Development of a Chemiluminescence Presumptive Assay for Peroxide-based Explosives" (2011). *Student Research Projects, Dissertations, and Theses - Chemistry Department*. 19.

<https://digitalcommons.unl.edu/chemistrydiss/19>

This Article is brought to you for free and open access by the Chemistry, Department of at DigitalCommons@University of Nebraska - Lincoln. It has been accepted for inclusion in Student Research Projects, Dissertations, and Theses - Chemistry Department by an authorized administrator of DigitalCommons@University of Nebraska - Lincoln.

Characterization of Novel Macrocyclic Polyether Modified Pseudostationary Phases

for use in Micellar Electrokinetic Chromatography and

Development of a Chemiluminescence Presumptive Assay for Peroxide-based Explosives

by

Raychelle M. Burks

A DISSERTATION

Presented to the Faculty of

The Graduate College at the University of Nebraska

In Partial Fulfillment of Requirements

For the Degree of Doctor of Philosophy

Major: Chemistry

Under the Supervision of Professor David S. Hage

Lincoln, Nebraska

May, 2011

CHARACTERIZATION OF NOVEL MACROCYCLIC POLYETHER MODIFIED  
PSEUDOSTATIONARY PHASES FOR USE IN MICELLAR ELECTROKINETIC  
CHROMATOGRAPHY AND DEVELOPMENT OF A CHEMILUMINESCENCE  
PRESUMPTIVE ASSAY FOR PEROXIDE-BASED EXPLOSIVES

Raychelle M. Burks, Ph.D.

University of Nebraska, 2011

Adviser: David S. Hage

This work describes the first use and characterization of macrocyclic polyether (MP) modified sodium dodecyl sulfate (SDS) pseudostationary phases (PSPs) for use in micellar electrokinetic chromatography (MEKC), as well as the development of a presumptive chemiluminescence assay for peroxide-based explosives. In MEKC separation and detection, resolution is optimized by using various PSPs or by altering the properties of a single PSP using different class I or class II modifiers. Class I modifiers target the PSP through direct interaction with micelles, while class II organic modifiers operate by altering the BGE. The of MPs 18-crown-6, 15-crown-5, and 12-crown-4 were used to modify SDS, with their effect on the SDS PSP and solute partitioning characterized using a linear solvation energy relationship (LSER) and select thermodynamic properties. Over two dozen solutes were used to probe the MP modified SDS PSPs, many of them nitro-based explosives (NBEs), precursors and/or additives to NBE compositions.

Easy-to-monitor presumptive assays are routinely used by forensic scientists, law enforcement and military personnel to screen for drugs of abuse and explosives. For

peroxide-based explosives (PBEs), such assays are often indirect, monitoring the PBE precursor and degradation product hydrogen peroxide ( $\text{H}_2\text{O}_2$ ) by utilizing peroxidase-based luminescence. As with most enzyme-based methods, peroxidase methods can be a challenge to integrate into field test kits. Presented here is an attractive alternative based on the  $\text{H}_2\text{O}_2$  - acetonitrile - luminol (HPAL) chemiluminescence reaction. This assay requires four simple reagents and no instrumentation for the visual detection of commonly encountered PBEs (TATP and HMTD) as well as  $\text{H}_2\text{O}_{2(l)}$ . Limits of detection were in the low mg range for PBEs and  $4 \mu\text{g/mL}$  for  $\text{H}_2\text{O}_{2(l)}$ . This HPAL assay can also act as a color test, with reaction solutions changing from colorless or white to yellow, probably due to the formation of 3-aminophthalate anion.

**DEDICATION**

*To my parents, who taught me to learn from success and failure.*

---

I have learned throughout my life as a composer chiefly through my mistakes and pursuits of false assumptions, not by my exposure to founts of wisdom and knowledge.

~ Igor Stravinsky

## ACKNOWLEDGMENTS

I wish to thank Dr. Hage for giving me the opportunity to join his research lab and pursue a variety of research interests. I sincerely thank each member of my committee including Dr. Redepening, Dr. Carr, Dr. Wehling and Dr. George for their patience and encouragement over the (far too many) years it took to complete this process. Dr. George passed away before I finished; his support and advice were invaluable.

My gratitude to past and present members of Hage Lab, with who space, supplies and sometimes, classes, was shared. Special thanks to Mary Anne, Annette, Cory, Abby, John S., Rangan, Lancia, Arthur and Erika. Beyond the lab, UNL has incredible dedicated technical and administrative staff that make the entire endeavor of higher education run smoothly. To the unsung heroes of the libraries, stockrooms, department offices, fabrication shops, Officer of Graduate Studies, Student Services and Academic Services: THANK YOU.

To my family, who has expanded considerably during the (far too many) years it took me to complete this process, my love and many thanks.

**TABLE OF CONTENTS****CHAPTER 1**

GENERAL INTRODUCTION.....	1
1.1 Unifying theme .....	1
1.2 PSPs for MEKC.....	2
1.2.1 Micellar Electrokinetic Chromatography.....	2
1.2.2 Modifying PSPs.....	5
1.2.3 Sample matrix for MEKC.....	6
1.3 Detection of PBEs.....	7
1.4 References.....	8

**CHAPTER 2**

USE OF A WATER MISCIBLE ORGANIC SOLVENT SAMPLE MATRIX IN MICELLAR ELECTROKINETIC CHROMATOGRAPHY .....	13
2.1 Introduction.....	13
2.1.1 Use of miscible organic solvents in sample solutions.....	15
2.1.2 Miscible organic solvents and peak deformity.....	16

2.1.3 OSM selection.....	19
2.1.3 OSM evaluation and optimization.....	20
2.2 Experimental.....	21
2.2.1 Instruments and Material.....	21
2.2.2 Solute set and determination of log $P_{mw}$ values.....	22
2.2.3 Modification of sample plug length.....	23
2.2.4 Modification of injection-to-separation delay time.....	23
2.3 Results and Discussion.....	24
2.4 Conclusion and Future Work.....	30
2.5 References.....	32
APPENDIX A Solute Set.....	37
APPENDIX B Solute McGowan's volume values.....	44
 <b>CHAPTER 3</b>  	
18-CROWN-6 AS A CLASS I ORGANIC MODIFIER IN MICELLAR ELECTROKINETIC CAPILLARY CHROMATOGRAPHY.....	47
3.1 Introduction.....	47



3.1.1 Class I Modifiers.....	48
3.2 Experimental.....	53
3.2.1 Instruments and Materials.....	53
3.2.2 Determination of CMC.....	53
3.2.3 Determination of $k$ and $\alpha$ .....	54
3.3 Results and Discussion.....	54
3.3.1 CMC observations.....	54
3.3.2 Nitrotoluene isomer series observations.....	55
3.3.3 Nitrophenol isomer series observations.....	57
3.3.4 $k$ and $\alpha$ observations for isomers studied.....	60
3.4 Conclusion and Future Work.....	65
3.5 References.....	67
APPENDIX B Current titration method for the determination of CMC.....	72

## **CHAPTER 4**

CHARACTERIZATION OF CROWN ETHERS AS CLASS I ORGANIC MODIFIERS USING MICELLAR ELECTROKINETIC CHROMATOGRAPHY.	76
--	----

4.1 Introduction.....	76
4.1.1 Macrocyclic polyethers.....	77
4.1.2 PSP characterization.....	82
4.2 Experimental.....	87
4.2.1 Instrumentation and Materials.....	87
4.2.2 Determination of LSER descriptors.....	88
4.2.3 Determination of $\Delta\Delta G_R^\circ$ .....	89
4.2.4 Determination of CMC.....	89
4.2.5 Determination of $\beta$ and $\Delta G_{MC}^\circ$ .....	89
4.3 Results and Discussion.....	90
4.3.1 LSER analysis.....	90
4.3.2 $\Delta\Delta G_R^\circ$ observations.....	109
4.3.3 Effect of MPs on micelle physicochemical properties.....	117
4.4 Conclusion and Future Work.....	121
4.5 References.....	124
APPENDIX A LSER Solute Descriptors.....	131

APPENDIX B	Current titration method for the determination of CMC	137
APPENDIX C	Current titration data for the determination of CMC	141
APPENDIX D	Influence of MPs on $\Delta\Delta G_R^\circ$	144

## CHAPTER 5

CURRENT TRENDS PEROXIDE-BASED EXPLOSIVES DETECTION.....	146
5.1 Introduction.....	146
5.2 Luminescence Methods.....	152
5.3 Infrared and Raman Spectroscopy .....	158
5.4 Ion Mobility and Mass Spectrometry.....	163
5.5 Electrochemical Methods.....	173
5.6 Other Methods.....	176
5.7 Conclusion.....	177
5.8 References.....	179

**CHAPTER 6**

PRESUMPTIVE ASSAY FOR PEROXIDE-BASED EXPLOSIVES USING THE HYDROGEN PEROXIDE - ACETONITRILE - LUMINOL CHEMILUMINESCENCE REACTION.....	186
6.1 Introduction.....	186
6.1.1 HPAL reaction.....	187
6.2 Experimental.....	189
6.2.1 Instruments and Consumables.....	189
6.2.2 General assay procedure.....	190
6.2.3 Analysis of H <sub>2</sub> O <sub>2</sub> .....	190
6.2.4 PBE sample analysis.....	191
6.2.5 UV spectra collection.....	193
6.3 Results and Discussion.....	193
6.3.1 Observations from H <sub>2</sub> O <sub>2</sub> analysis.....	195
6.3.2 Observations from PBE sample analysis.....	198
6.4 Conclusion and Future Work.....	207
6.5 References.....	208

## CHAPTER 1

### GENERAL INTRODUCTION

#### *1.1 Unifying theme*

The work presented in this dissertation covers two broad topics: pseudostationary phases (PSPs) for micellar electrokinetic chromatography (MEKC) and the detection of peroxide-based explosives (PBEs). While these may seem to be disparate topics, many of the solutes used to probe the PSPs presented here are nitro-based explosives (NBEs), precursors and/or additives to NBE compositions. MEKC, and other PSP-based capillary electrophoresis (CE) methods, have seen increased use in the detection of NBE and related compounds.<sup>1-4</sup> The increased use of NBEs and PBEs in acts of terrorism, as well as NBE remediation projects, has corresponded to an increased interest in detection schemes for explosives.<sup>5-7</sup> A brief introduction to MEKC and the PSP research presented in **CHAPTERS 3** and **4** is given in section *1.2*, as is the background for **CHAPTER 2**. PBE detection, the subject of **CHAPTERS 5** and **6**, is introduced in section *1.3*.

## ***1.2 PSPs for MEKC***

### *1.2.1 Micellar electrokinetic chromatography*

Twenty-five years ago, Shigeru Terabe and colleagues brought the analytical power of CE to neutral solutes by employing the anionic surfactant SDS at a concentration above its critical micelle concentration (CMC).<sup>8,9</sup> Separation was achieved through the differential partitioning of solutes into micelles, leading Terabe et al.<sup>8,9</sup> to dub micelles a “pseudostationary phase” (PSP) and to call this new mode of CE micellar electrokinetic chromatography (MEKC).

Though the aggregation numbers of surfactant micelles are too low to classify micelles as a truly distinct phase, these numbers are too high for micelles to be considered a chemical species.<sup>10,11</sup> The association of surfactant monomers into micelles in aqueous solvents shares several features in common with the formation of a separate liquid phase, given the quasi-liquid state of the micelle’s hydrophobic core.<sup>8,12</sup> Though for ionic surfactants the existence of a charged interface presents a challenge to a simple two-phase solvation model, the depiction of micelles as a distinct phase separate from the bulk aqueous phase has gained general acceptance.<sup>8-10,12-17</sup>

In MEKC, neutral solutes are separated based on their differential partitioning into migrating micelles, allowing comparisons to be made between this method and conventional high performance liquid chromatography (HPLC). MEKC is often compared to reversed phase liquid chromatography given that both rely on a polar mobile phase (i.e., an aqueous buffer solution) and a less polar stationary phase (i.e., a micellar

PSP). Work by Terabe and others showed that much of the theory developed for conventional liquid chromatography applied to MEKC with a few modifications.<sup>8,9,17-19</sup> In conventional liquid chromatography, the retention factor ( $k$ ) is defined as the ratio of the number of solute molecules in the stationary phase to the number in the mobile phase, as calculated by using **Equation 1**.<sup>17-19</sup>

$$k = \frac{t_R - t_0}{t_0} \quad \text{Equation 1}$$

In the above equation, the retention time of the solute is given by  $t_R$ , and the elution time of a completely non-retained solute is given by  $t_0$ . In MEKC, the PSP travels at an electrophoretic velocity that requires an additional term in the equation for  $k$ .<sup>17-19</sup> The migration time of the PSP, denoted  $t_{mc}$ , can be approximated by using the migration time of a highly retained compound. For MEKC, **Equation 1** becomes **Equation 2**.

$$k = \frac{[t_m - t_{eo}]}{t_{eo}[1 - t_m/t_{mc}]} \quad \text{Equation 2}$$

The term  $t_m$  is the MEKC version of  $t_R$ , and represents the migration time of the solute. The migration time of a non-retained solute, denoted by  $t_{eo}$ , takes the place of  $t_0$  and represents electroosmotic flow (EOF).

Under common anionic MEKC experimental conditions, the selected surfactant is dissolved in a high pH buffered solution referred to as the background electrolyte (BGE). Anionic surfactant MEKC operates in the so-called “normal mode”, in which injection occurs at the anode and detection near the cathode. **Figure 1** illustrates a MEKC separation for neutral solutes. In **Figure 1**, the solutes (●) partition between phases

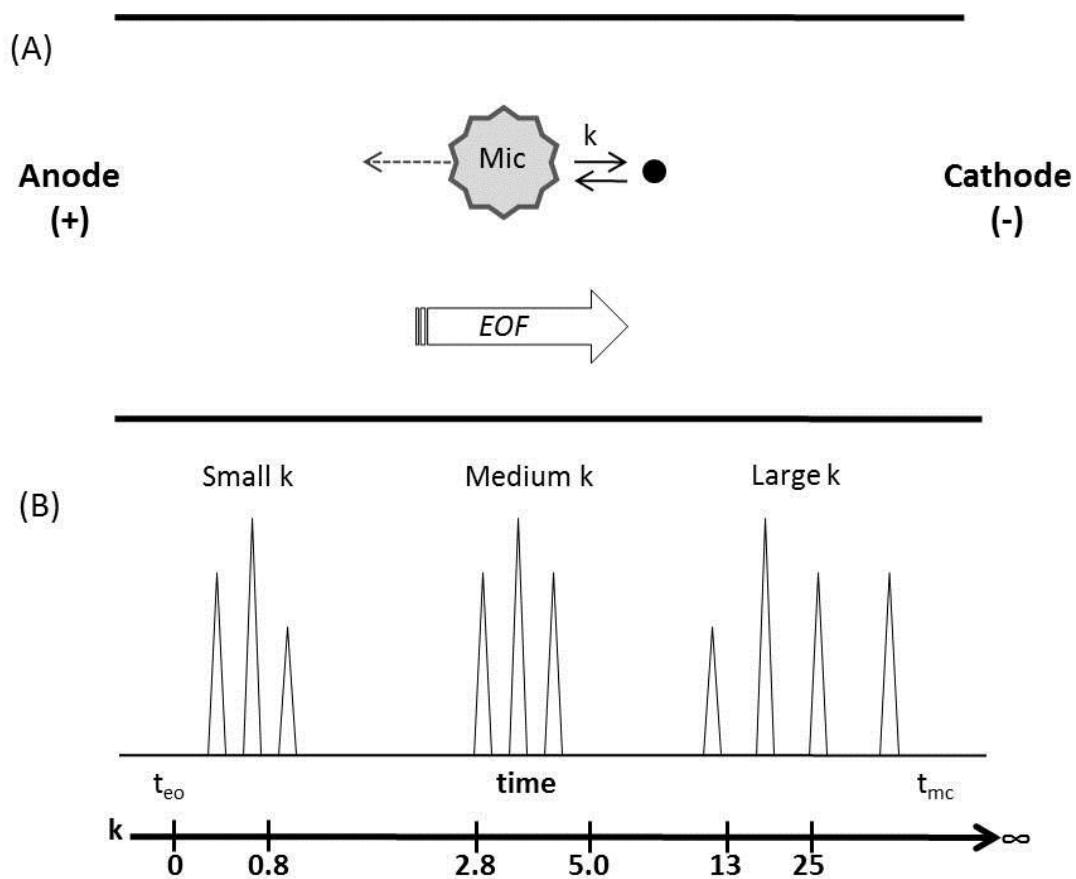


**Figure 1:** Illustration of a MEKC separation of neutral solutes. EOF is electroosmotic flow,  $k$  is the retention factor (**Equation 2**),  $t_{eo}$  is the migration time of a non-retained solute, and  $t_{mc}$  is the migration time of the PSP. This figure was constructed using information from several references.<sup>18, 20-23</sup>



differentially, as illustrated by their various retention factor values. Anionic micelles are attracted to the anode, but EOF forces travel to the cathode where a detector is located.

### 1.2.2 Modifying PSPs

In MEKC separation and detection, one way to optimize separation resolution is to utilize different PSPs (i.e., surfactants).<sup>18, 21, 24, 25</sup> Though a number of surfactants are commercially available, SDS remains the most popular PSP.<sup>18, 21, 22</sup> Rather than utilizing alternative surfactants, researchers often use different class I and II modifiers to affect the PSP and, thus, selectivity and resolution.<sup>24, 26-29</sup> Class I modifiers target the PSP through direct interaction with micelles<sup>12, 18, 24, 26, 30, 31</sup>, while class II organic modifiers operate by altering the BGE.<sup>12, 18, 24, 26-32</sup> In **CHAPTER 3**, the use of a novel class I modifier, the macrocyclic polyether (MP) 18-crown-6 (18C6), is presented for augmentation of SDS MEKC. For this study, nitrotoluene and nitrophenol positional isomers are used as model compounds to investigate 18C6-SDS PSP.

A robust characterization of this 18C6 modified PSP, along with 15-crown-5 (15C5) and 12-crown-4 (12C4) modified PSPs, is presented in **CHAPTER 4**. The characterization of these MP modified PSPs utilizes over two dozen probe solutes, including nitroaromatics. The work presented in **CHAPTER 3** marks the first use<sup>33</sup> of a MP as a class modifier in MEKC and was highlighted in Silva's<sup>34</sup> 2011 review on current methodological and instrumental advances in MEKC for *Electrophoresis*. To this author's knowledge, **CHAPTER 4** presents the first use of 15C5 and 12C4 as class modifiers in

MEKC, as well as being the first detailed investigation of the influence of MPs on solute partitioning in micelles.

The effect of these MPs on SDS has applications beyond MEKC. Surfactants like SDS have long been used to mimic cellular membranes.<sup>31, 32, 35</sup> As described in **CHAPTER 4**, solute partitioning is used to characterize unmodified SDS PSP and MP modified SDS PSP. With crown ethers integrated into drug delivery systems<sup>36, 37</sup>, serving as anti-tumor agents<sup>38</sup>, and used to study cellular ion transport<sup>39-41</sup>, information on the influences of these MPs on solute partitioning is valuable to these fields.

### *1.2.3 Sample matrix for MEKC*

For every CE method, a number of experimental parameters require optimization. One of these parameters is the sample matrix. Unlike PSPs, sample matrices have received little attention beyond an admonishment – do not use a complex sample matrix. Complex sample matrices can cause peak deformities, which can negatively impacting separation resolution.<sup>18, 19, 21, 42</sup> A sample matrix is “complex” if it is different from the BGE. Thus, a water miscible organic solvent is a complex sample matrix.<sup>43-45</sup> A prohibition on such sample matrices can increase analysis times, as samples extracted in organic solvents or in other complex matrices will have to be “cleaned-up” or diluted with aqueous background electrolyte (BGE).<sup>43-45</sup>

**CHAPTER 2** details work done to select and optimize a water miscible organic solvent sample matrix (OSM). Studies done by this author show with proper OSM selection, sample preparation for subsequent CE experiments can be straightforward.

Beyond saving time, OSMs also address those situations where “clean-up” or dilution protocols are unwanted, such as might occur during the analysis of a reaction mixture to monitor its progress. In fields like forensic science, the use of an OSM would alleviate concerns over sample preparation using multiple dilutions and/or solvent exchange protocols.<sup>46</sup>

### ***1.3 Detection of PBEs***

Current trends in the detection of peroxide-based explosives (PBEs) are reviewed in **CHAPTER 5**. The two most popular PBEs are triacetone triperoxide (TATP) and hexamethylene triperoxide diamine (HMTD). Designing a detection scheme for these PBEs is challenging as they are sensitive to mechanical stress, are relatively unstable, lack of UV absorbance or fluorescence, and have limited solubility.<sup>47-53</sup> As discussed in **CHAPTER 5**, a common way around these challenges to PBE detection is to target the common PBE ingredient, hydrogen peroxide.<sup>49, 52, 54-57</sup> This common ingredient was also the focus of this author’s development of a simple wet chemical assay for the presumptive detection of PBEs, as described in **CHAPTER 6**.

#### 1.4 References

1. Giordano, B. C.; Copper, C. L.; Collins, G. E., *Electrophoresis* **2006**, 27 (4), 778-786.
2. Pumera, M., *Electrophoresis* **2006**, 27 (1), 244-256.
3. Pumera, M., *Electrophoresis* **2008**, 29 (1), 269-273.
4. Sarazin, C.; Delaunay, N.; Varenne, A.; Costanza, C.; Eudes, V.; Gareil, P., *Sep. Purification Rev.* **2010**, 39 (1), 63-94.
5. Marshall, M.; Oxley, J. C., *Aspects of Explosives Detection*. Elsevier: 2008.
6. Burks, R.; Hage, D., *Anal. Bioanal. Chem.* **2009**, 395, 301-313.
7. Schubert, H.; Kuznetsov, A., *Detection and Disposal of Improvised Explosives*. Springer: 2006.
8. Terabe, S.; Otsuka, K.; Ando, T., *Anal. Chem.* **1985**, 57, 834-841.
9. Terabe, S.; Otsuka, K.; Ichikawa, K.; Tsuchiya, A.; Ando, T., *Anal. Chem.* **1984**, 56, 111-113.
10. Poole, C.; Poole, S., *J. Chromatogr., A* **2008**, 1182, 1-24.
11. Moroi, Y., *Micelles: Theoretical and Applied Aspects*. Plenum Press: New York, 1992.
12. Zana, R., *Dynamics of Surfactant Self-Assemblies*. Taylor & Francis: Boca Raton, 2005; Vol. 125.
13. Evans, D.; Wennerström, H., *The Colloidal Domain: Where Physics, Chemistry, Biology, and Technology Meet*. Wiley-VCH: New York, 1999; p 672.
14. Muijselaar, P. G.; Otsuka, K.; Terabe, S., *J. Chromatogr., A* **1997**, 780 (1-2), 41-61.

15. Poole, C.; Poole, S., *J. Chromatogr., A* **1997**, 792, 89-1007.
16. Pliska, V.; Testa, B.; van de Waterbeemd, H., *Lipophilicity in Drug Action and Toxicology*. VCH: Weinheim, 1996.
17. Poole, C., *The Essence of Chromatography*. Elsevier: Amsterdam, 2003; p 925.
18. Camilleri, P., *Capillary Electrophoresis*. 2 ed.; CRC Press: Boca Raton, 1997.
19. Landers, J., *Handbook of Capillary Electrophoresis*. CRC Press: Boca Raton, 1993.
20. Mazzeo, J., Micellar Electrokinetic Chromatography. In *Handbook of Capillary Electrophoresis*, 2 ed.; Landers, J., Ed. CRC Press LLC: Boca Raton, 1996; pp 49-70.
21. Landers, J., *Handbook of Capillary and Microchip Electrophoresis and Associated Microtechniques*. 3 ed.; CRC Press: Boca Raton, 2008.
22. Terabe, S., Micellar Electrokinetic Chromatography. In *Handbook of Capillary and Microchip Electrophoresis and Associated Microtechniques*, 3 ed.; Landers, J., Ed. CRC Press, Inc.: Boca, 2008.
23. Silva, M., *Electrophoresis* **2009**, 30 (1), 50-64.
24. Wall, W. E.; Allen, D. J.; Denson, K. D.; Love, G. I.; Smith, J. T., *Electrophoresis* **1999**, 20 (12), 2390-9.
25. Foley, J.; Nielsen, K., Micellar Electrokinetic Chromatography. In *Capillary Electrophoresis*, 2 ed.; Camilleri, P., Ed. CRC Press LLC: Boca Raton, 1998.
26. Allen, D. J.; Wall, W. E.; Denson, K. D.; Smith, J. T., *Electrophoresis* **1999**, 20 (1), 100-10.
27. Katsuta, S.; Saitoh, K., *J. Chromatogr. A* **1997**, 780, 165-178.

28. Seals, T., *Chromatographia* **2000**, *51*, 669-680.
29. Seifar, R.; Kraak, J.; Kok, W., *Anal. Chem.* **1997**, *69*, 2772-2778.
30. Pascoe, R.; Foley, J. P., *Electrophoresis* **2002**, *23* (11), 1618-27.
31. Rosen, M., *Surfactants and Interfacial Phenomena*. 2 ed.; John Wiley and Sons: New York, 1988.
32. Elworthy, P.; Florence, A.; Macfarlane, C., *Solubilization by Surface-Active Agents*. Chapman and Hall LTD: London, 1968.
33. Burks, R. M.; Hage, D. S., *Electrophoresis* **2009**, *30* (4), 657-660.
34. Silva, M., *Electrophoresis* **2011**, *32* (1), 149-165.
35. Hiemenz, P. C.; Rajagopalan, R., *Principles of Colloid and Surface Chemistry*. Marcel Dekker: 1997.
36. Darwish, I. A.; Uchegbu, I. F., *Int. J. Pharm.* **1997**, *159* (2), 207-213.
37. Muzzalupo, R.; Nicoletta, F. P.; Trombino, S.; Cassano, R.; Iemma, F.; Picci, N., *Colloids Surf., B* **2007**, *58* (2), 197-202.
38. Marjanovic, M.; Kralj, M.; Supek, F.; Frkanec, L.; Piantanida, I.; Smuc, T.; Tusek-Bozic, L., *J. Med. Chem.* **2007**, *50* (5), 1007-1018.
39. Kudo, Y.; Takeda, Y.; Matsuda, H., *J. Electroanal. Chem.* **1995**, *396* (1-2), 333-338.
40. He, G.-X.; Kurita, M.; Ishii, I.; Wada, F.; Matsuda, T., *J. Membr. Sci.* **1992**, *69* (1-2), 61-73.
41. Izatt, R. M.; Bruening, R. L.; Clark, G. A.; Lamb, J. D.; Christensen, J. J., *J. Membr. Sci.* **1986**, *28* (1), 77-86.
42. Altria, K., *Capillary Electrophoresis Guidebook*. Humana Press: Totowa, 1996.

43. Shihabi, Z.; Garcia, L., Effects of sample matrix on separation by capillary electrophoresis. In *Handbook of Capillary Electrophoresis*, Landers, J., Ed. CRC Press, Inc.: Boca Raton, 1994; pp 537-548.
44. Thibault, P.; Dovichi, N., General instrumentation and detection systems including mass spectrometric interfaces. In *Capillary Electrophoresis*, 2 ed.; Camilleri, P., Ed. CRC Press LLC: Boca Raton, 1997; pp 26-35.
45. Altria, K., Method Development/Optimization. In *Capillary Electrophoresis Guidebook*, Altria, K., Ed. Humana Press: Totowa, 1996; pp 39-40.
46. United Nations Office on Drugs and Crime. Laboratory and Scientific, S., *Methods for Impurity Profiling of Heroin and Cocaine: Manual for Use by National Drug Testing Laboratories*. United Nations: 2005.
47. Dubnikova, F.; Kosloff, R.; Almog, J.; Zeiri, Y.; Boese, R.; Itzhaky, H.; Alt, A.; Keinan, E., *J. Am. Chem. Soc.* **2005**, *127*, 1146-1159.
48. Oxley, J., Peroxide Explosives. In *Detection and Disposal of Improvised Devices*, Schubert, H.; Kuznetson, A., Eds. Springer: New York, 2006.
49. Oxley, J.; Smith, J.; Chen, H.; Cioffi, E., *Thermochim. Acta* **2002**, *338*, 215-225.
50. Schulte-Ladbeck, R.; Vogel, M.; Karst, U., *Anal. Bioanal. Chem.* **2006**, *386*, 559-565.
51. Wilson, P.; Prince, B.; McEwan, M., *Anal. Chem.* **2006**, *78*, 575-579.
52. McKay, G., *Kayaku Gakkaishi* **2002**, *63*, 323-329.
53. Bellamy, A., *J. Forensic. Sci.* **1999**, *44*, 603-608.
54. Woffenstein, R., *Chem. Ber.* **1895**, *28*, 2265-2269.

55. Yeager, K., Dangerous innovations. In *Trace Chemical Sensing of Explosives*, Woodfin, R., Ed. Wiley-Interscience: Hoboken, 2007.
56. Evans, H.; Tulleners, A.; Sanchez, B.; Rasmussen, C., *J. Forensic. Sci.* **1986**, *31*, 1119-1125.
57. Legler, L., *Chem. Ber.* **1881**, *14*, 602-604.



## CHAPTER 2

### USE OF A WATER MISCIBLE ORGANIC SOLVENT SAMPLE MATRIX IN MICELLAR ELECTROKINETIC CHROMATOGRAPHY

#### *2.1 Introduction*

The development of micellar electrokinetic chromatography (MEKC) addressed the major challenge neutral solutes presented to capillary electrophoresis (CE). Whether the solute was charged or neutral, in a CE technique with or without a pseudo-stationary phase (PSP) a common feature is the impact sample matrix has on peak deformity and separation resolution.<sup>1-4</sup> Though the volume of a sample solution that is typically injected onto a CE capillary is <1% of the total capillary volume, the composition of the sample matrix is considered to have a large effect on a separation's peak shape and resolution.<sup>5-9</sup> This chapter focuses on the selection and optimization of a water miscible organic solvent sample matrix (OSM).

To minimize peak deformity and maximize separation resolution, the general rule in CE sample preparation is to (1) avoid complex sample matrices, (2) “clean-up” sample solutions or (3) dilute complex matrices with aqueous background electrolyte (BGE).<sup>6, 8, 9</sup> The definition of “complex” as used here for the sample matrix is relative in nature (i.e., compared to the run buffer), with sample matrices containing, or wholly comprised of, water miscible organic solvents often being classified as such.<sup>6, 8, 9</sup> For a number of

solutes, the complex matrix avoidance dictum is easy to abide by because many solutes can be dissolved in water or dilute BGE.<sup>6, 8, 9</sup> The biggest test for this rule occurs when working with neutral hydrophobic solutes of various aqueous solubilities.

For these solutes, one would think that MEKC would be the answer. However, the sample matrix in MEKC is often surfactant-free, containing water, BGE or dilute BGE.<sup>10, 11</sup> Use of these sample matrices departs the benefits of field-enhanced sample-stacking (FESS) onto a given separation.<sup>5, 6, 8-13</sup> Though FESS techniques were first developed for conventional CE of ionic analytes, hydrophobic neutral compounds analyzed by MEKC can be concentrated due to their solubilization by micelles. In a typical FESS MEKC protocol, the sample is prepared in a low conductivity matrix (e.g., BGE) relative to the run buffer (BGE + micelles), which leads to a narrow, concentrated sample zone that often corresponds to narrow, well-resolved peaks.<sup>10, 11, 13</sup> To deal with solutes that are slow to dissolve in aqueous solutions, surfactants (i.e., micelles) can be added to the sample matrix, imparting increased solubility while minimizing or eliminating FESS benefits, depending on surfactant concentration.<sup>10-13</sup> Even with the addition of surfactants to the sample matrix, some hydrophobic solutes with *extremely* limited aqueous phase solubility can still prove a challenge to analyze by MEKC.<sup>10, 14-18</sup>

The use of an OSM would provide the benefits of FESS techniques, while potentially meeting the challenge of working with the most hydrophobic solutes. In addition, the proper selection of an OSM would address those situations where “clean-up” or dilution protocols are unwanted. One example is the analysis of a reaction mixture to monitor its progress. Another example is high throughput screening, where additional sample preparation steps are not preferred. The use of an OSM would also assuage

sampling concerns in fields where multiple dilutions and/or solvent exchange protocols are problematic, such as in forensic science.<sup>19</sup>

### *2.1.1 Use of miscible organic solvents in sample solutions*

Water-miscible organic solvents such as methanol (MeOH) and acetonitrile (ACN) are frequently added to background electrolyte (BGE) solutions and/or aqueous sample solutions to address solubility issues.<sup>2,4</sup> Modifying BGEs with organic solvents has created CE modes employing binary (organic solvent – aqueous phase) BGEs and non-aqueous capillary electrophoresis (NACE), expanding the range of compounds for CE analysis.<sup>1-3</sup>

The employment of an OSM is relatively rare<sup>15, 18, 20-25</sup>, though reports in the literature that discourage the use of an OSM are plentiful<sup>1-4, 14, 16, 20, 26-30</sup>. Caution against the use of an OSM is often given under the general heading of “sample matrix effects” which lead to peak deformity.<sup>1-3</sup> This admonition is at odds with common practice and emerging CE trends. As mentioned above, the addition of ACN and MeOH to aqueous sample solutions is routine as they aid in solubilization. Miscible organic solvents, such as ACN and MeOH, are successfully used in stacking regimes (e.g., FESS) that are employed to concentrate solutes on-column, leading to high efficiency and resolution.<sup>31-33</sup>

In MEKC, two markers are required in each sample: (1) an electroosmotic force (EOF) marker, which is a non-retained solute (migration time denoted  $t_{eo}$ ), and (2) a PSP marker, which is some highly retained compound. Most relevant to this discussion is the

EOF marker, which is often a water miscible organic solvent, with MeOH, ACN and acetone being commonly used for this purpose.<sup>34</sup> Both  $t_{eo}$  and  $t_{mc}$  are required to calculate a solute's retention factor ( $k$ ; **Equation 1**), which is a measure of how well solubilized a solute is by the PSP.<sup>2,4</sup>

$$k = \frac{[t_m - t_{eo}]}{t_{eo}[1 - t_m/t_{mc}]} \quad \text{Equation 1}$$

In Equation 1,  $t_m$  is the migration time of an analyte. Miscible organic solvents are routinely used in sample solutions without negative effects.

### *2.1.2 Miscible organic solvents and peak deformity*

Strong admonishments against the use of OSM began when Crabtree and colleagues first investigated the role of OSMs in peak deformity in 1994<sup>16</sup>, noting that for select solutes, split peaks were induced by the use of ACN as the sample matrix. **Figure 1** illustrates Crabtree and colleagues' explanation of OSM induced peak splitting. In this four step model<sup>16</sup>, a solute in an OSM is injected into the capillary, yielding an organic solvent-aqueous phase interface (**a**). Upon application of the separation voltage, a second organic solvent-aqueous phase interface develops (**b**). The solute begins partitioning from the OSM into the PSP across both interfaces, giving two zones of high solute concentration (**c**). Eventually, the OSM, completely non-retained and travelling at the same velocity as EOF, migrates past the leading zone. By overtaking the leading zone, the OSM dissolves micelles that contain solutes, causing the solutes to re-partition. This process is repeated until longitudinal diffusion reduces the

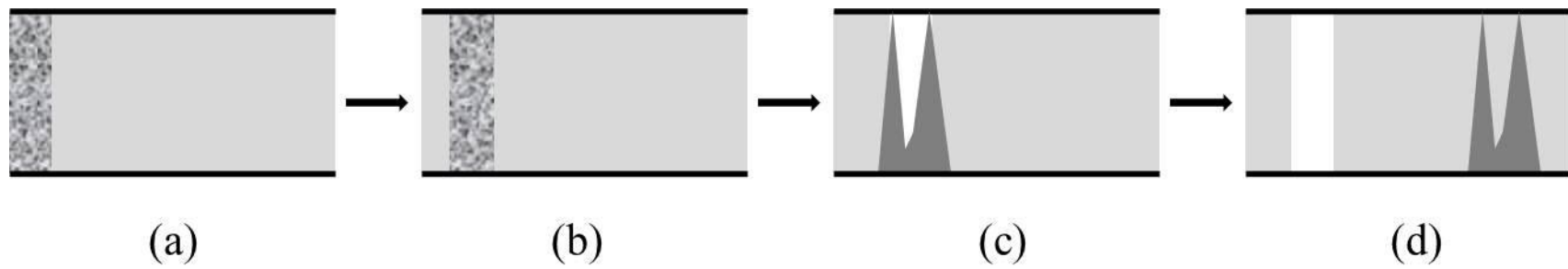


**Figure 1:** A schematic representation of the four step model developed by Crabtree and colleagues<sup>16</sup> to explain OSM induced peak splitting. See text for explanation of steps (a) – (d).

concentration of organic solvent until it can no longer dissolve micelles in the leading zone. The result is a split peak for a single solute (**d**).

Crabtree's model is generally accepted, with a handful of supporting investigations using a sodium dodecyl sulfate (SDS) PSP being conducted in the intervening years.<sup>14, 30, 35</sup> Examination of these studies<sup>14, 30, 35</sup>, however, reveals that OSM induced peak deformity is *extremely* selective; is seen mainly for large solutes (as measured by McGowan's characteristic volume<sup>14</sup>), is found at low surfactant concentrations (e.g., 12 mM SDS), and is often seen at moderate separation voltages (e.g., 15 kV). In regards to SDS concentration, peak splitting is generally not been observed in these studies<sup>14, 30, 35</sup> for SDS concentrations  $\geq 40$  mM in a variety of aqueous BGEs.

In MEKC, one would expect a change in a solute's bulk aqueous phase - PSP partitioning if the Crabtree model (**c**) is accurate. The selective nature of peak splitting indicates the use of OSMs does not affect solute bulk aqueous-PSP partitioning in a general fashion or to a substantial degree. In addition, given the use of ACN, MeOH or acetone as EOF markers and in stacking regimes<sup>31-33</sup>, the role of these solvents seems either benign or beneficial.

In light of the observations regarding the selective nature of peak splitting, it is perhaps likely that the OSM does play a role in peak splitting, but perhaps this role is due to diffusion prior to the application of the separation voltage. Due to CE instrument design, there is a delay between the formation of solvent interface 1 (at the time of injection) and interface 2 (when the separation voltage is applied).<sup>36, 37</sup> During this delay

diffusion can occur<sup>36</sup>, with the OSM being diluted and an OSM concentration gradient being allowed to develop. During this time, solutes are partitioning as shown in (c) of Crabtree's model (section 2.1.2). Depending on the size of the solute and/or its preference for the OSM versus an aqueous environment, this "delay activity" may result in peak deformity.

Given the many benefits of an OSM and a possible "delay activity" cause of OSM-related peak splitting, an OSM was selected and optimized for use in MEKC experiments involving aromatic solutes, such as those detailed in **CHAPTERS 3 and 4**. The selection of this OSM is discussed in section 2.1.3, with optimization experiments are detailed in sections 2.2 and 2.3.

### *2.1.3 OSM selection*

The initial selection of the OSM was based on the solute set (see **APPENDIX A**) of interest in experiments discussed in **CHAPTERS 3 and 4**, along with commonly employed EOF markers. For the experiments described herein, a 1:1 v/v ACN:MeOH OSM was used due to the benefits each of these solvents brings to solubilizing solutes of the type studied in this chapter. ACN is a dipolar and aprotic solvent that engages in donor-acceptor complexation with aromatic rings to which electron-withdrawing groups are attached.<sup>38, 39</sup> Given the solute set used in this work, ACN was a good choice as a solvent for many of the solutes. MeOH was also a good choice because it is a protic solvent with pronounced hydrogen bonding abilities.<sup>39</sup>

The properties of density, viscosity and dielectric constants are known for various mixtures of ACN and MeOH.<sup>40-42</sup> The nature of hydrogen bonding in mixtures of ACN–MeOH has also been studied.<sup>43</sup> At ratios less and greater than 1:1 v/v, ACN–MeOH solutions are less cohesive than either ACN, MeOH or water.<sup>44</sup> A less cohesive OSM would be a benefit to solutes partitioning from the OSM to the aqueous environment in an MEKC separation mode (e.g., micelles in a BGE).

### *2.1.3 OSM evaluation and optimization*

To evaluate the selected OSM (i.e., a 1:1 v/v mixture of ACN:MeOH), solute peak shape under MEKC conditions employed in CHAPTERS 3 and 4 (section 2.3) was monitored. For those solutes for which peak splitting was observed, two remedies based on the “delay activity” cause of peak splitting (section 2.1.2) were used. These were: (1) modifying the injection protocol for a shorter sample plug and (2) increasing the delay time between injection and separation to allow for longer OSM – aqueous environment mixing.

As stated in section 2.1.2, one would expect to see changes to a solute’s bulk aqueous phase - PSP partitioning if the Crabtree model is accurate. Based on the selective nature of OSM-induced peak splitting, this does not appear to be the case. To investigate the impact of the selected OSM on solute bulk aqueous-PSP partitioning, the micellar phase to aqueous phase partition coefficient ( $P_{mw}$ ; section 2.2.2) for each solute was determined and compared to previously-published values for which an aqueous sample matrix had been used to determine  $P_{mw}$ .



## ***2.2 Experimental***

### ***2.2.1 Instruments and Materials***

CE experiments were done at 25°C and 25 kV using a Beckman Coulter P/ACE MDQ CE with DAD (Fullerton, CA). An unmodified silica capillary (75  $\mu\text{m}$  inner diameter, 60 cm total length, and 50 cm effective length) was purchased from Polymicro Technologies (Phoenix, AZ).

Buffer reagents, SDS (the PSP used in this work), methanol, acetonitrile and test solutes were purchased from Sigma-Aldrich (St. Louis, MO). All solute solutions were made at a concentration of 150  $\mu\text{g}/\text{mL}$  using an OSM of 1:1 v/v ACN:MeOH. For all MEKC experiments, the background electrolyte (BGE) was 10 mM, pH 8.5 sodium borate buffer with added SDS concentrations, as already noted. All aqueous solutions were made using water obtained from a Millipore NANOpure system (Bedford, MA).

### 2.2.2 Solute set and determination of $\log P_{mw}$ values

A diverse set of twenty-six solutes (see **APPENDIX A**) was used to determine solute water-micelle partition coefficients ( $P_{mw}$  in **Equation 2**).

$$k = P_{mw}V_{sf}([\text{surfactant}] - \text{CMC}) \quad \text{Equation 2}$$

In **Equation 2**<sup>45</sup>,  $V_{sf}$  is the partial molar volume of the surfactant in the micelles,  $[\text{surfactant}]$  is the concentration of the surfactant used as the PSP, and CMC is the critical micelle concentration. At  $[\text{surfactant}] \geq \text{CMC}$ , the surfactant forms micelles, thus serving as the PSP.

A well-established MEKC method was used to determine of retention factors ( $k$ ) for the calculation of  $P_{mw}$ , as described previously.<sup>45,46</sup> This method involved determining the retention factor ( $k$  in **Equation 1**; see section 2.1.1) for each solute at various concentrations of the PSP.  $P_{mw}$  can be calculated, if  $V_{sf}$  is known, by plotting  $k$  versus  $[\text{SDS}]$  (**Equation 2**).

For the determination of  $P_{mw}$  values, a SDS concentration range of 15-40 mM was used. A known value for the  $V_{sf}$  of SDS at 25 °C was used (i.e.,  $2.478 \times 10^{-4}$  L/mmol), which is a value routinely employed for  $P_{mw}$  determination experiments involving SDS.<sup>45-47</sup> All measurements of  $k$  were done in triplicate. Conveniently, both methanol (MeOH) and acetonitrile (ACN) serve as EOF markers<sup>34</sup>, allowing the migration of the solute solution matrix to be used to determine the EOF migration time ( $t_{eo}$ ). The micelle migration times ( $t_{mc}$ ) were determined using Sudan III or decanophenone.<sup>34</sup> A sample injection program of 0.5 psi for 3 s or 0.3 psi for 3 s was used initially (see sections 2.2.3 and 2.3), along with a separation voltage of 20 kV.

### *2.2.3 Modification of sample plug length*

The injection was modified to 0.3 psi and 3 sec using operation software accompanying the Beckman Coulter P/ACE MDQ CE instrument for those solutes in which peak splitting was observed (four out of twenty-six during experiments to determine  $P_{mw}$  values and using an initial injection program of 0.5 psi-3 sec). Sample plug lengths were estimated as described by Weinberger<sup>5</sup>, using a published viscosity value for the selected OSM ratio<sup>41</sup>; the injection specifics are detailed above, and the column dimensions are listed in section 2.2.1.

### *2.2.4 Modification of injection-to-separation delay time*

For those solutes for which split peaks were observed (four out to twenty-six during experiments to determine  $P_{mw}$  values using an injection program of 0.5 psi-3 sec), the delay between injection and application of separation voltage was extended. This delay was introduced by adding a “wait” command between sample injection and separation using operation software accompanying the Beckman Coulter P/ACE MDQ CE instrument. To minimize diffusive sample solution loss out of the capillary<sup>36</sup>, and based on initial experiments, the “wait” command location was occupied by a vial containing the selected OSM.

### 2.3 Results and Discussion

Peak splitting was observed for the four largest solutes, as characterized by the McGowan's characteristic volume (see **APPENDIX B**), during initial retention factor (*k*) determination experiments. These four compounds were naphthalene, 1-naphthol, 2-naphthol, and diphenylamine. To eliminate the peak splitting observed for these four compounds, the modifications described in sections 2.2.3 and 2.2.4 were utilized.

To bypass peak deformity due to disparate run buffer and sample matrices, it has been suggested that sample plug lengths be limited to 1-2% of the total capillary length.<sup>30</sup> This suggestion is general in nature and may not address a solute's unique partitioning behavior between the specific phases (or pseudophases) that are present. It should be noted that stacking regimes (see section 2.1) which employ a miscible organic solvent typically utilize a range of solvent plugs, some far greater in length than that which corresponds to 1-2% of the total capillary length.<sup>32</sup>

Though the initial injection plug length was 0.5 psi for 3 sec (1.35% total capillary length) for early retention factor (*k*) determination experiments, split peaks were observed for naphthalene, 1-naphthol, 2-naphthol, and diphenylamine at various concentrations of SDS. Injection plug length was reduced further using 0.3 psi for 3 sec, giving  $\approx$  0.81% total capillary length. This injection protocol adjustment saw the complete elimination of peak deformity for all of the tested compounds. **Figure 2** is a comparison of peak shapes for 2-naphthol for both two injection protocols over a wide SDS concentration range. Utilizing the injection program of 0.3 psi for 3 sec resulted in single, sharp peaks for naphthalene, 1-naphthol, and

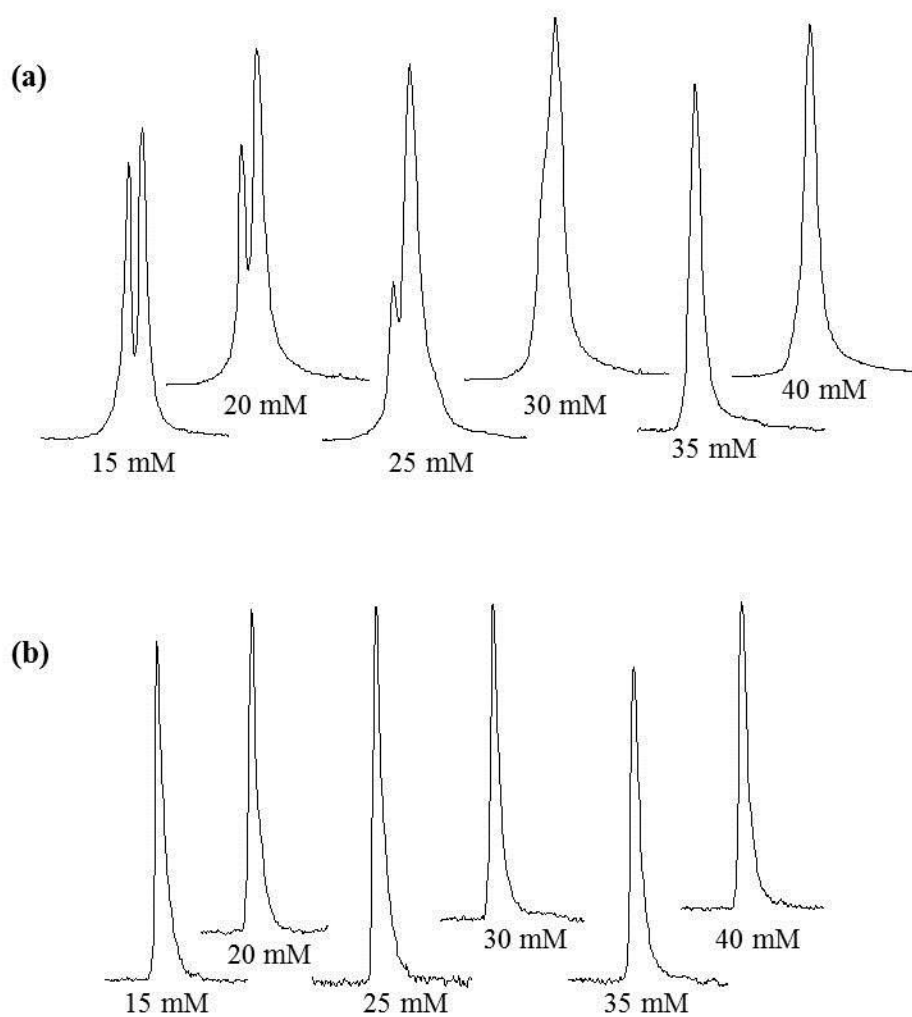


**Figure 2:** Electropherogram for 2-naphthol peaks over the designated SDS concentration range when using an injection program of (a) 0.5 psi for 3 sec or (b) 0.3 psi for 3 sec.

diphenylamine, in addition to 2-naphthol, with no negative effects being noted for smaller solutes.

The usefulness of injection-to-separation delay time modifications was investigated to ascertain if the split peaks observed using the initial injection plug length of 0.5 psi for 3 sec could be eliminated. Using 2-naphthol as a test solute, the effect of increasing the delay time between injection and separation was examined. A “wait” time of 0 sec eliminated the peak splitting, though times of 15 and 30 sec were also tested. The CE system used here is fully automated; requiring specific trays and vial locations are used based on specific commands. Such idiosyncrasies correspond to no “wait” command, or a “wait” time of 0 sec, corresponding to several seconds.

For the particular instrument used in this study, with *no* “wait” command used, the delay between sample injection and application of the separation voltage was determined to be approximately 25 sec (i.e., the approximate delay time). A “wait” command of 0 min added approximately 20 sec (delay time  $\approx$  45 sec). **Figure 3** is a comparison of electropherograms for 2-naphthol that shows the elimination of a split peak upon inclusion of a “wait” command of 0 min in the separation program. As with the injection program modification, the aforementioned “wait” time of “0” resulted in single, sharp peaks for naphthalene, 1-naphthol, and diphenylamine, in addition to 2-naphthol, with no negative effects being noted for smaller solutes.

Though this “wait” command eliminated the split peaks observed for naphthalene, 1-naphthol, 2-naphthol, and diphenylamine, to minimize the total analysis time, the 0.3 psi for 3 sec option for injection was used to collect the  $k$  values necessary to calculate

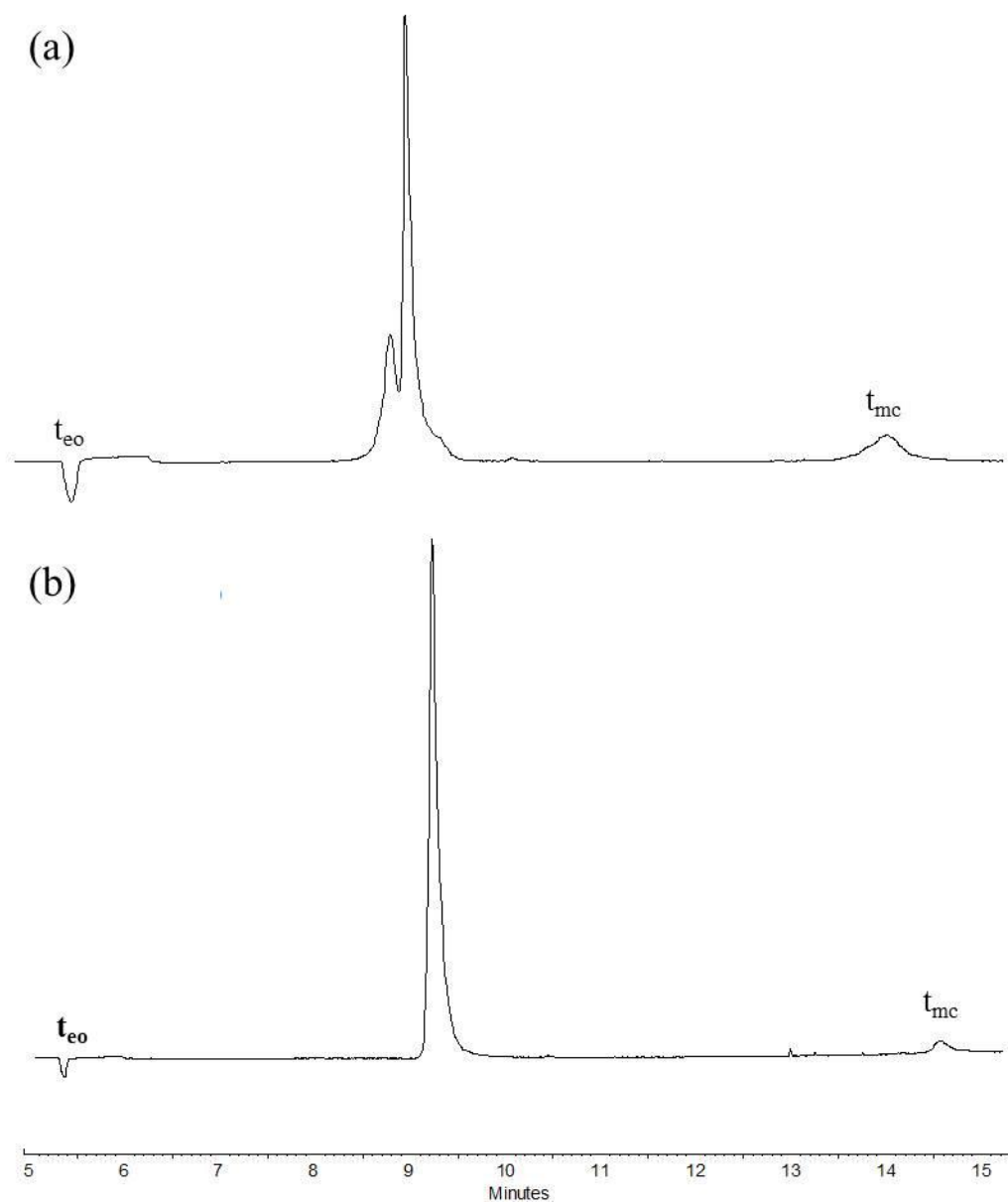


**Figure 3:** Electropherograms for 2-naphthol where (a) no “wait” command preceded the solute injection program of 0.5 psi for 3 sec (delay time  $\approx$  25 sec) or (b) a “wait” command of 0 min preceded the solute injection program of 0.5 psi for 3 sec (delay time  $\approx$  45 sec).

**Table 1:** Comparison of experimentally determined log micelle-water partition coefficients ( $\log P_{mw}$ ; **Equation X**) with published  $\log P_{mw}$  values or  $\log P_{mw}$  values calculated using published data. Lower case letters indicate values that were taken or calculated from the following references: *a* - values taken from (Katsuta, S.; Saitoh, K.)<sup>45</sup>, *b* - values taken from (Kelly et al.)<sup>48</sup>, *c* - values taken from (Kord et al.)<sup>49</sup>, *d* - values calculated using data from (Sprunger et al.)<sup>50</sup>, *e* - values taken from (Gavenda et al.)<sup>51</sup>, *f* - values calculated using data from (Vitha et al.)<sup>52</sup>, *g* - values calculated using data from (Garcia, M.A.; Marina, M.L.; Diez-Masa, J.C.)<sup>53</sup>. An average ( $\bar{x}$ )  $\log P_{mw}$  value was calculated using experimentally determined and previously published data for solutes with three or more  $\log P_{mw}$  values. For these average  $\log P_{mw}$  values, standard deviation ( $\sigma$ ) values are given.



Solute	log P <sub>mw</sub>							$\bar{x}$	$\sigma$
	<i>this work</i>	<i>a</i>	<i>b</i>	<i>c</i>	<i>d</i>	<i>e</i>	<i>f</i>		
phenylamine	1.60		1.61		1.78			1.66	0.08
phenol	1.65	1.69	1.66		1.82			1.58	0.09
benzyl alcohol	1.69	1.76	1.70		1.72			1.60	0.06
benzene	1.93	2.02	1.94		1.81	1.97	2.01	1.92	0.07
1,3-dinitrobenzene	2.01								
3-methylphenol	2.03				2.00			2.05	0.03
nitrobenzene	2.04	2.13	2.05	2.10	1.84			2.04	0.10
4-methylphenol	2.07	2.12			2.00				0.06
anisole	2.16	2.24	2.15		2.06				0.07
acetophenone	2.17	2.29	2.17		2.20			2.39	0.09
toluene	2.38	2.50	2.38	2.47	2.31	2.37	2.42	2.38	0.06
2-nitrotoluene	2.45							2.50	0.03
chlorobenzene	2.48	2.57	2.50		2.50			2.50	0.03
4-nitrotoluene	2.49		2.49						
3-nitrotoluene	2.56								
bromobenzene	2.63		2.65		2.90				0.15
1,2-dimethylbenzene	2.76	2.86							
ethylbenzene	2.76		2.77		2.84		2.78	2.36	0.19
1-naphthol	2.77	2.85			2.87			2.73	0.07
2-naphthol	2.79	2.83						2.76	0.03
1,3-dimethylbenzene	2.80	2.91							
1,4-dimethylbenzene	2.81	2.91	2.81		3.03				0.10
1,4-dichlorobenzene	2.93	3.00	2.95		3.46				0.25
naphthalene	3.07	3.15	3.07		3.05			3.07	0.04
diphenylamine	3.31		3.30						
2-bromonaphthalene	3.87				3.87				

solute  $P_{mw}$  values (see section 2.2.2). The  $P_{mw}$  values determined for the test solutes are listed in **Table 1**. These experimentally determined values were compared to  $P_{mw}$  values obtained or calculated from previously published data where SDS was the PSP, a similar BGE was used and the sample matrix was aqueous. There was good agreement between the  $P_{mw}$  values determined in this study using an OSM and those determined when using an aqueous sample matrix.

While this abbreviated evaluation of a selected OSM is not definitive, the observed selective nature of peak splitting, the easy fixes employed to eliminate peak splitting, and the good agreement between the  $P_{mw}$  values determined here using an OSM and those determined using an aqueous sample matrix all led credence to the “delay activity” explanation of differential peak splitting. However, it should be noted that due to diffusive sample solution loss out of the capillary<sup>36</sup>, there is a chance the elimination of split peaks is simply due to a smaller sample band. As stated in 2.2.4, the “wait” command location was a vial containing the selected OSM to minimize such a loss of sample.

## ***2.4 Conclusion and Future Work***

The aim of this work was to illustrate that with proper selection and fast optimization, an OSM can be used with no negative effects. In addition, the selected OSM was used to determine solute  $P_{mw}$  values and it was found that these values were in-line with those determined using an aqueous sample solution.

The benefits of this work were discussed in section 2.1. One such benefit is a reduced analysis time due to fewer sample preparation steps. For  $P_{mw}$  value determination experiments involving dozens of solutes, or high volume testing such as in a forensic or hospital laboratory, this approach saves valuable time. Simple split peak fixes such as modified injection programs and “wait” commands may open the door for direct sampling of complex reaction mixtures.

Additional work may confirm “delay activity” as the source of peak splitting. One possibility is to conduct similar experiments using a different instrument capable of delay times less than 25 sec to evaluate the prevalence of peak splitting for a solute set. Use of other OSMs (acetone, ethanol, etc.) may reveal more nuances in peak splitting behavior. Computation work, employing mathematical modeling of “delay activity” and the Crabtree model of peak splitting would also provide valuable insight.

## 2.5 References

1. Altria, K., *Capillary Electrophoresis Guidebook*. Humana Press: Totowa, 1996.
2. Camilleri, P., *Capillary Electrophoresis*. 2 ed.; CRC Press: Boca Raton, 1997.
3. Landers, J., *Handbook of Capillary Electrophoresis*. CRC Press: Boca Raton, 1993.
4. Landers, J., *Handbook of Capillary and Microchip Electrophoresis and Associated Microtechniques*. 3 ed.; CRC Press: Boca Raton, 2008.
5. Weinberger, R., Injection Techniques for Capillary Electrophoresis. In *Encyclopedia of Chromatography*, Cazes, J., Ed. Marcel Dekker, Inc.: New York, 2001; Vol. 1, pp 435-437.
6. Shihabi, Z.; Garcia, L., Effects of sample matrix on separation by capillary electrophoresis. In *Handbook of Capillary Electrophoresis*, Landers, J., Ed. CRC Press, Inc.: Boca Raton, 1994; pp 537-548.
7. Wu, X., *Trends Anal. Chem.* **2003**, 22 (1), 48-58
8. Thibault, P.; Dovichi, N., General instrumentation and detection systems including mass spectrometric interfaces. In *Capillary Electrophoresis*, 2 ed.; Camilleri, P., Ed. CRC Press LLC: Boca Raton, 1997; pp 26-35.
9. Altria, K., Method Development/Optimization. In *Capillary Electrophoresis Guidebook*, Altria, K., Ed. Humana Press: Totowa, 1996; pp 39-40.
10. Terabe, S., Micellar Electrokinetic Chromatography. In *Handbook of Capillary and Microchip Electrophoresis and Associated Microtechniques*, 3 ed.; Landers, J., Ed. CRC Press, Inc.: Bocoa, 2008.

11. Mazzeo, J., Micellar Electrokinetic Chromatography. In *Handbook of Capillary Electrophoresis*, 2 ed.; Landers, J., Ed. CRC Press LLC: Boca Raton, 1996; pp 49-70.
12. Foley, J.; Nielsen, K., Micellar Electrokinetic Chromatography. In *Capillary Electrophoresis*, 2 ed.; Camilleri, P., Ed. CRC Press LLC: Boca Raton, 1998.
13. Terabe, S., *Analytical Chemistry* **2004**, 76 (13), 240-246.
14. Rafols, C.; Poza, A.; Fuguet, E.; Roses, M.; Bosch, E., *Electrophoresis* **2002**, 23 (15), 2408-16.
15. Huhn, C.; Putz, M.; Holthausen, I.; Pyell, U., *Electrophoresis* **2008**, 29, 526-537.
16. Crabtree, H., *J. Chromatogr., A* **1994**, 1994, 263-267.
17. Crabtree, H.; Ireland, I.; Dovichi, N., *J. Chromatogr., A* **1994**, 669, 263-267.
18. Hsiao, H.; Cheng, T.; Yang, G.; Huang, I.; Chen, R., *Phytochem. Anal.* **2008**, 19, 136-140.
19. United Nations Office on Drugs and Crime. Laboratory and Scientific, S., *Methods for impurity profiling of heroin and cocaine: manual for use by national drug testing laboratories*. United Nations: 2005.
20. Cifuentes, A.; Bernal, J.; Diez-Masa, J., *J. Chromatogr., A* **1998**, 824, 99-108.
21. Hasemann, P.; Balk, M.; Preu, L.; Watzig, H., *Electrophoresis* **2007**, 28, 1779-1787.
22. Kavran, G.; Erim, F. B., *J. Chromatogr., A* **2002**, 949, 301-305.
23. Lee, M. C.; Chuang, W. C.; Sheu, S. J., *J. Chromatogr., A* **1996**, 755, 113-119.
24. Shihabi, Z., *Electrophoresis* **2008**, 29, 1672-1675.
25. Taylor, R.; Reid, R., *J. Pharm. Biomed. Anal.* **1993**, 11, 1289-1294.

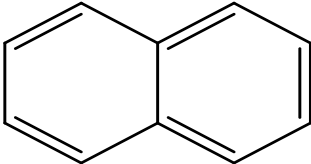
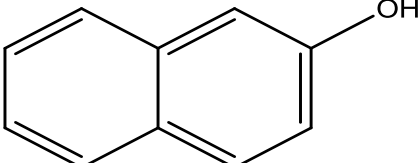
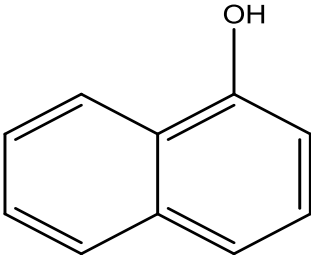
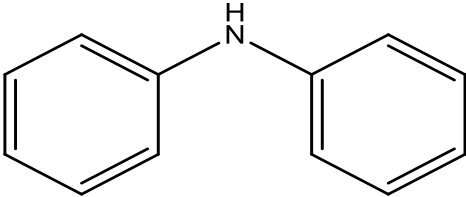
26. Altria, K.; Clark, B.; Kelly, M., *J. High Resol. Chromatogr.* **1999**, 22, 55-58.
27. Huie, C. W., *Anal. Bioanal. Chem.* **2002**, 373 (1-2), 23-30.
28. Huie, C. W., *Electrophoresis* **2003**, 24 (10), 1508-29.
29. Porras, S. P.; Kenndler, E., *Electrophoresis* **2005**, 26 (17), 3203-20.
30. Stapf, F. I.; Oehme, M.; Kiessig, S.; Schwarz, M. A.; Kalman, F., *Electrophoresis* **2007**, 28 (20), 3625-38.
31. Silva, M., *Electrophoresis* **2009**, 30 (1), 50-64.
32. Malá, Z.; Šlampová, A.; Gebauer, P.; Boček, P., *Electrophoresis* **2009**, 30 (1), 215-229.
33. Quirino, J. P., *J. Chromatogr., A* **2009**, 1216 (2), 294-299.
34. Fuguet, E.; Rafols, C.; Bosch, E.; Roses, M., *Electrophoresis* **2002**, 23 (1), 56-66.
35. Chen, X.; Xie, J.; Li, C.; Hu, Z.; Chen, X., *J. Sep. Sci.* **2004**, 27 (12), 1005-1010.
36. Colyer, C. L.; Myland, J. C.; Oldham, K. B., *J. Chromatogr., A* **1996**, 732 (2), 335-343.
37. Steiner, F.; Scherer, B., *J. Chromatogr., A* **2000**, 887 (1-2), 55-83.
38. Leggett, D. C.; Miyares, P. H.; Jenkins, T. F., *J. Solution Chem.* **1992**, 21 (1), 105-108-108.
39. Subirats, X.; Reinstadler, S.; Porras, S. P.; Raggi, M. A.; Kenndler, E., *Electrophoresis* **2005**, 26 (17), 3315-3324.
40. Coplan, M. A.; Fuoss, R. M., *J. Phys. Chem.* **1964**, 68 (5), 1181-1185.
41. Nikam, P. S.; Shirsat, L. N.; Hasan, M., *J. Chem. Eng. Data* **1998**, 43 (5), 732-737.

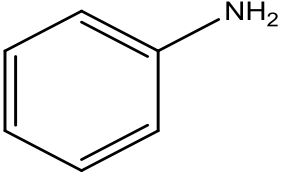
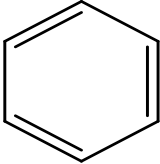
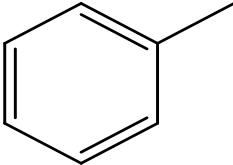
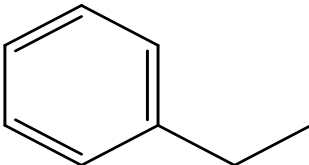
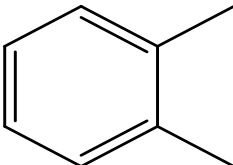
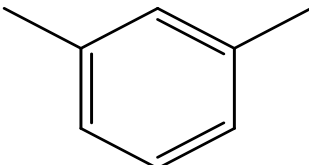
42. Krasnoperova, A.; Kovalenko, L.; Gracheva, E., *J. Struct. Chem.* **1978**, *19* (1), 67-70-70.
43. Sathyan, N.; Santhanam, V.; Sobhanadri, J., *J. Mol. Struc.* **1995**, *333* (1-2), 179-189.
44. Conti, F.; Pistoia, G., *J. Phys. Chem.* **1968**, *72* (6), 2245-2248.
45. Katsuta, S.; Saitoh, K., *J. Chromatogr., A* **1997**, *780*, 165-178.
46. Terabe, S.; Otsuka, K.; Ando, T., *Anal. Chem.* **1985**, *57*, 834-841.
47. Shinoda, K.; Soda, T., *J. Phys. Chem.* **1963**, *67* (10), 2072-2074.
48. Kelly, K. A.; Burns, S. T.; Khaledi, M. G., *Anal. Chem.* **2001**, *73* (24), 6057-62.
49. Kord, A. S.; Strasters, J. K.; Khaledi, M. G., *Anal. Chim. Acta* **1991**, *246* (1), 131-137.
50. Sprunger, L.; Acree, W. E., Jr.; Abraham, M. H., *J. Chem. Inf. Model.* **2007**, *47* (5), 1808-17.
51. Gavenda, A.; Bednář, P.; Barták, P.; Adamovský, P.; Ševčík, J.; Tzoumas, P.; Ulrichová, J., *J. Sep. Sci.* **2001**, *24* (9), 723-728.
52. Vitha, M.; Weckwerth, J.; Odland, K.; Dema, V.; Carr, P., *J. Phys. Chem.* **1996**, *100*, 18823-18828.
53. García, M. A.; Marina, M. L.; Díez-Masa, J. C., *J. Chromatogr., A* **1996**, *732* (2), 345-359.
54. Jover, J.; Bosque, R.; Sales, J., *J. Chem. Inf. Comput. Sci.* **2004**, *44* (3), 1098-1106.
55. Werlich, S.; Andersson, J., *Fresen. J. Anal. Chem.* **1999**, *364*, 3-14.

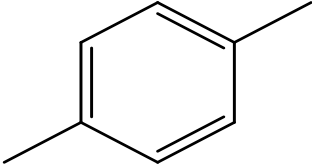
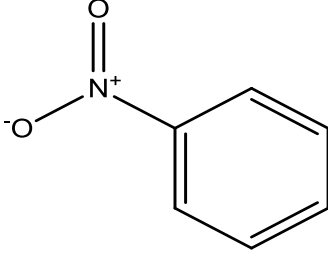
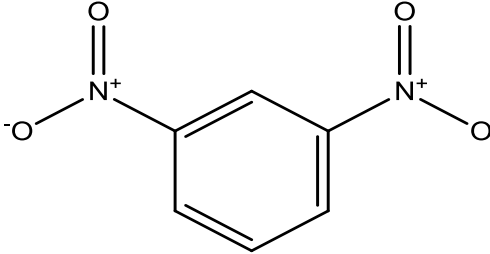
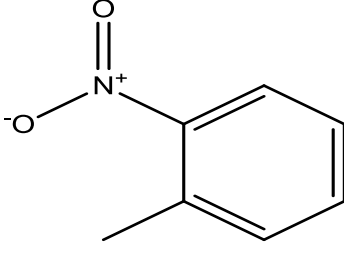
56. Bui, H.; Masquelin, T.; Perun, T.; Castle, T.; Dage, J.; Kuo, M. S., *J. Chromatogr., A* **2008**, *1206* (2), 186-95.
57. Berthod, A.; Mitchell, C. R.; Armstrong, D. W., *J. Chromatogr., A* **2007**, *1166* (1-2), 61-9.
58. Ahmed, H.; Poole, C. F., *J. Chromatogr., A* **2006**, *1104* (1-2), 82-90.

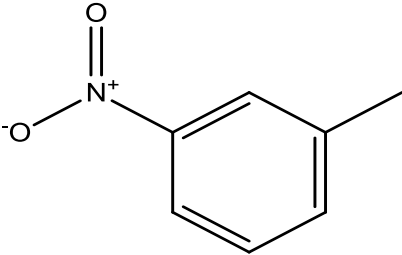
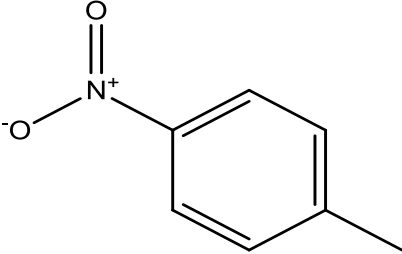
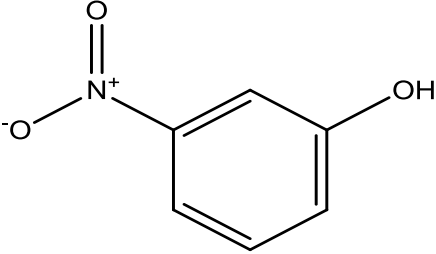
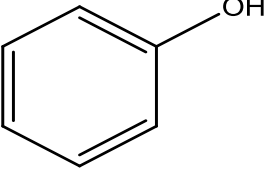
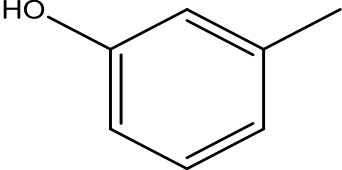


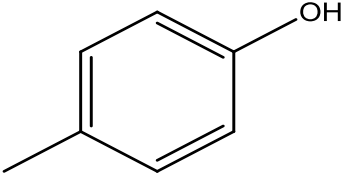
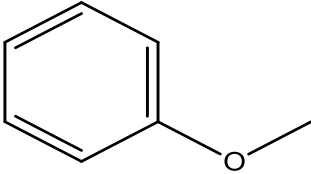
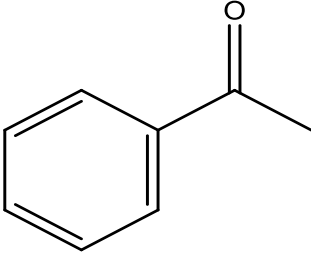
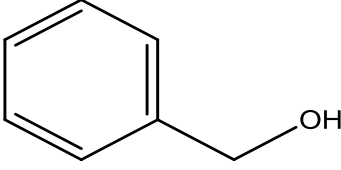
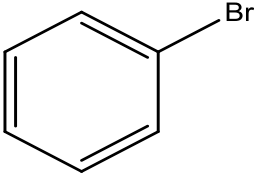
**APPENDIX A****Solute Set**

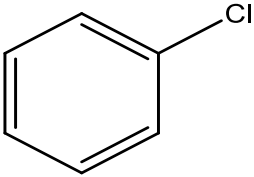
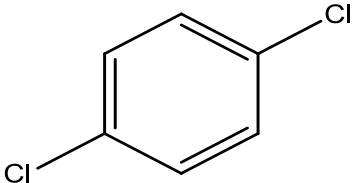
Solute	Solute structure
naphthalene	 $C_{10}H_8$
2-naphthol	 $C_{10}H_8O$
1-naphthol	 $C_{10}H_8O$
diphenylamine	 $C_{12}H_{11}N$

Solute	Solute structure	
phenylamine		$C_6H_7N$
benzene		$C_6H_6$
toluene		$C_7H_8$
ethylbenzene		$C_8H_{10}$
1,2-dimethylbenzene		$C_8H_{10}$
1,3-dimethylbenzene		$C_8H_{10}$

Solute	Solute structure
1,4-dimethylbenzene	
	$C_8H_{10}$
nitrobenzene	
	$C_6H_5NO_2$
1,3-dinitrobenzene	
	$C_6H_4N_2O_4$
2-nitrotoluene	
	$C_7H_7NO_2$

Solute	Solute structure
3-nitrotoluene	 <chem>Cc1cccc([N+](=O)[O-])c1</chem> $C_7H_7NO_2$
4-nitrotoluene	 <chem>Cc1ccc([N+](=O)[O-])cc1</chem> $C_7H_7NO_2$
3-nitrophenol	 <chem>Oc1cccc([N+](=O)[O-])c1</chem> $C_6H_5NO_3$
phenol	 <chem>Oc1ccccc1</chem> $C_6H_6O$
3-methylphenol	 <chem>Cc1cccc(O)c1</chem> $C_7H_8O$

Solute	Solute structure	
4-methylphenol		$C_7H_8O$
anisole		$C_7H_8O$
acetophenone		$C_8H_8O$
benzyl alcohol		$C_7H_8O$
bromobenzene		$C_6H_5Br$

Solute	Solute structure
chlorobenzene	 $C_6H_5Cl$
1,4-dichlorobenzene	 $C_6H_4Cl_2$

**APPENDIX B****Solute McGowan's volume values**



The McGowan's volume (V) values listed in the proceeding table were taken from (Jover, J.; Bosque, R.; Sales, J.)<sup>54</sup> except for 2-nitrotoluene (Werlich, S.; Andersson, J.)<sup>55</sup>; 1,3-dinitrobenzene (Bui et al.)<sup>56</sup>; the dimethylbenzene isomers (Berthod, A.; Mitchell, C.; Armstrong, D.)<sup>57</sup>; diphenylamine (Ahmed, H.; Poole, C.)<sup>58</sup>.

<b>Solute</b>	<b>V</b>
benzene	0.7164
phenol	0.7751
phenylamine	0.8162
chlorobenzene	0.8388
toluene	0.8573
nitrobenzene	0.8906
bromobenzene	0.8914
anisole	0.916
4-methylphenol	0.916
3-methylphenol	0.916
benzyl alcohol	0.916
1,4-dichlorobenzene	0.9612
1,2-dimethylbenzene	0.9982
1,3-dimethylbenzene	0.9982
1,4-dimethylbenzene	0.9982
ethylbenzene	0.9982
acetophenone	1.014
2-nitrotoluene	1.032
4-nitrotoluene	1.032
3-nitrotoluene	1.032
1,3-dinitrobenzene	1.06
naphthalene	1.0854
1-naphthol	1.144
2-naphthol	1.1441
diphenylamine	1.424

**Table 1:** McGowan's characteristic volume values for solutes studied.

## CHAPTER 3

### 18-CROWN-6 AS A CLASS I ORGANIC MODIFIER IN MICELLAR ELECTROKINETIC CAPILLARY CHROMATOGRAPHY

#### 3.1 Introduction

In capillary electrophoresis (CE) method development, a variety of conditions can be adjusted to produce the desired selectivity and resolution.<sup>1</sup> Selectivity ( $\alpha$ ), a ratio of solute retention factors ( $k$ ) values (**Equation 1**), measures the ability of a micellar system to separate two or more analytes differing by one or more chemical groups.

$$\alpha = \frac{k_2}{k_1} \quad \text{Equation 1}$$

Where  $k$  is a ratio of the moles of solute in the pseudostationary phase (PSP) divided by the moles in the mobile phase and is typically expressed as in **Equation 2**.

$$k = \frac{[t_m - t_{eo}]}{t_{eo}[1 - t_m/t_{mc}]} \quad \text{Equation 2}$$

In **Equation 2**, the migration time of a non-retained solute, which marks electroosmotic force (EOF), is denoted  $t_{eo}$ . The migration time of the PSP, marked by a highly retained compound, is denoted  $t_{mc}$ . The solute's migration time is given by  $t_m$ . The degree of separation or resolution ( $R$ ) of two solutes is defined as in **Equation 3**.

$$R_s = \underbrace{\left(\frac{\sqrt{N}}{4}\right)}_{\text{efficiency}} \underbrace{\left(\frac{k_2+1}{k_2}\right) \left(\frac{1 - \frac{t_{eo}}{t_{mc}}}{1 + \left(\frac{t_{eo}}{t_{mc}}\right) k_1}\right)}_{\text{retention}} \underbrace{\left(\frac{\alpha-1}{\alpha}\right)}_{\text{selectivity}} \quad \text{Equation 3}$$

Class I and II organic modifiers are routinely used in sodium dodecyl sulfate (SDS) mediated micellar electrokinetic chromatography (MEKC) to tune selectivity and resolution.<sup>2-6</sup> Class II organic modifiers operate by altering the aqueous phase and are used more extensively in capillary electrophoresis (CE) than class I modifiers.<sup>1-10</sup> Widely used class II modifiers include acetonitrile, short chain ( $C \leq 4$ ) alcohols, tetrahydrofuran, urea, and glucose.<sup>3,9,10</sup> Class I modifiers target the pseudostationary phase (PSP) through direct interaction with micelles and are used at much lower concentrations than class II modifiers.<sup>1,2,6,8-10</sup> While not as popular in CE as class II modifiers, class I modifiers have seen increased use in MEKC and vesicle electrokinetic chromatography (VEKC) over the past decade.

### 3.1.1 Class I Modifiers

Class I modifiers employed in MEKC and VEKC include medium-to-long chain ( $C \leq 5$ ) alcohols and diols.<sup>2,3,6,9</sup> As an alternative to these class I modifiers, the use of 18-crown-6 (18C6; **Figure 1**) as a class I modifier in SDS MEKC was investigated using nitrotoluene and nitrophenol positional isomers as model compounds. Nitrotoluenes and nitrophenols are of intense environmental and forensic interest.<sup>11-13</sup> Both isomer series (which include *ortho*, *meta*, and *para* members; **Figure 2**) are well characterized<sup>12,14-18</sup>,

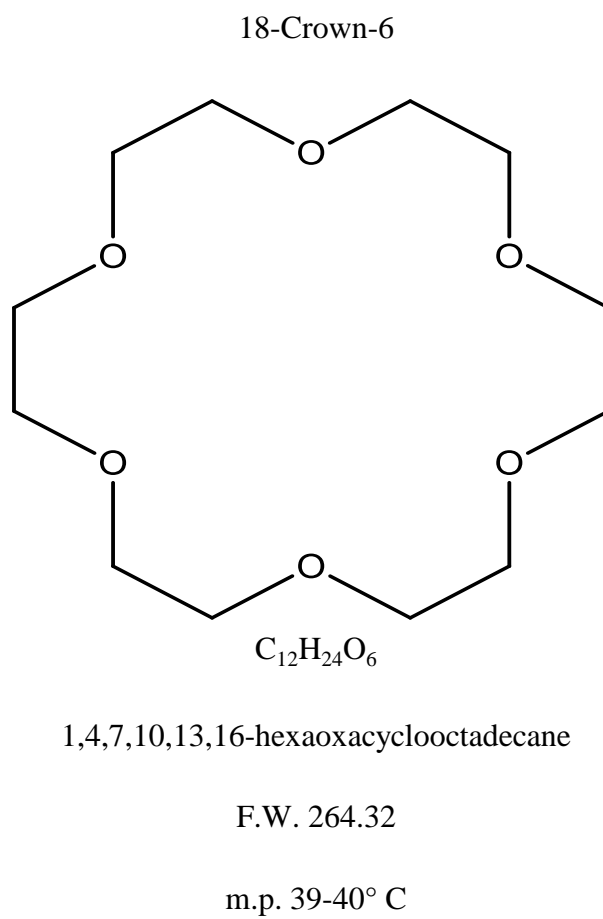
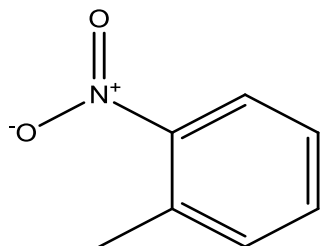


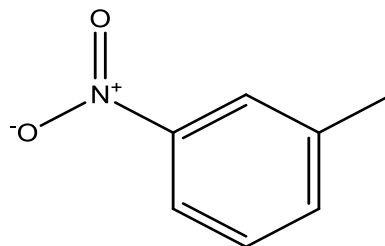
**Figure 1:** structure and select properties of 18C6

**nitrotoluene  
isomers**



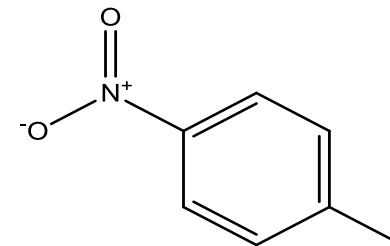
$C_7H_7NO_2$

**ortho**



$C_7H_7NO_2$

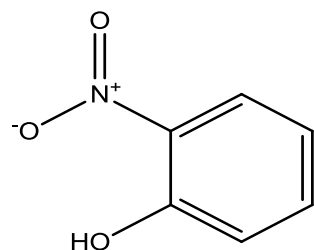
**meta**



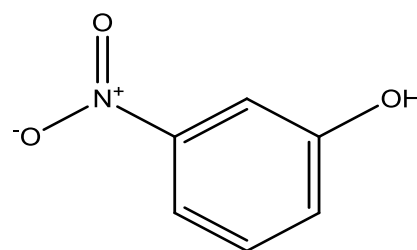
$C_7H_7NO_2$

**para**

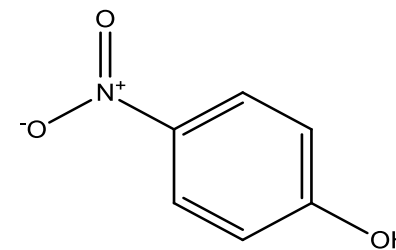
**nitrophenol  
isomers**



$C_6H_5NO_3$



$C_6H_5NO_3$



$C_6H_5NO_3$

**Figure 2:** Nitrotoluene and nitrophenol positional isomers model compounds

with the nitrotoluenes previously being used to examine class I and II modifiers in VEKC<sup>9</sup>.

Class I modifiers are characterized by their direct interactions with micelles, which can result in depression of the critical micelle concentration (CMC) and decreased micelle surface polarity.<sup>2, 6-8, 10</sup> Based on these criteria, 18C6 is a class I modifier. This macrocyclic polyether is well known for its ability to form host-guest complexes with various metal cations,  $\text{NH}_4^+$ , and primary amines.<sup>19</sup> Of particular interest to SDS MEKC is the formation of a 18C6- $\text{Na}^+$  complex and the effect of this complexation on the SDS PSP. 18C6 and  $\text{Na}^+$  form a 1:1 complex that is stable as a result of strong ion-dipole interactions ( $K_{\text{stab}} = 6.6 \text{ M}^{-1}$  at 25 °C).<sup>19-24</sup> When introduced to an aqueous solution of SDS, 18C6 sequesters  $\text{Na}^+$ , leading to an increase in  $\text{SO}_4^-$  head group repulsion and altered micelle interfacial electrostatic properties. These property changes have been linked to decreased micelle size, surface charge density, surface polarity, and CMC values.<sup>20-22, 25-33</sup>

Three features distinguish 18C6 from other class I modifiers in SDS MEKC: the shallow solubilization of 18C6 near the micelle surface, non-contact with other solubilizates (analytes), and this macrocycle's use in CE as an inclusion compound. In aqueous solutions, class I modifiers, which are generally small polar organic molecules, first adsorb at or near the micelle surface in the Stern layer.<sup>2, 7, 8, 10</sup> Penetration to greater micelle depths is governed by the ratio of polar (hydrophilic) to non-polar (hydrophobic) structures in the solubilizate.<sup>7, 8, 10</sup> Straight chain alcohol or diol class I modifiers "puncture" the micelle surface, with hydrophilic portions residing in the Stern layer and the chain penetrating to a depth dictated by its length.<sup>2, 3, 6-10, 34</sup> 18C6, via  $\text{Na}^+$

complexation, is localized to the external Stern layer with no penetration to lower Stern layers or the micelle core.<sup>20, 21, 25, 26, 28, 29, 33</sup> This complexation also effectively eliminates 18C6-analyte interactions, unlike alcohol or diol class I modifiers which are free to interact with analytes.<sup>2, 3</sup> 18C6 modifies the SDS PSP, and thus MEKC, through purely electrostatic interactions with the micelles.

Unlike other class I modifiers that have been used in CE, 18C6 and its chiral derivative, (+)-(18-crown-6)-tetracarboxylic acid (18C6H<sub>4</sub>), are used in CE for their host-guest abilities. 18C6 is often used for cation separations<sup>23, 35-38</sup>, while 18C6H<sub>4</sub> is extensively utilized as a chiral selector for primary amines, including amino acids<sup>39-43</sup>. The use of 18C6 or its derivatives in MEKC<sup>44, 45</sup> and microemulsion electrokinetic chromatography (MEEKC)<sup>46</sup> has been limited, with these macrocycles acting as secondary inclusion compounds to the PSP for the separation of cations or primary amines. The host-guest nature of 18C6 is far from a hindrance to the application of 18C6 as a class I modifier because its list of possible guests is quite exclusive. In addition, at the low concentrations at which class I modifiers are typically used<sup>2, 6, 9, 10</sup>, 18C6 could likely be used as a modifier in the SDS MEKC separation of primary amines, given the greater affinity 18C6 has for Na<sup>+</sup><sup>47-49</sup>. The work presented in this chapter is the first use of 18C6 as a class I modifier in PSP-modified CE and the first discussion of the effect of 18C6 on a PSP.



## 3.2 *Experimental*

### 3.2.1 *Instruments and Materials*

CE experiments in this report were done at 25°C and 25 kV using a Beckman Coulter P/ACE MDQ CE with DAD (Fullerton, CA). An unmodified silica capillary (75  $\mu\text{m}$  inner diameter, 60 cm total length, and 50 cm effective length) was purchased from Polymicro Technologies (Phoenix, AZ). SDS, 18C6, and buffer reagents were purchased from Sigma (St. Louis, MO). All aqueous solutions were made using water obtained from a Millipore NANOpure system (Bedford, MA).

Nitrotoluene and nitrophenol isomers were obtained either from Sigma (St. Louis, MO) or AccuStandard (New Haven, CT). Isomers stock solutions were made using 1:1 v/v mixtures of methanol and acetonitrile. The BGE was 10 mM, pH 8.5 sodium borate buffer with (or without) 18C6 and SDS, depending on the specific experiment being performed. For 18C6 modified SDS MEKC, a variety of 18C6 to SDS concentration ratios ( $[\text{18C6}]/[\text{SDS}]$ ) ranging from 0 to 1 were evaluated. Based on initial SDS MEKC experiments with each isomer series (to be described later), a single SDS concentration of 35 mM was selected.

### 3.2.2 *Determination of CMC*

The degree of SDS CMC depression over the selected range of  $[\text{18C6}]/[\text{SDS}]$  values was evaluated using a previously described CMC determining method<sup>50</sup> which

does not require a micelle-interacting marker. For a detailed discussion of this method, please see **APPENDIX A**. Method validation was done by determining the CMC of SDS in water at 25°C.

### *3.2.3 Determination of $k$ and $\alpha$*

Solute retention factors ( $k$ ) and separation selectivity ( $\alpha$ ) were calculated using **Equation 2** and **Equation 1**, respectively. Electroosmotic force (EOF) and micelle migration times ( $t_{eo}$  and  $t_{mc}$ , respectively) were determined using methanol ( $t_{eo}$ ) and Sudan III ( $t_{mc}$ ). Calculations were done using Excel software.

## ***3.3 Results and Discussion***

### *3.3.1 CMC observations*

The range of 18C6 concentrations utilized were within the typical range of use for class I modifiers<sup>2, 6, 9, 10</sup> and less than concentrations needed for 18C6 to display class II behavior (i.e. by altering the aqueous phase)<sup>21, 28</sup>. The calculated CMC of 8.3 ( $\pm$  0.1) mM for SDS was in excellent agreement with the accepted range of 7.9-8.4 mM at 25°C.<sup>1, 7, 10, 50, 51</sup> The CMC of SDS in the BGE was determined to be 4.5 ( $\pm$  0.1) mM, a value in-line with the known effect of electrolytes on a surfactant's CMC.<sup>1, 7, 8, 10, 50, 52</sup> At

low [18C6]/[SDS], the CMC of SDS decreased in a linear manner ( $y = -10.4 + 4.6x$ ,  $R^2 = 0.997$ ,  $n = 4$ ) with asymptotic-like behavior being observed for  $[18C6]/[SDS] \geq 0.5$ , as noted previously<sup>21, 26, 28, 53</sup> (**Figure 3**). The y-intercept for a plot of SDS CMC versus [18C6] was  $4.6 (\pm 0.1)$  mM, in good agreement with the experimentally determined CMC of SDS in the BGE. Though the BGE contained  $Na^+$ , bulk aqueous phase 18C6- $Na^+$  complexation did not limit the ability of 18C6 to modify the PSP. Counter-ion condensation caused free 18C6 and 18C6- $Na^+$  to engage/exchange with  $Na^+$  at the micelle surface rather than in the aqueous bulk phase<sup>28, 30, 52</sup>, which left the class I modifying abilities of 18C6 intact.

### 3.3.2 Nitrotoluene isomer series observations

Initial experiments of the nitrotoluene isomer series using 18C6 modified SDS MEKC revealed the subtle, yet easily apparent, effect of 18C6 on neutral polar analyte partitioning in SDS micellar solutions. The nitrotoluenes were neutral at the BGE pH of 8.5 and, as expected, co-migrated in capillary zone electrophoresis (CZE) at a migration time ( $t_m$ ) equal to  $t_{eo}$  in the SDS MEKC analysis these isomers. In SDS MEKC experiments, 35 mM SDS provided good resolution of nitrotoluene isomers, with a migration order of 2-nitrotoluene (2NT) < 4-nitrotoluene (4NT) < 3-nitrotoluene (3NT), as predicted by the octanol/water partition coefficients ( $\log P_{o/w}$ ) for these analytes (2NT, 2.30; 4NT, 2.42; 3NT, 2.45).<sup>18</sup> At  $[18C6]/[SDS] = 0$ , 2NT migrated ahead of the closely migrating, but fully resolved, peaks of 4NT and 3NT. By  $[18C6]/[SDS] = 0.20$ , 2NT and

### Effect of 18C6 on CMC of SDS

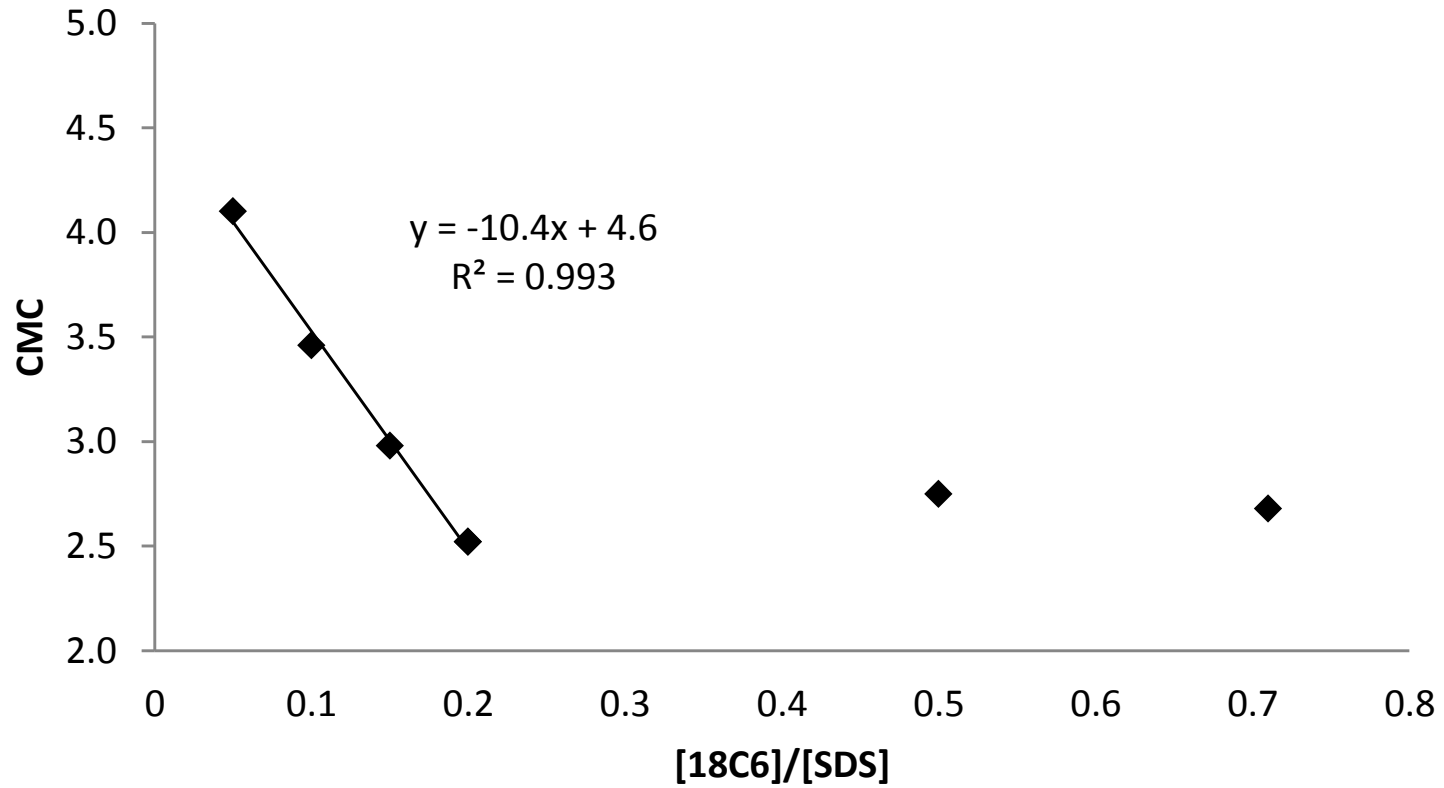


**Figure 3:** Effect of 18C6 concentration on the CMC of SDS.

4NT were paired peaks and 3NT was the trailing peak (see **Figure 4**). The isomer 3NT showed nearly no change in its retention factor ( $k$ ), while the  $k$  values decreased for 4NT and increased for 2NT. These changes are not due to 18C6 – nitrotoluene interactions, as the literature clearly indicates that there are no substantial interactions between 18C6 and nitrotoluenes in aqueous solutions.<sup>19,54</sup>

These shifts in retention are easily explained if nitrotoluene charge separation/local polarity ( $\Pi$ ) values are considered. The  $\Pi$  values decrease in going from 4NT (11.24 kcal/mol) to 3NT (11.07 kcal/mol) and 2NT (10.65 kcal/mol).<sup>18</sup> An overall retention increase of the most non-polar nitrotoluene, 2NT, is observed while a decrease in retention is seen for the most polar nitrotoluene, 4NT. This indicates the surface of the micelle is becoming less polar. Two previous studies<sup>31,55</sup>, which employed a single probe molecule, found that addition of 15C5 and 18C6 to aqueous SDS solutions resulted in a decrease of SDS interfacial polarity.

### 3.3.3 Nitrophenol isomer series observations

Unlike the nitrotoluene series, the nitrophenol isomers 2-nitrophenol (2NP), 3-nitrophenol (3NP), and 4-nitrophenol (4NP) were charged under the given experimental conditions, as predicted from their  $pK_a$  values (4NP, 6.90; 2NP, 6.92; 3NP, 8.10)<sup>15</sup> and confirmed by CZE. In the CZE analysis of a nitrophenol isomer mixture, the elution order followed the  $pK_a$  values from high to low (i.e. 3NP < 4NP < 2NP), with 2NP and 4NP migrating closely together (**Figure 5(a)**). The use of 25 mM 18C6 in CZE analysis

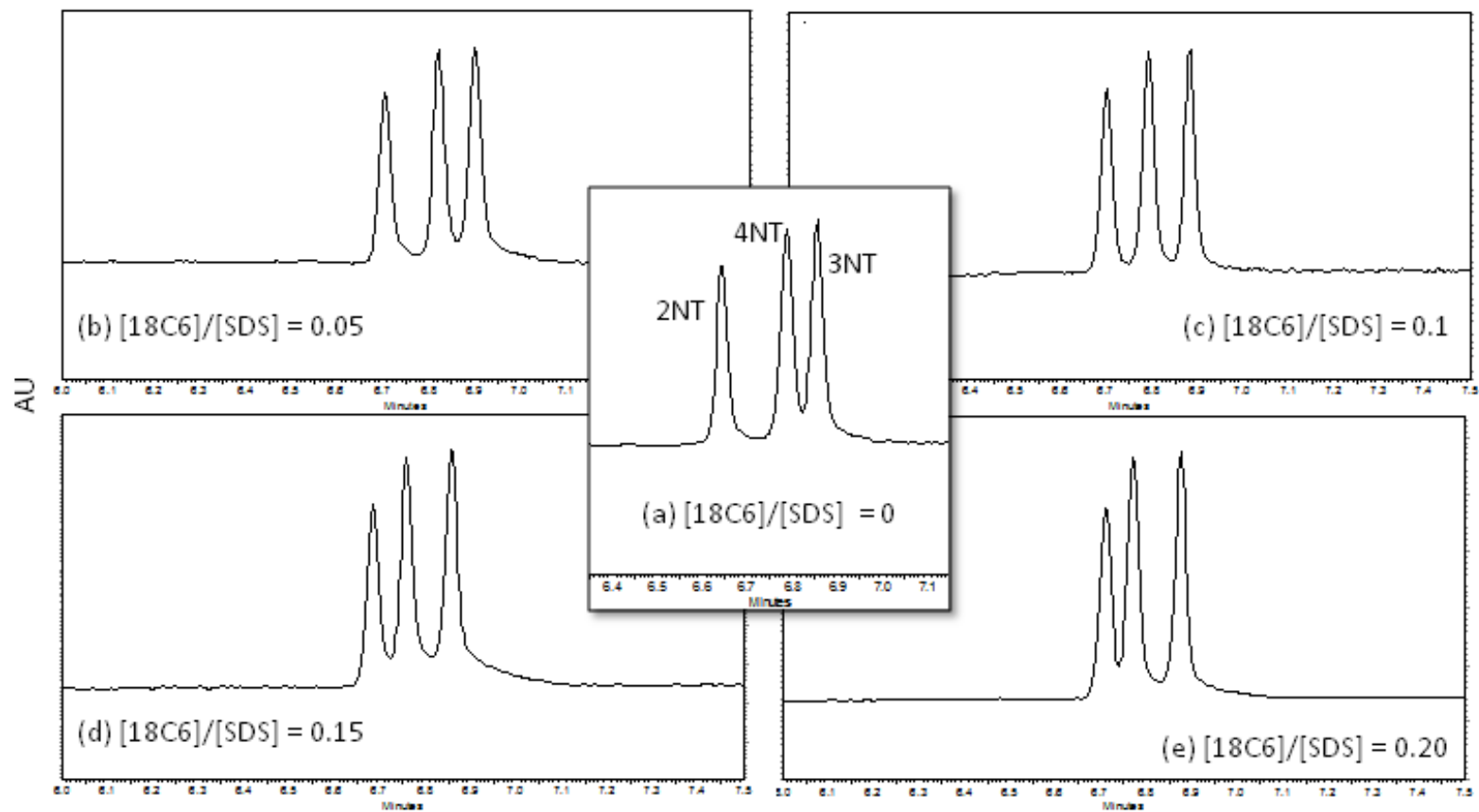


**Figure 4:** Electropherograms obtained for nitrotoluenes at various [18C6]/[SDS]. The migration order for each separation was the same as noted in (a).

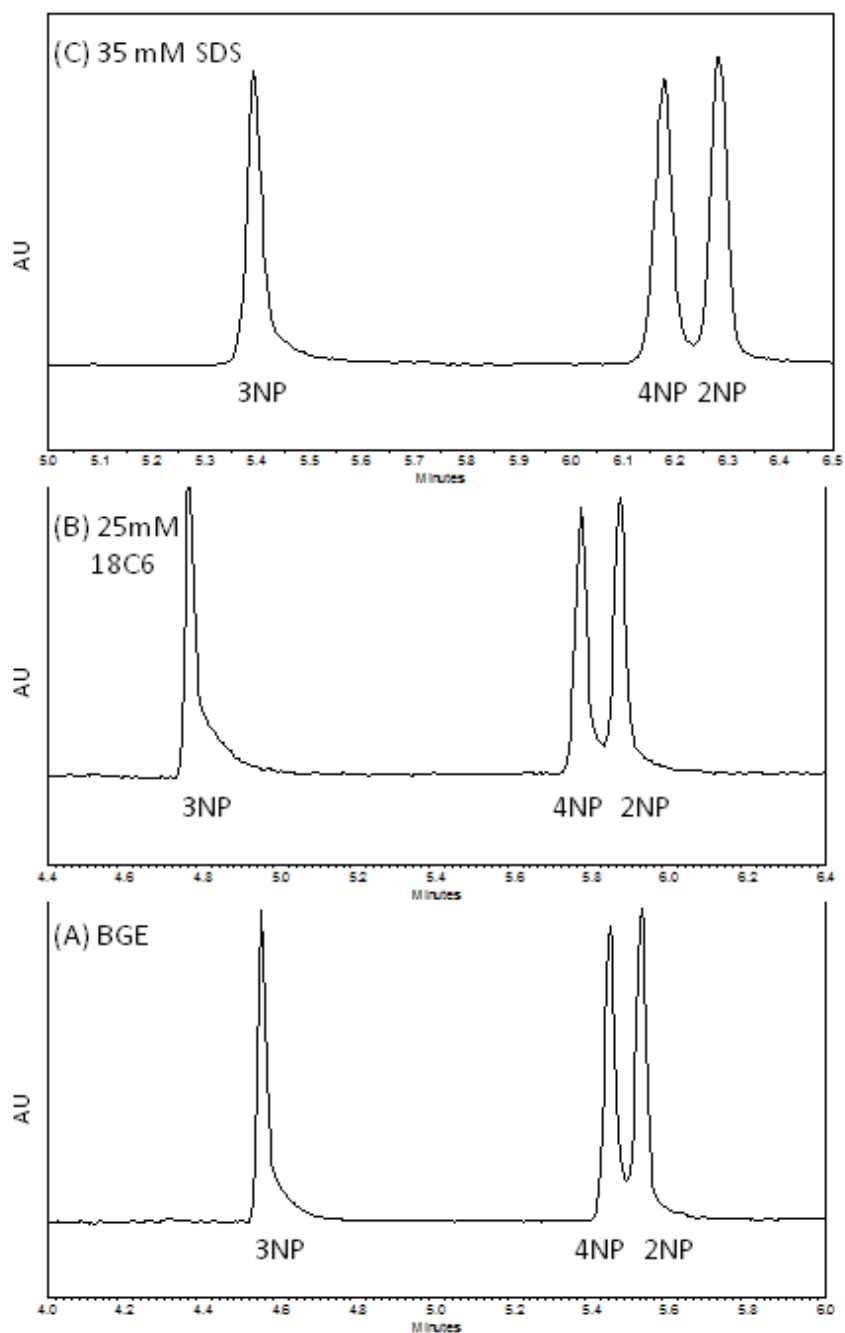


**Figure 5:** Electropherograms obtained from nitrophenol (NP) experiments. **(a)** CZE analysis of a NP isomer mixture with migration following  $pK_a$  values **(b)** the use of 25 mM 18C6 in CZE analysis of NP and **(c)** the use of 35 mM SDS in MEKC analysis of NP isomer mixture.

of nitrophenols yielded a slight improvement in resolution for 2NP and 4NP peaks along with increased  $t_m$  for each isomer (**Figure 5(b)**). This slight improvement in resolution is due to 18C6 modification of EOF through association with BGE sodium ions<sup>56</sup>, rather than an interaction between 18C6 and nitrophenol anions<sup>19</sup>. Indeed, SDS MEKC analysis of a nitrophenol isomer mixture using 35 mM SDS gave approximately the same improvements to resolution and shifts in  $t_m$  as 25 mM 18C6 alone (**Figure 6(c)**).

Over the [18C6]/[SDS] range of 0-0.20 used in analysis of nitrotoluenes, little to no change was observed in retention or resolution for nitrophenols. This is perhaps not surprising given the high degree of repulsion between anions and anionic micelles. As such, the [18C6]/[SDS] was extended for determination of  $k$  for all isomers and for isomer mixture analysis. **Figure 6** shows the changes in isomer retention with [18C6]/[SDS] (also see  $k$  values in **Table 1**).

### *3.3.4 $k$ and $\alpha$ observations for isomers studied*

Retention factors ( $k$ ) for all isomers were calculated using (**Equation 2**), which is an appropriate course when comparing  $k$  values in MEKC.<sup>57</sup> Over this extended [18C6]/[SDS] range, nitrotoluenes exhibited the same shifts in retention, as discussed previously. The most non-polar nitrotoluene (2NT) saw approximately a 3% increase in  $k$  over this range, while retention for the most polar nitrotoluene (4NT) decreased by nearly 7.5%. The isomer with intermediate polarity (3NT) gave virtually no change in  $k$ , decreasing by only 0.2%. As seen in initial nitrotoluene 18C6 modified SDS MEKC



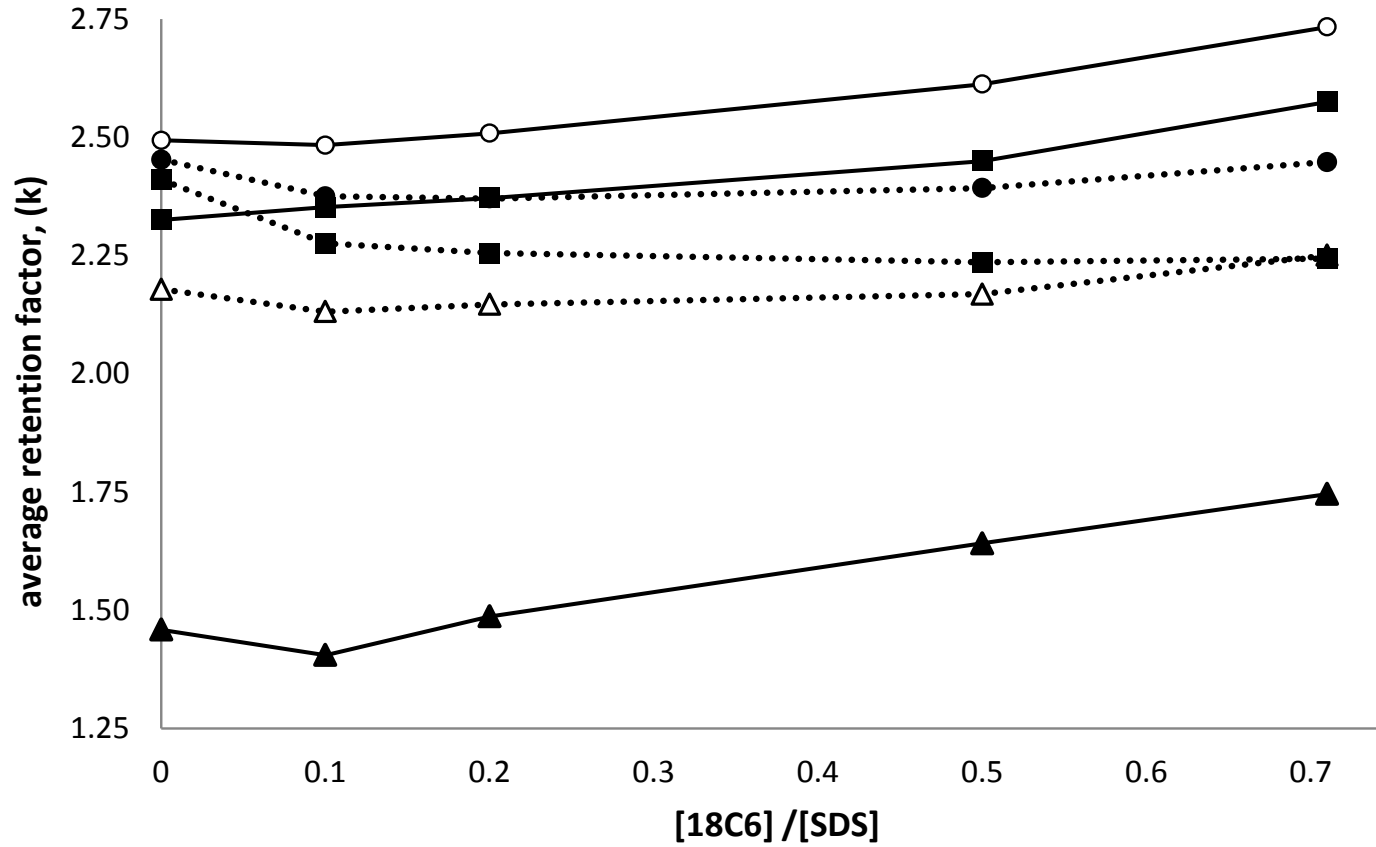


**Figure 6:** Observed trends in retention factor ( $k$ ) for various values of  $[18C6]/[SDS]$ . Symbols: ( $\cdot\Delta\cdot$ ) 2NT; ( $\cdot\blacksquare\cdot$ ) 4NT; ( $\cdot\bullet\cdot$ ) 3NT; ( $\text{---}\blacktriangle\text{---}$ ) 3NP; ( $\text{---}\blacksquare\text{---}$ ) 4NP; ( $\text{---}\circ\text{---}$ ) 2NP

[18C6]/[SDS]	average retention factor (k)					
	2NT	4NT	3NT	3NP	4NP	2NP
0	2.18 [.01]	2.41 [.07]	2.45 [.01]	1.46 [.01]	2.33 [.03]	2.49 [.07]
0.1	2.13 [.01]	2.28 [.01]	2.37 [.01]	1.40 [.01]	2.35 [.01]	2.48 [.02]
0.2	2.15 [.01]	2.25 [.01]	2.37 [.01]	1.49 [.01]	2.37 [.03]	2.51 [.03]
0.5	2.17 [.04]	2.24 [.04]	2.39 [.01]	1.64 [.01]	2.45 [.01]	2.61 [.02]
0.7	2.25 [.01]	2.24 [.04]	2.45 [.01]	1.75 [.01]	2.57 [.02]	2.73 [.02]

**Table 1:** Change in average retention factors (k) with increasing [18C6]/[SDS]. Beneath each k value is the calculated standard deviation in brackets.

experiments, 2NT and 4NT began to co-migrate with increasing [18C6]/[SDS]. This path to co-migration can be seen in **Figure 6**. At the highest [18C6]/[SDS] value, which was also the value giving the best resolution of isomers, 2NT and 4NT co-migrated and gave a single peak, as seen in **Figure 7(b)**.

In addition to lowering the surface polarity in SDS micelles, 18C6 depressed surface charge density, a phenomenon impacting nitrophenol anion retention. Over the extended [18C6]/[SDS] range, retention for all nitrophenols increased (**Figure 6**). Isomers 2NP and 4NP had a similar increase in  $k$  values at nearly 9% and 10%, respectively. The largest increase in retention was seen for 3NP at over 16% (**Table 1**). These shifts in nitrophenol retention were likely due to the same forces that influence acid strength. Both 2NP and 4NP are able to delocalize a negative charge due to hydroxyl group deprotonation over their aromatic rings, providing greater anion stability which results in lower and nearly identical  $pK_a$  values relative to 3NP.<sup>15, 16</sup> Such delocalization is not an option for 3NP due to structure induced resonance limitations.<sup>15, 16</sup> 3NP likely experienced a greater repulsion to SDS micelles compared to 2NP and 4NP; thus a decrease in micelle surface charge density had a greater impact on 3NP. Isomers 2NP and 4NP, with similar  $pK_a$  values, displayed nearly identical increases in retention.

Equivalent trends in phenolic anion retention through surface charge density has been seen through the use of anionic-zwitterionic mixed micelles.<sup>58</sup> Under experimental conditions used in this study, nitrotoluene and nitrophenols had quite close  $k$  values, with the exception of 3NP. **Figure 7** demonstrates that while 35 mM SDS may have been suitable for good resolution of each isomer series, it provided poor peak separation for

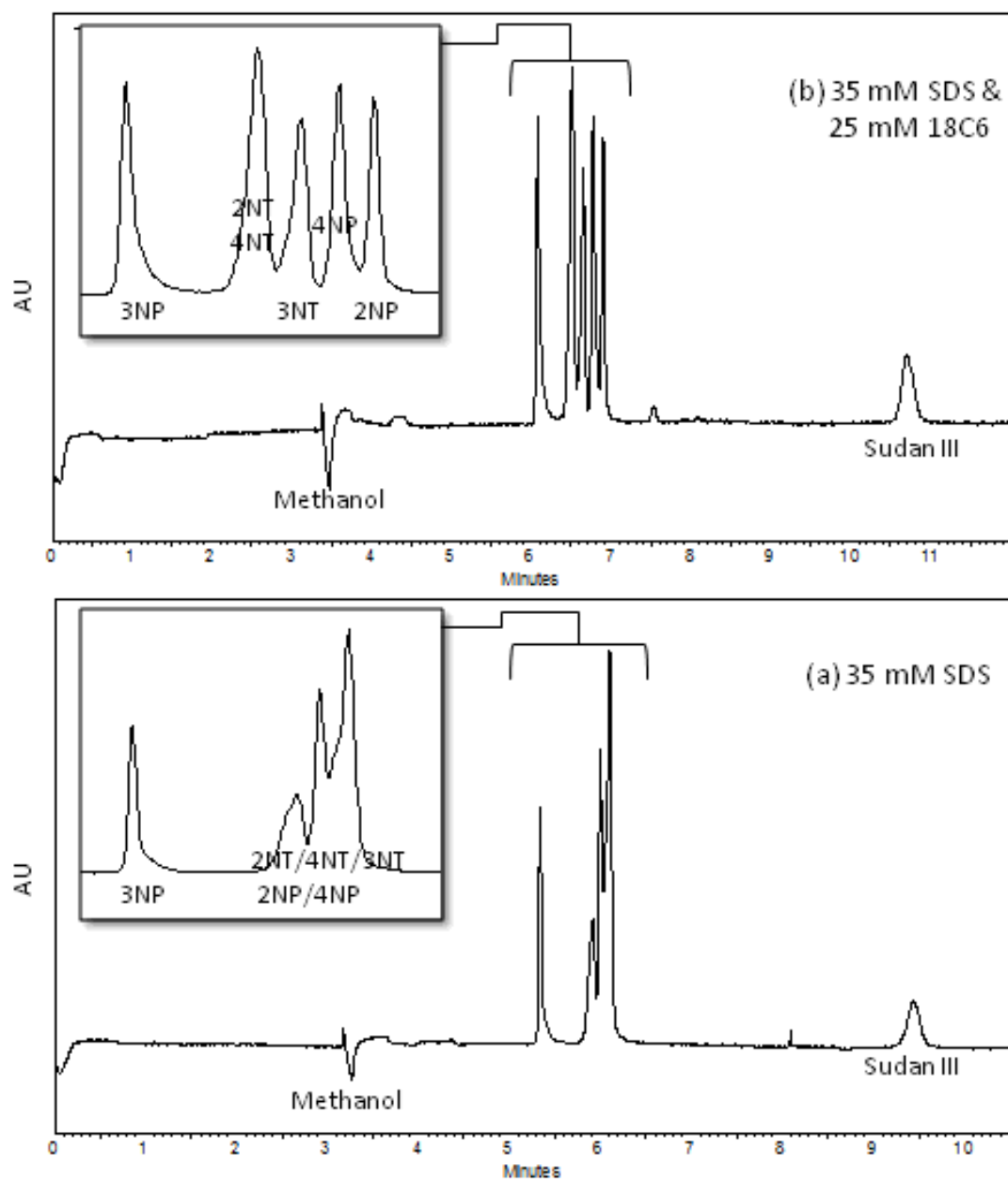


**Figure 7:** Electropherograms obtained for the mixture analysis of nitrotoluene and nitrophenol isomers in the presence of (a) SDS and (b) 18C6 modified SDS MEKC.

the analysis of a nitrotoluene–nitrophenol mixture (**Figure 7(a)**). Over the [18C6]/[SDS] range of 0 to 1, the best resolution was achieved by the addition of 25 mM 18C6, giving [18C6]/[SDS]  $\approx$  0.70. By depressing both SDS micelle surface polarity and charge density, 18C6 dramatically improved the resulting separation (see **Figure 7(b)**). It should be noted that in line with observations made for other class I modifiers in CE<sup>6,9</sup>, 18C6 was found to have virtually no impact on the ratio  $t_{eo}/t_{mc}$ , which averaged  $0.33 \pm 0.01$  for all experiments over the [18C6]/[SDS] range 0 to 1.

### ***3.4 Conclusion and Future Work***

The use of 18C6 as a class I organic modifier for SDS MEKC was probed using positional isomer series, one neutral (nitrotoluenes) and one anionic (nitrophenols). The macrocycle 18C6 allowed for the modification of SDS micelle surface polarity and charge density for easy manipulation of analyte retention. As the nitrotoluene and nitrophenol data presented here indicates, both neutral polar and anion organic analyte retention can be tuned by this approach for improved separations.

The promising results shown here for 18C6 prompted study into the modifying abilities of 15-crown-5 and 12-crown-4. An in-depth study of all three crown ethers is presented in CHAPTER 4, using the solvation parameter (SP) model and linear solvation energy relationships to robustly characterize said abilities. Future work should include a greater application of crown ethers as class I modifiers in MEKC, MEEKC and VEKC. The unique way in which crown ethers influence analyte partitioning would allow for subtle phase interactions to be examined in greater detail. As surfactants are popular mimic systems for cells and soils<sup>7,8,10</sup>, crown modified PSP CE is a tool researchers

could use to probe electrostatics in cell membrane interactions. Crown ethers effects on ion transport across cell membranes is well known<sup>59-65</sup>, but the influence of their cation binding ability on the partitioning of organic molecules into cells is relatively unexplored area<sup>59, 66, 67</sup>.

### 3.5 References

1. Camilleri, P., *Capillary Electrophoresis*. 2 ed.; CRC Press: Boca Raton, 1997.
2. Allen, D. J.; Wall, W. E.; Denson, K. D.; Smith, J. T., *Electrophoresis* **1999**, *20* (1), 100-10.
3. Katsuta, S.; Saitoh, K., *J. Chromatogr., A* **1997**, *780*, 165-178.
4. Seals, T., *Chromatographia* **2000**, *51*, 669-680.
5. Seifar, R.; Kraak, J.; Kok, W., *Anal. Chem.* **1997**, *69*, 2772-2778.
6. Wall, W. E.; Allen, D. J.; Denson, K. D.; Love, G. I.; Smith, J. T., *Electrophoresis* **1999**, *20* (12), 2390-9.
7. Elworthy, P.; Florence, A.; Macfarlane, C., *Solubilization by Surface-Active Agents*. Chapman and Hall LTD: London, 1968.
8. Zana, R., *Dynamics of Surfactant Self-Assemblies*. Taylor & Francis: Boca Raton, 2005; Vol. 125.
9. Pascoe, R.; Foley, J. P., *Electrophoresis* **2002**, *23* (11), 1618-27.
10. Rosen, M., *Surfactants and Interfacial Phenomena*. 2 ed.; John Wiley and Sons: New York, 1988.
11. Cledera-Castro, M.; Santos-Montes, A.; Izquierdo-Hornillos, R.; Gonzalo-Lumbreras, R., *J. Sep. Sci.* **2007**, *30* (5), 699-707.
12. Isayev, O.; Rasulev, B.; Gorb, L.; Leszczynski, J., *Mol. Divers.* **2006**, *10* (2), 233-245.
13. Zemann, A.; Volgger, D., *Anal. Chem.* **1997**, *69*, 3243-3250.
14. Chen, P.; Wu, C., *J. Mol. Struct.* **1995**, *357*, 87-95.

15. Bouchard, G.; Carrupt, P.-A.; Testa, B.; Gobry, V.; Girault, H., *Chem. Eur. J.* **2002**, *8* (15), 3478-3484.
16. Huang, X.; Kong, L.; Li, X.; Zheng, C.; Zou, H., *J. Mol. Recognit.* **2003**, *16*, 406-411.
17. Ma, Y.; Gross, K. C.; Hollingsworth, C. A.; Seybold, P. G.; Murray, J. S., *J. Mol. Model.* **2004**, *10*, 235-239.
18. Murray, J.; Brinck, T.; Politzer, P., *J. Phys. Chem.* **1993**, *97*, 13807-13809.
19. Izatt, R.; Pawlak, K.; Jerald, S., *Chem. Rev.* **1995**, *95*, 2529-2586.
20. Bakshi, M.; Crisantino, R.; Lisi, R.; Milioto, S., *Langmuir* **1994**, *10*, 423-431.
21. Caponetti, E.; Martino, D.; Floriano, M.; Triolo, R.; Wignall, G., *Langmuir* **1995**, *11*, 2464-2470.
22. Evans, D.; Sen, R.; Warr, G., *J. Phys. Chem.* **1986**, *90*, 5500-5502.
23. Manège, L.; Takayanagi, T.; Oshima, M.; Motomizu, S., *Analyst* **2000**, *125*, 1928-1932.
24. Muzikar, M.; Havel, J.; Macka, M., *Electrophoresis* **2002**, *23*, 1796-1802.
25. Baglioni, P.; Kevan, L., *J. Chem. Soc. Faraday Trans.* **1988**, *84*, 467-472.
26. Caponetti, E.; Chillura-Martino, D.; Pedone, L., *Langmuir* **2004**, *20*, 3854-3862.
27. Chillura-Martino, D.; Caponetti, E.; Pedone, L., *J. Appl. Cryst.* **2003**, *36*, 562-567.
28. Crisantino, R.; De Lisi, R.; Milioto, S.; Pellerito, A., *Langmuir* **1996**, *12*, 890-901.
29. Evans, D.; Evans, J.; Radha, S.; Warr, G., *J. Phys. Chem.* **1988**, *92*, 784-790.
30. Loginovaa, L.; Samokhina, L.; Mchedlov-Petrosyan, N.; Alekseevab, V.; Savvina, L., *Colloids Surf. A* **2001**, *193*, 207-219.



31. Myassoedova, T.; Grand, D.; Hauteclouque, S., *J. Photochem. Photobiol., A* **1992**, *64*, 159-169.
32. Stilbs, P., *J. Colloid Interface Sci.* **1982**, *87*, 385-394
33. Stilbs, P., *J. Colloid Interface Sci.* **1983**, *94*, 463-469
34. Caponetti, E.; Martino, D.; Floriano, M.; Triolo, R., *Langmuir* **1997**, *13*, 3277-3283.
35. Hopper, K.; LeClair, H.; McCord, B., *Talanta* **2005**, *67*, 304–312.
36. Okada, T., *J. Chromatogr., A* **1999**, *834*, 73-87
37. Padarauskas, A.; Olauskaite, V.; Paliulionyte, V.; Pranailyte, B., *Chromatographia* **2000**, *52*, 133-136.
38. Wang, J.; Pumera, M.; Collins, G.; Frantisek, O.; Jelínek, I., *Analyst* **2002**, *127*, 719–723.
39. Chen, Z.; Uchiyama, K.; Hobo, T., *Electrophoresis* **2001**, *22*, 2136–2142.
40. Ha, P. T.; Hoogmartens, J.; Van Schepdael, A., *J. Pharm. Biomed. Anal.* **2006**, *41* (1), 1-11.
41. Kahle, K. A.; Foley, J. P., *Electrophoresis* **2007**, *28* (15), 2503-26.
42. Kuhn, R., *Electrophoresis* **1999**, *20* (13), 2605-13.
43. Vespalec, R.; Bocek, P., *Chem. Rev.* **2000**, *100*, 3715-3753.
44. Liu, G.; Chen, J.; Ma, Y., *J. Chromatogr., B: Anal. Technol. Biomed. Life Sci.* **2004**, *805* (2), 281-8.
45. Vaidya, B.; Porter, M.; Utterback, M.; Bartsch, R., *Anal. Chem.* **1997**, *69*, 2688-2693.

46. Cook, H. A.; Klampfl, C. W.; Buchberger, W., *J. Chromatogr., A* **2005**, *1085* (1), 164-9.
47. Cho, S.; Jung, H.; Chung, D., *Electrophoresis* **2000**, *21*, 3618-3624.
48. Cho, S.; Lee, K.; Kim, Y.; Jang, J.; Chung, D., *Electrophoresis* **2002**, *23*, 972-977.
49. Frensdorff, H., *J. Am. Chem. Soc.* **1970**, *93*, 600-606.
50. Cifuentes, A.; Bernal, J.; Diez-Masa, J., *Anal. Chem.* **1997**, *69*, 4271-4274.
51. Rahman, A.; Brown, C., *J. Appl. Polym. Sci.* **1982**, *28*, 1331-1334.
52. Hsiao, C. C.; Wang, T. Y.; Tsao, H. K., *J. Chem. Phys.* **2005**, *122* (14), 144702.
53. Seno, M.; Namba, T.; Kise, H., *Bull. Chem. Soc. Jpn.* **1981**, *54*, 2841-2842.
54. Izatt, R. M.; Bradshaw, J. S.; Pawlak, K.; Bruening, R. L.; Tarbet, B. J., *Chem. Rev.* **1992**, *92*, 1261-1354.
55. Baglioni, P.; Kevan, L., *J. Chem. Soc. Faraday Trans.* **1988**, *84*, 467-472.
56. Lamb, J. D.; Edwards, B. R.; Smith, R. G.; Garrick, R., *Talanta* **1995**, *42*, 109-117.
57. Otsuka, K.; Terabe, S., pH, Effect on MEKC separation. In *Encyclopedia of Chromatography* Cazes, J., Ed. Marcel Dekker, Inc.: New York, 2001; pp 604-606.
58. Monton, M. R.; Otsuka, K.; Terabe, S., *J. Chromatogr., A* **2003**, *985* (1-2), 435-445.
59. Boojar, M.; Goodarzi, F., *Clin. Chim. Acta* **2006**, *364*, 321-327.
60. Izatt, R.; Bruening, R.; Clark, G.; Lamb, J.; Christensen, J., *J. Membr. Sci.* **1986**, *28*, 77-86.

61. Arenaz, P.; Bitticks, L.; Pannell, K.; Garcia, S., *Mutagenesis* **1989**, *4*, 437-438.
62. Arenaz, P.; Bitticks, L.; Pannell, K.; Garcia, S., *Mutat. Res.* **1992**, *280*, 109-115.
63. He, G.; Kurita, M.; Ishii, I.; Wada, F.; Matsuda, T., *J. Membr. Sci.* **1992**, *69*, 61-74.
64. Kudo, Y.; Takeda, Y.; Matsuda, H., *J. Electroanal. Chem.* **1995**, *396*, 333-338.
65. Christensen, J.; Eatough, D.; Izatt, R., *Chem. Rev.* **1974**, *74* (3), 351-384.
66. Darwish, I.; Uchegbu, I., *Int. J. Pharm.* **1997**, *159*, 207-213.
67. Muzzalupo, R.; Nicoletta, F.; Trombino, S.; Cassano, R.; Iemma, F.; Picci, N., *Colloids Surf., B* **2007**, *58*, 197-202.
68. Landers, J., *Handbook of Capillary Electrophoresis*. CRC Press: Boca Raton, 1993.
69. Lin, C. E., *J. Chromatogr. A* **2004**, *1037* (1-2), 467-78.
70. Lu, Y.; Stellwagen, E.; Stellwagen, N., *Anal Biochem* **2004**, *332*, 191-192.
71. Nesmerak, K.; Nemcova, I., *Anal. Lett.* **2006**, *39*, 1023-1040.
72. Coury, L., *Curr. Sep.* **1999**, *18*, 91-96.
73. Evans, H., *J. Chem. Soc.* **1956**, 579 - 586.

## **APPENDIX B**

### **Current titration method for the determination of CMC**

In a capillary electrophoresis (CE), the magnitude of the current observed obeys Ohm's Law<sup>50, 68-71</sup>, as given in **Equation 1**.

$$V=IR \quad \text{Equation 1}$$

The term V is the applied voltage, I is the measured current, and R is the resistance of the solution between the inlet and outlet electrodes. The reciprocal of R, conductance, is given by **Equation 2**.<sup>70, 72</sup>

$$\frac{1}{R} = \kappa \frac{\pi r^2}{L_t} \quad \text{Equation 2}$$

Conductivity is denoted by  $\kappa$ , the total length of the capillary is given by  $L_t$ , and r is the radius of the capillary. Combining **Equations 1** and **2** gives **Equation 3**.

$$I = \kappa \frac{V\pi r^2}{l} \quad \text{Equation 3}$$

In CE,  $V/l$  denotes electric field strength<sup>1, 68</sup>, E (V/cm), allowing **Equation 3** to be written as **Equation 3a**.

$$I = \kappa E \pi r^2 \quad \text{Equation 3a}$$

Molar conductivity,  $\Lambda$ , is the solution conductivity ( $\kappa$ ) normalized by the total ionic concentration (C)<sup>72</sup> and is given by **Equation 4**.

$$\Lambda = \frac{\kappa}{C} \quad \text{Equation 4}$$

Substituting **Equation 4** into **Equation 3a** gives **Equation 5**.

$$I = E \Lambda \pi r^2 C \quad \text{Equation 5}$$

For an SDS solution of concentration [SDS], **Equation 5** can be written as **Equation 5a**.

$$I_{\text{SDS soln}} = E\Lambda_{\text{SDS soln}}\pi r^2[\text{SDS}] \quad \text{Equation 5a}$$

Considering **Equation 4**, the molar conductivity of a SDS solution,  $\Lambda_{\text{SDS soln}}$ , can be written as **Equation 6**.

$$\Lambda_{\text{SDS soln}} = \frac{\kappa_{\text{SDS solution}}}{[\text{SDS}]} \quad \text{Equation 6}$$

The conductivity of the SDS solution,  $\kappa_{\text{SDS}}$ , is equal to the sum of conductivity values of relevant species in solution<sup>50, 73</sup>, as illustrated by **Equation 7**.

$$\kappa_{\text{SDS soln}} = \kappa_{\text{monomer}} + \kappa_{\text{Na}^+} + \kappa_{\text{micelle}} \quad \text{Equation 7}$$

Thus, **Equation 6** can be written as **Equation 6a**.

$$\Lambda_{\text{SDS soln}} = \frac{\kappa_{\text{monomer}}}{[\text{SDS}]} + \frac{\kappa_{\text{Na}^+}}{[\text{SDS}]} + \frac{\kappa_{\text{micelle}}}{[\text{SDS}]} \quad \text{Equation 6a}$$

Inserting **Equation 6a** into **Equation 5a** produces the following expression for  $I_{\text{SDS soln}}$  (**Equation 5b**).

$$I_{\text{SDS soln}} = E \left( \frac{\kappa_{\text{monomer}}}{[\text{SDS}]} + \frac{\kappa_{\text{Na}^+}}{[\text{SDS}]} + \frac{\kappa_{\text{micelle}}}{[\text{SDS}]} \right) \pi r^2 [\text{SDS}] \quad \text{Equation 5b}$$

At [SDS] below the critical micelle concentration (CMC), the contribution of the term  $\frac{\kappa_{\text{micelle}}}{[\text{SDS}]}$  to  $I_{\text{SDS soln}}$  is very small<sup>50, 73</sup> and **Equation 5b** can be written as **Equation 5c**.

$$I_{\text{SDS solution}} = E \left( \frac{\kappa_{\text{monomer}}}{[\text{SDS}]} + \frac{\kappa_{\text{Na}^+}}{[\text{SDS}]} \right) \pi r^2 [\text{SDS}] = I_{\text{pre-CMC}} \quad \text{Equation 5c}$$

Alternatively, above the CMC, the contribution of  $\left(\frac{\kappa_{\text{monomer}}}{[\text{SDS}]} + \frac{\kappa_{\text{Na}^+}}{[\text{SDS}]}\right)$  is very small<sup>50, 73</sup>

and  $I_{\text{SDS soln}}$  can be written as **Equation 5d**.

$$I_{\text{SDS soln}} = E \left( \frac{\kappa_{\text{micelle}}}{[\text{SDS}]} \right) \pi r^2 [\text{SDS}] = I_{\text{post-CMC}} \quad \text{Equation 5d}$$

In practice, plotting  $I_{\text{SDS soln}}$  vs.  $[\text{SDS}]$  reveals a sharply increasing slope up to the CMC and a “slower” increasing slope after the CMC due to changes in conductivity with  $[\text{SDS}]$ . The conductivity of a SDS solution pre-CMC increases over the  $[\text{SDS}]_{<\text{CMC}}$  range yet decreases over the range  $[\text{SDS}]_{>\text{CMC}}$  such that the slope of  $I_{\text{pre-cmc}}$  vs.  $[\text{SDS}]_{<\text{CMC}}$  is greater than  $I_{\text{post-CMC}}$  vs.  $[\text{SDS}]_{>\text{CMC}}$ . The ordered structure of the anionic micelle, where approximately half of the surfactants counterions (e.g.  $\text{Na}^+$ ) are localized to the Stern layer and the other half distributed in the Gouy-Chapman region, translates into an increased resistance to migration by the micelle explaining the conductivity decrease for SDS solutions above the CMC.<sup>50, 71, 73</sup>

Conductivity has been utilized for nearly 100 years to study surfactant solution behavior<sup>7, 10, 73</sup>, with simple  $[\text{surfactant}]$  vs.  $\kappa$  or  $I$  plots readily revealing the monomer-to-micelle transition region.<sup>50</sup> This region is called, somewhat erroneously, *the CMC*.<sup>7, 8, 10, 73</sup> As detailed above, two linear curves of different slopes are easily seen in  $[\text{surfactant}]$  vs.  $\kappa$  or  $I$  plots when the  $[\text{surfactant}]$  range encompassing several points above and below the CMC. To determine the CMC, the linear trend line equations are determined for both curves. The intersection of these two lines gives the CMC.

## CHAPTER 4

### CHARACTERIZATION OF CROWN ETHERS AS CLASS I ORGANIC MODIFIERS USING MICELLAR ELECTROKINETIC CHROMATOGRAPHY

#### 4.1 Introduction

Since its introduction in 1984, micellar electrokinetic chromatography (MEKC) has emerged as a powerful separation technique. Conceived to enable the electrophoretic separation of neutral analytes by using surfactants as a pseudostationary phase (PSP)<sup>1,2</sup>, MEKC is routinely applied to the analysis of neutral, ionic and mixed samples.<sup>3-6</sup> To improve resolution in MEKC, three separation parameters are routinely adjusted: efficiency, retention and selectivity.<sup>3,4,7,8</sup> Resolution ( $R_s$ ) in MEKC is defined as

$$R_s = \underbrace{\left(\frac{\sqrt{N}}{4}\right)}_{\text{efficiency}} \underbrace{\left(\frac{k_2+1}{k_2}\right) \left(\frac{1 - \frac{t_{eo}}{t_{mc}}}{1 + \left(\frac{t_{eo}}{t_{mc}}\right) k_1}\right)}_{\text{retention}} \underbrace{\left(\frac{\alpha-1}{\alpha}\right)}_{\text{selectivity}} \quad \text{Equation 1}$$

where  $N$  is the average plate number and  $k$  is the retention factor,  $k_1$  of the first migrating peak and  $k_2$  of the later, neighboring peak. (**Equation 2**). The migration time of a non-retained solute, which marks electroosmotic force (EOF), is denoted by the term  $t_{eo}$  while  $t_{mc}$  is the migration time of the PSP, as marked by a highly retained compound.

Selectivity, a ratio of  $k$  values, is represented by  $\alpha$  and measures the ability of a micellar system to separate two or more analytes differing by one or more chemical groups.



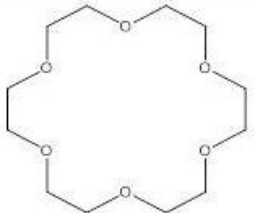
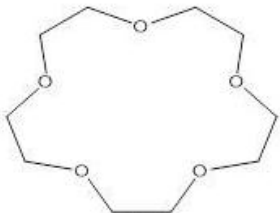
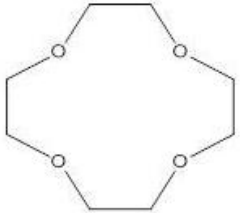
$$k = \frac{[t_m - t_{eo}]}{t_{eo}[1 - t_m/t_{mc}]} \quad \text{Equation 2}$$

In **Equation 2**,  $t_m$  is the migration time of the analyte.

Class I and II organic modifiers are often used in MEKC to adjust resolution.<sup>7-11</sup> Class I modifiers affect resolution through direct interaction with micelles while class II organic modifiers alter the aqueous phase.<sup>3, 7-15</sup> Class I modifiers employed in MEKC include medium-to-long chain ( $C \leq 5$ ) alcohols and diols.<sup>7-9, 14</sup> A new class I modifier, the macrocyclic polyether (MP) 18-crown-6 (18C6), was introduced in **CHAPTER 3**. The intriguing results seen with 18C6 modified sodium dodecyl sulfate (SDS) MEKC prompted the further studies of this MP in addition to 15-crown-5 (15C5) and 12-crown-4 (12C4), with the characterization of these MPs by MEKC being presented in this chapter.

#### 4.1.1 Macrocyclic polyethers

Macrocyclic polyethers (MPs) are well known for their ability to form host-guest complexes with various cations, usually metals.<sup>16, 17</sup> Of particular interest to SDS MEKC are the formation of MP-  $\text{Na}^+$  complexes and the effect of complexation on the SDS PSP. Factors affecting MP-cation complexation include: (1) relative sizes of cation and macrocyclic cavity, (2) steric hindrance in the ring and (3) solvent identity and extent of solvation of both the cation and MP.<sup>16-18</sup> **Table 1** provides the structure of the three MPs that were studied, along with the diameter of MP cavities and common target cations. Almost exclusively, the MPs 18C6, 15C5 and 12C4 form 1:1 complexes with  $\text{Na}^+$  of

Crown ethers	Cavity diameter (Å)	Cation	Ionic Diameter (Å)
 $C_{12}H_{24}O_6$	2.6 – 3.2	$Cs^+$ $NH_4^+$ $Tl^+$ $Rb^+$	3.34 2.84 2.98 2.96
 $C_{10}H_{20}O_5$	1.7 – 2.2	$Ba^{2+}$ $K^+$ $Ag^+$ $Pb^{2+}$	2.70 2.66 2.52 2.36
 $C_8H_{16}O_4$	1.2 – 1.4	$Na^+$ $Li^+$	1.90 1.20

**Table 1:** Macrocyclic polyether (MP) structures, MP cavity diameter and common target cation diameters. Values taken from (Frensdorff, H. K.).<sup>19</sup>

varying strengths and stabilities (**Table 2**). Interestingly, “sandwich” complexes [i.e.  $(MP)_2 + Na^+$ ] have been observed for 15C5 and 12C4 in the gas phase<sup>20</sup>, with a  $(12C4)_2 + Na^+$  complex being incorporated into an electrically conducting salt<sup>21</sup>.

When 18C6 and 15C5 are added to an aqueous solution of SDS, they are localized to the external Stern layer (**Figure 1**) via  $Na^+$  complexation, with no penetration to lower Stern layers or the micelle core.<sup>22-28</sup> This sequestration of  $Na^+$  by 18C6 or 15C5 leads to an increase in  $SO_4^-$  head group repulsion. This increased repulsion, in turn, results in decreased micelle size, and the alternated electrostatics of the micelle is thought to cause a decrease in CMC values.<sup>22-33</sup> The formation of a  $15C5 + Na^+$  or  $18C6 + Na^+$  complex, and its localization to the micelle Stern layer, also results in a decrease in surface charge density<sup>22-33</sup>, with some studies also showing a decrease in surface (interfacial) polarity.<sup>32, 34</sup> The influence of MPs on the electrostatic properties of SDS is particularly interesting given that for this surfactant, electrostatic interactions appear to exert significant control over separations.<sup>35</sup>

Though 18C6–SDS and 15C5–SDS interactions in aqueous solutions have been studied, similar work with 12C4 is very rare.<sup>33, 36</sup> This is likely due to this MP’s cavity size (**Table 1**) and the high concentration of 12C4 required for  $Na^+$  complexation. While the aforementioned  $(12C4)_2 + Na^+$  sandwich complex has been noted in both the gas and solid phase, this author has found no characterization of such an aqueous phase complex in literature, though it has been suggested to explain certain 12C4–SDS interactions.<sup>37</sup> Select partitioning and solubilization constants for 12C4 in aqueous SDS solutions have been calculated (**Table 2**), leading this author to target 12C4 as a potential class I

**Macrocyclic polyether solubilization and binding constants**

	$K_{\text{Na}^+} (\text{M}^{-1})$ 25 °C	$\log P_{\text{mw}}$	$f_{\text{mc}}$ 25 °C	$\log K_{\text{sol}}$ 25 °C	$\log K_{\text{mc}}$ 25 °C
18C6	6.6	2.77	0.90	2.17	0.80
15C5	4.7	2.05	0.86	2.00	0.70
12C4	—	1.28	0.57	1.34	—

**Table 2:**  $K_{\text{Na}^+}$ : MP-  $\text{Na}^+$  binding constants calculated using a NaCl solution<sup>37</sup>,  $\log P_{\text{mw}}$ : water-micelle partition coefficient<sup>36</sup>,  $f_{\text{mc}}$ : fraction of MP associated with SDS micelle compared to bulk aqueous phase<sup>33</sup>,  $\log K_{\text{sol}}$ : solubilization equilibrium constant for MPs in aqueous SDS solutions<sup>33</sup> and  $\log K_{\text{mc}}$ : association constant for MP in aqueous micelle solution<sup>38</sup>. Values for each constant were taken from the reference noted for each definition.

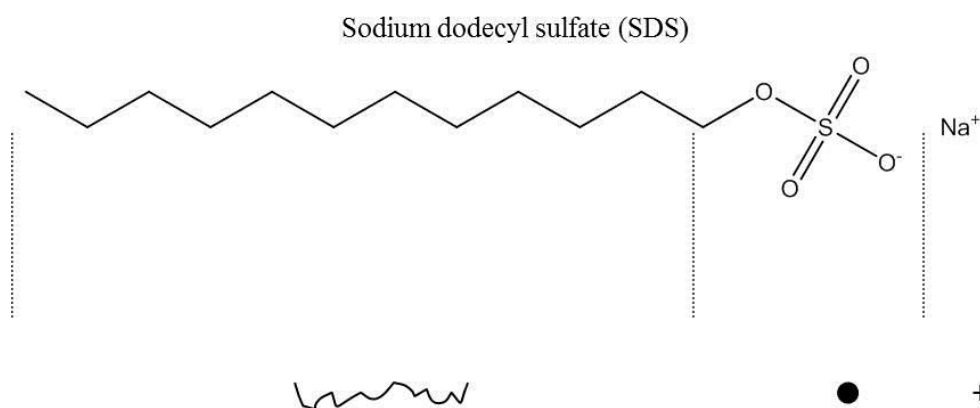
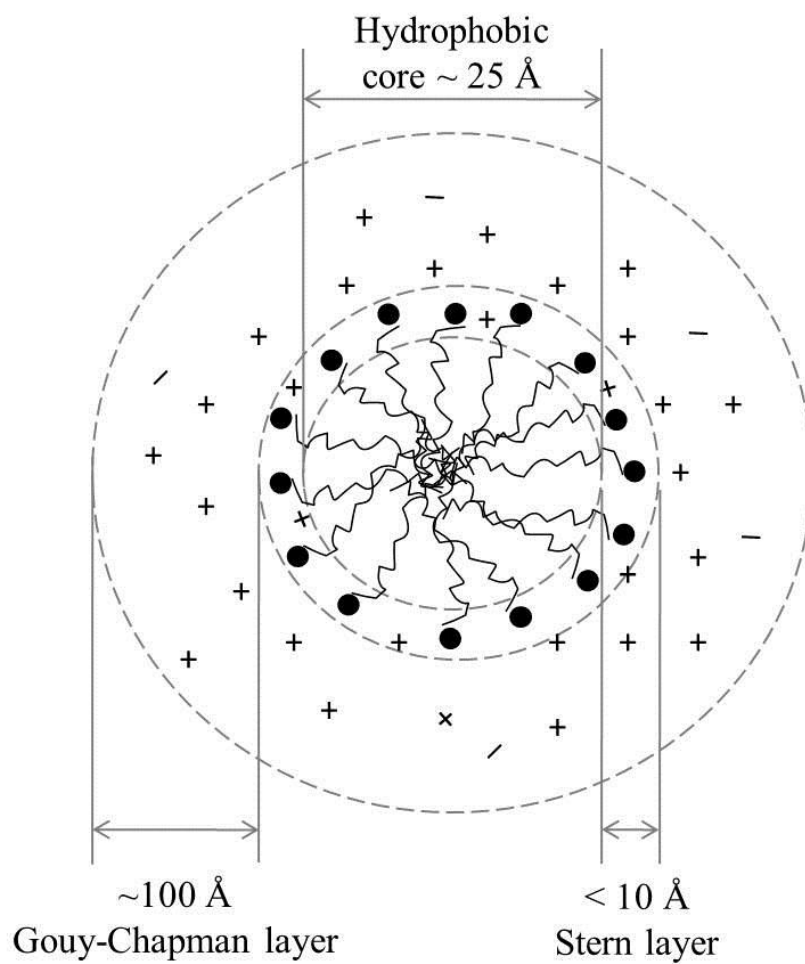


**Figure 1:** Cross section schematic structure of an SDS micelle. Representation based on information from various sources.<sup>12, 13, 15, 39</sup>

modifier. The work presented in this dissertation is the first detailed study of MPs as class I modifiers in MEKC.

#### 4.1.2 PSP characterization

In MEKC, the mechanism of the separation is based on differential solute partitioning. Thus, it is essential to determine the physiochemical properties of the PSP solution and the factors exerting the strongest influence on solute-PSP interactions. To this end, the linear solvation energy relationships (LSER) method was adopted. In this method, a linear sum of product terms comprised of solute factors and complementary solvent properties representing individual intermolecular interactions is employed.<sup>40</sup> Such LSER equations have been extensively used in a variety of applications<sup>41-59</sup> including drug design, or prediction and evaluation studies of toxicity, biological activity, environmental transport, chromatographic and electrophoretic retention.

Employed in this study was the most commonly used LSER in MEKC, the Abraham model<sup>60</sup>, as given in **Equation 3**.

$$\log k = c + vV + eE + sS + aA + bB \quad \text{Equation 3}$$

The term  $k$  is the solute retention factor, as introduced earlier (**Equation 2**). In **Equation 3**, solute descriptors are in uppercase, while solvent (herein, the PSP) properties are in lowercase. The cavity effect is represented by  $V$ , the solute's volume, with the McGowan's characteristic volume often used (units  $\text{cm}^3\text{mol}^{-1}/100$ ). For cavity formation in the micelle phase, micelle-micelle and micelle-water interactions must be disrupted.

Cavity formation in the micellar phase is often favorable compared to the bulk electrolyte, which is typically more cohesive.<sup>45, 48</sup> Disruption caused by cavity formation is minimized by the reorganization of water and surfactant molecules, which orientate for more favorable solute-water or solute-surfactant interactions.<sup>48, 60</sup> The final step is the insertion of the solute into the cavity and the establishment of solute-solvent or solute-surfactant interactions.<sup>48</sup> For nonionic solutes, to which MEKC is most often employed, these interactions include dispersion, induction, orientation and hydrogen bonding<sup>45, 46, 48, 55, 60</sup>, which are represented by other terms in the LSER.

McGowan's volume shows up again in the excess molar refraction,  $E$ , which is defined as the molar refraction of the solute minus the molar refraction of a hypothetical  $n$ -alkane with the same  $V$  value. Values for  $E$  are calculated using the refractive index of the solute at 20 °C for the sodium D-line,  $\eta$ , using **Equation 4**<sup>60</sup> in units  $\text{cm}^3 \text{mol}^{-1}/10$ .

$$E = 10V \left[ \frac{\eta^2 - 1}{\eta^2 + 2} \right] - 2.832V + 0.526 \quad \text{Equation 4}$$

The excess molar refraction represents additional dispersion forces arising from the greater polarizability of solutes with  $\pi$ - and  $n$ -electrons.<sup>60</sup> Interactions associated with dipoles and induced dipoles are described by  $S$ , the dipolarity/polarizability descriptor. As either dipole or induced dipole interactions cannot be independently described, these interactions are grouped. Terms  $A$  and  $B$  both describe hydrogen bonding (H-bonding); solute descriptor  $A$  refers to H-bond donor ability while  $B$  refers to H-bond accepting ability.

The PSP descriptors (lowercase) complement the solute descriptors, describing each phase's ability for a particular interaction. Each descriptor is actually a ratio of

micelle phase to aqueous phase. Positive descriptors indicate the particular interaction favors partitioning into the micellar phase, while negative descriptors mean partitioning into the aqueous phase is preferred. The phase ratio is represented by  $c$ ;  $v$  is a measure of the ease of cavity formation in the micelle phase relative to the aqueous phase;  $e$  is a constant that represents the ability of the phases to interact with solute  $n$ - or  $\pi$ -electrons;  $s$  represents the ability the phases to take part in dipole-dipole and dipole-induced dipole interactions;  $a$  measures the difference in hydrogen bond acceptor ability; and  $b$  represents the difference in hydrogen bond donor ability.

From studies of a wide range of anionic and cationic surfactants, general trends in solute and solvent descriptors relating to partitioning have been observed.<sup>40, 60, 61</sup> The trends seen for solutes are illustrated in **Figure 2**. Increased solute  $V$  and  $E$  values favor solute partitioning in the micellar phase. Micelles are less cohesive than water or aqueous buffer solutions, allowing for easier cavity formation. For a wide range of surfactants, their head groups are capable of greater solute  $n$ - or  $\pi$ -interactions than the aqueous phase. Given the polar nature of water, it is not surprising that the greater the  $S$  values is for a solute the more partitioning will occur into the aqueous phase, with the  $s$  coefficients for the diverse set of surfactants being negative. Preferences based on the hydrogen bond accepting ability, as represented by  $A$ , will depend on the surfactant polar head group.<sup>60, 61</sup> Sulfate polar group surfactants (e.g. SDS) display poorer hydrogen bond accepting ability compared to an aqueous phase, having negative  $a$  coefficients.<sup>60, 61</sup>

The properties of the PSP elucidated by LSER studies are well complemented by functional groups selectivity ( $\tau$ ) determinations. Functional groups selectivity ( $\tau$ ) for a group  $R$  is defined as the ratio of the retention factors (or partition coefficients)



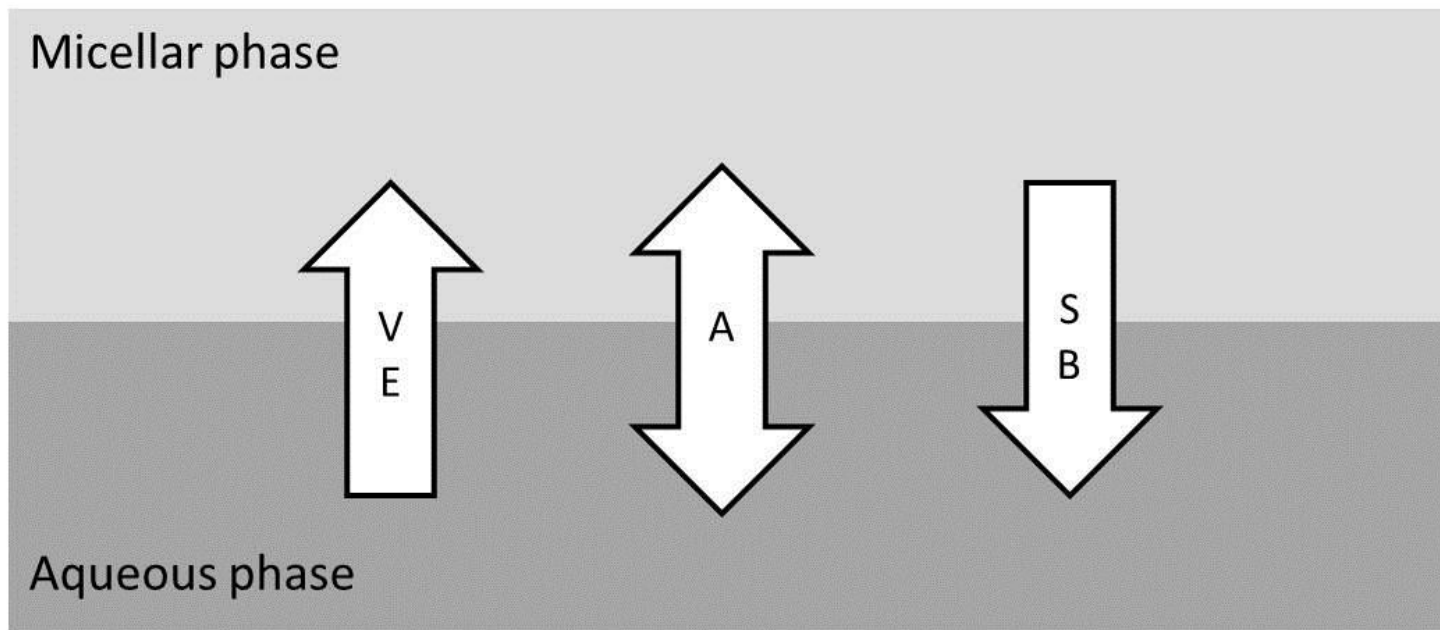


**Figure 2:** General trends in solute descriptors relating to partitioning.

between a mono-substituted aromatic compound (typically  $C_6H_5-R$ ) and the parent aromatic compound (typically  $C_6H_6$ ), as given by **Equation 5**.<sup>62, 63</sup>

$$\tau = \frac{k_{C_6H_5-R}}{k_{C_6H_6}} \quad \text{Equation 5}$$

The transfer free energy of functional group  $R$  ( $\Delta\Delta G_R^\circ$ ) from the aqueous phase to the micellar phase can be derived from **Equation 5** and expressed as **Equation 6**.<sup>62, 63</sup>

$$\Delta\Delta G_R^\circ = -RT \ln \tau \quad \text{Equation 6}$$

Examination of  $\Delta\Delta G_R^\circ$  may provide additional information on the effect of MPs on solute-micelle interactions and/or confirm observation made during LSER analysis.

In addition to using LSER and functional group selectivity to study PSP solubilization and partitioning properties, the effect of each MP on the micelle physicochemical properties of critical micelle concentration (CMC), micellar ionization degrees ( $\beta$ ) and free energy of micellization ( $\Delta G_{MC}^\circ$ ) were determined. An ionic surfactant's CMC is the result of the interplay between *hydrophobic (surfactant's long-chain alkane "tail")* and *electrostatic (surfactant's charged hydrophilic "head")* interactions.<sup>12, 13, 15</sup> Thus, by monitoring CMC, the effect of MPs on electrostatic interactions controlling aggregation can be probed. From the literature<sup>22-33</sup> and studies presented in **CHAPTER 3**, a decrease in CMC for MP modified SDS relative to unmodified SDS is expected.

Upon formation of micelles, a fraction of an ionic surfactant's counter-ions are dissociated from the micelles, leaving the micelles charged.<sup>64, 65</sup> This fraction is

commonly referred to as micellar ionization degree ( $\beta$ ). The degree of ionization of a micelle is associated with the hydration of the hydrophilic “head” and the association of counter-ions.<sup>64-66</sup> For a given ionic surfactant (here a PSP), a  $\beta$  value can be calculated. Given the role electrostatics plays in ionic surfactant aggregation and MEKC separations,  $\beta$  values provide insight into a particular PSP’s behavior, including micelle stability, growth and shape, as well the solubilization behavior of organic substrates and hydrophilic ions.<sup>65</sup>

Determinations of CMC and  $\beta$  values enable the Gibbs free energy of micellization ( $\Delta G_{MC}^{\circ}$ ) for each PSP to be calculated using **Equation 7**.<sup>67</sup>

$$\Delta G_{M}^{\circ} = RT(1 + \beta)\ln CMC \quad \text{Equation 7}$$

$\Delta G_{MC}^{\circ}$  is also the free energy of transfer of one surfactant from the aqueous phase to the micellar pseudophase. Calculations of  $\Delta G_{MC}^{\circ}$  give insight into the interplay between *hydrophobic* and *electrostatic* interactions that control micellization, with the effect of adding MPs examined herein.

## 4.2 Experimental

### 4.2.1 Instrumentation and Materials

CE experiments were done at 25°C and 25 kV using a Beckman Coulter P/ACE MDQ CE with DAD (Fullerton, CA). An unmodified silica capillary (75  $\mu\text{m}$  inner

diameter, 60 cm total length, and 50 cm effective length) was purchased from Polymicro Technologies (Phoenix, AZ).

Buffer reagents, SDS, solvents and test solutes were purchased from Sigma-Aldrich (St. Louis, MO). All aqueous solutions were made using water obtained from a Millipore NANOpure system (Bedford, MA). All solute solutions were made to a concentration of 150  $\mu\text{g/mL}$  using 1:1 v/v mixtures of methanol (MeOH) and acetonitrile (ACN). For MEKC studies, the background electrolyte (BGE) was 10 mM, pH 8.5 sodium borate. Based on initial experiments with MPs, a MP concentration of 25 mM and a SDS concentration of 35 mM was chosen to study the MP effect on surfactant aggregation, as well as PSP solubilization and partitioning.

#### 4.2.2 Determination of LSER descriptors

For the determination of LSER descriptors for each PSP, a diverse set of solutes (**APPENDIX A**) were selected. Solute sets of this size and variety have been used for LSER analysis.<sup>35, 42, 48, 68-70</sup> Solute LSER descriptors were taken from<sup>43, 47, 51, 69, 71</sup> and are given in **APPENDIX A**. These descriptors, along with experimentally determined solute retention factors ( $k$ ), were used to determine SDS micelle phase LSER coefficients by using multiple linear regression analysis, as described elsewhere.<sup>48, 72</sup>

Solute retention factors ( $k$ ) were calculated using **Equation 2**. Conveniently, both methanol (MeOH) and acetonitrile (ACN) serve as EOF markers<sup>73</sup>, allowing the migration of the solute solution matrix to be used as the EOF migration time ( $t_{\text{eo}}$ ). The micelle migration times ( $t_{\text{mc}}$ ) were determined using decanophenone.<sup>73</sup> For solute

solution injection, a 0.3 psi-3 sec program was used. All MEKC experiments were run at least in triplicate. All calculations were done using Excel software.

#### 4.2.3 Determination of $\Delta\Delta G_R^\circ$

Transfer free energy of functional group  $R$  ( $\Delta\Delta G_R^\circ$ ) values were calculated for mono-substituted aromatic compounds from the solute test pool (**APPENDIX A**) using **Equation 6**. All calculations were done using Excel software.

#### 4.2.4 Determination of CMC

The CMC of SDS in the BGE was found using a current titration method<sup>74</sup> (**APPENDIX B**) and validated by determining the CMC of SDS in water at 25°C. Typical titration results for each PSP studied are given in **APPENDIX C**. The calculated CMC of SDS in water was 8.1 ( $\pm$  0.05) mM, which was well within the accepted range of 7.9-8.4 mM at 25°C for SDS.<sup>3, 12, 15, 74, 75</sup> The CMC of SDS in the BGE was determined to be 4.5 ( $\pm$  0.1) mM, a value in-line with the known effect of electrolytes on a surfactant's CMC.<sup>3, 12, 13, 15, 74, 76</sup>

#### 4.2.5 Determination of $\beta$ and $\Delta G_{MC}^\circ$

Micellar ionization degree ( $\beta$ ) and free energy of micellization ( $\Delta G_{MC}^\circ$ ) were both calculated using current titration (see section 4.2.5) data. For a detailed discussion of the

current titration method, see **APPENDIX B**. The  $\beta$  value is calculated using a method described previously<sup>66</sup> in which  $\beta$  has been found to relate to the ratio of the slopes (S) of the two linear segments of the current titration post-CMC and pre-CMC (**Equation 8**).

$$\beta = \frac{S_{\text{post-CMC}}}{S_{\text{pre-CMC}}} \quad \text{Equation 8}$$

**Equation 7** was used to calculate  $\Delta G_{\text{MC}}^{\circ}$ . All calculations were done using Excel software.

### **4.3 Results and Discussion**

#### *4.3.1 LSER analysis*

A summary of LSER regression data is given in **Table 3**. A complementary histogram showing the variations of the LSER system parameters for the unmodified SDS and MP modified SDS PSPs is shown in **Figure 3**. In general, for a wide array of surfactants, cavity formation ( $v$ ) and hydrogen bond acceptor ( $a$ ) or hydrogen bond donor ( $b$ ) are the driving forces of solute partitioning.<sup>60, 61, 72</sup> The large positive value for  $v$  for the PSPs that were studied are expected as micellar phases are typically less cohesive than the aqueous phase.<sup>45, 48</sup> For both unmodified and MP modified SDS PSP,  $v$  is statistically constant.

**MP modification effects on the interactive properties of SDS PSP**

	PSP descriptors						Statistics		
	v	s	a	b	e	c	R <sup>2</sup>	F	SE
35 mM SDS	2.49 [0.18]	-0.60 [0.11]	-0.23 [0.10]	-1.59 [0.18]	0.50 [0.12]	-1.58 [0.13]	0.99	143	0.08
35 mM SDS 25 mM 18C6	2.38 [0.20]	-0.58 [0.12]	-0.04 [0.11]	-2.10 [0.20]	0.72 [0.13]	-1.52 [0.14]	0.99	143	0.09
35 mM SDS 25 mM 15C5	2.42 [0.19]	-0.61 [0.11]	-0.06 [0.10]	-2.22 [0.19]	0.80 [0.13]	-1.56 [0.14]	0.99	164	0.09
35 mM SDS 25 mM 12C4	2.41 [0.19]	-0.65 [0.11]	-0.12 [0.10]	-1.80 [0.19]	0.68 [0.13]	-1.55 [0.14]	0.97	140	0.09

**Table 3:** Solute descriptors  $v$ ,  $s$ ,  $a$ ,  $b$ ,  $e$  and  $c$  are as defined in section 4.1.2.  $R^2$  = coefficient of determination; F = F-statistic; SE is the standard error in the estimate; and the numbers in brackets are the standard deviation in the above descriptor.

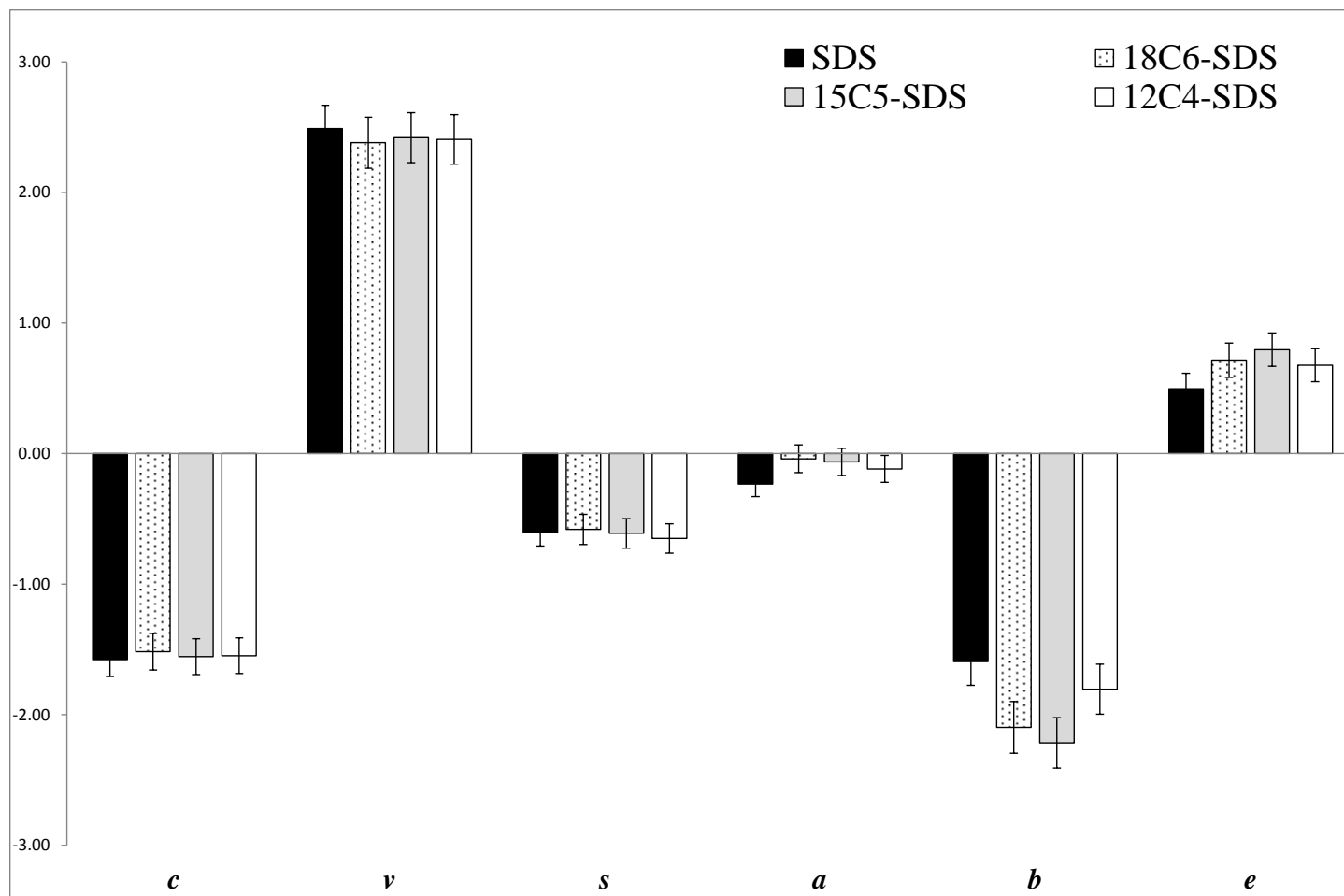


**Figure 3:** Histogram of MP modification effects on the LSER solvent (SDS PSP) descriptors. Error bars represent calculated standard deviations.



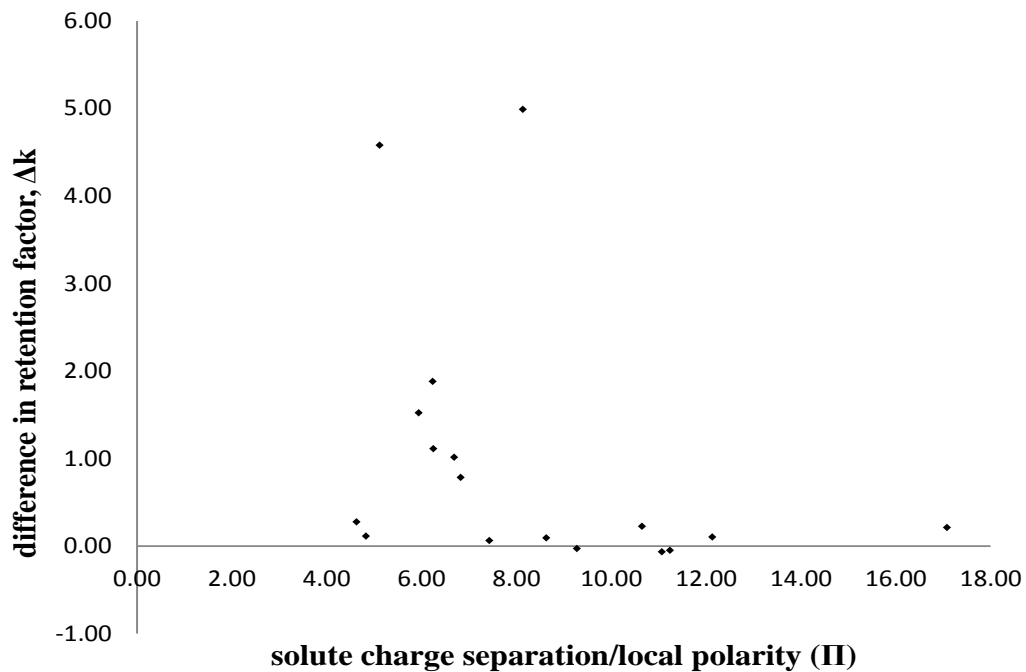
The solute coefficient of  $\nu$  (V, solute volume) is strongly correlated with molar refraction and polarizability, with V being used to calculate excess molar refraction (E) using **Equation 4**. The solvent coefficient of E,  $e$ , indicates the ability of the phases to interact with solute  $n$ - or  $\pi$ -electrons. Nearly all surfactant systems have positive values for  $e$ , with SDS being moderately polarizable<sup>61</sup>. With the addition of MPs to the SDS PSP, a slight increase in  $e$  was observed following the trend 12C4 < 18C6 < 15C5, with the  $e$  values for all three modified PSPs being nearly statistically equivalent (**Table 3**). Given that  $\nu$  remained statistically constant for all PSPs studied, it is likely that the addition of MPs had little effect on the cohesiveness of the PSP but did increase the polarizability of the micelles, making partitioning into the micellar phase more favorable by increasing its ability to interact with solute  $n$ - or  $\pi$ -electrons.

Turning from PSP polarizability to PSP surface polarity, introduction of MPs to the SDS PSP resulted in a decrease of micelle surface polarity. In **CHAPTER 3**, analysis of retention data ( $k$ ) of the nitrotoluene isomer series, for which charge separation/local polarity ( $\Pi$ ) values are known, confirmed that 18C6 causes a decrease in the polarity of the SDS PSP. Similar analysis was done for a subset of the LSER solute set for which  $\Pi$  values are known. **Figures 4 – 6** contain plots of the change in  $k$  ( $\Delta k$ ; **Equation 9**) versus  $\Pi$  values for this solute subset.

$$\Delta k = k_{\text{MP}} - k_{\text{SDS}} \quad \text{Equation 9}$$

In this equation,  $k_{\text{SDS}}$  is the  $k$  of a solute in unmodified SDS PSP and  $k_{\text{MP}}$  is the  $k$  of a solute in a MP modified SDS PSP. Evaluation of this data shows the more non-polar

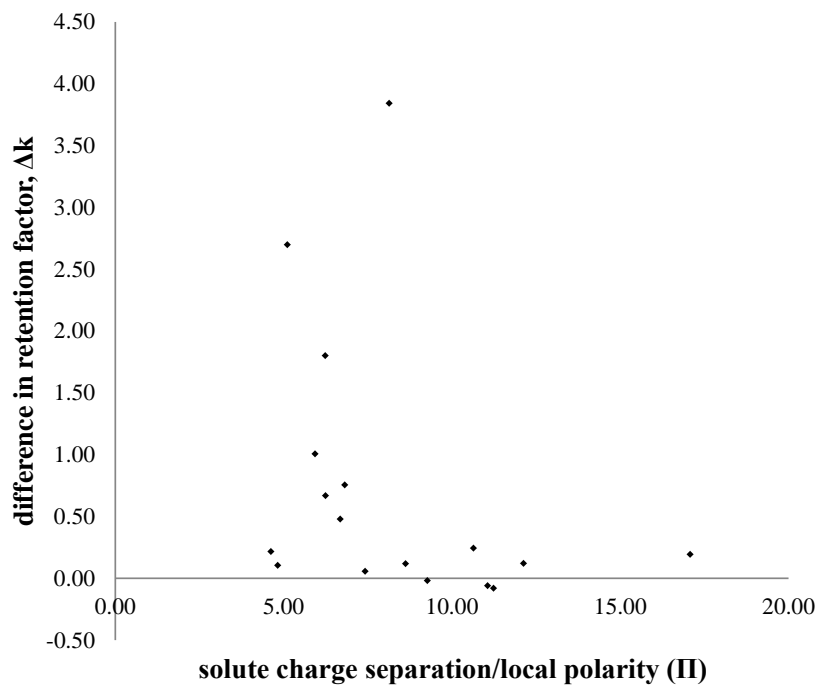
**Figure 4:** Plot of solute charge separation/local polarity ( $\Pi$ ) versus change in  $k$  ( $\Delta k$ ; **Equation 9**) for 15C5 modified SDS PSP.  $\Pi$  values for benzene, toluene, chlorobenzene, bromobenzene, anisole, phenol, phenylamine, 2-naphthol and 1,4-dichlorobenzene were taken from (Murray, J.S.; Brinck, T.; Politzer, P.)<sup>77</sup>.  $\Pi$  values for the nitrotoluene isomer series and nitrobenzene were taken from (Murray, J.S.; Brinck, T.; Politzer, P.)<sup>78</sup>.  $\Pi$  values for 1,3-dinitrobenzene and naphthalene taken from (Murray et al.)<sup>79</sup>.  $\Pi$  values for 1,3-dimethylbenzene and 1,4-dimethylbenzene were taken from (Zou, J.; Yu, Q.; Shang, Z.)<sup>80</sup>.



**Solute II values and  $\Delta k$  data**  
**35 mM SDS, 25 mM 15C5**

<b>solute</b>	<b>II</b>	<b><math>\Delta k</math></b>
3-nitrotoluene	11.07	-0.07
4-nitrotoluene	11.24	-0.05
phenylamine	9.28	-0.03
anisole	7.43	0.06
phenol	8.63	0.09
nitrobenzene	12.13	0.10
benzene	4.83	0.11
1,3-dinitrobenzene	17.08	0.21
2-nitrotoluene	10.65	0.22
toluene	4.63	0.27
1,3-dimethylbenzene	6.83	0.78
1,4-dimethylbenzene	6.69	1.02
chlorobenzene	6.25	1.11
bromobenzene	5.94	1.52
1,4-dichlorobenzene	6.24	1.88
naphthalene	5.12	4.58
2-naphthol	8.14	4.99

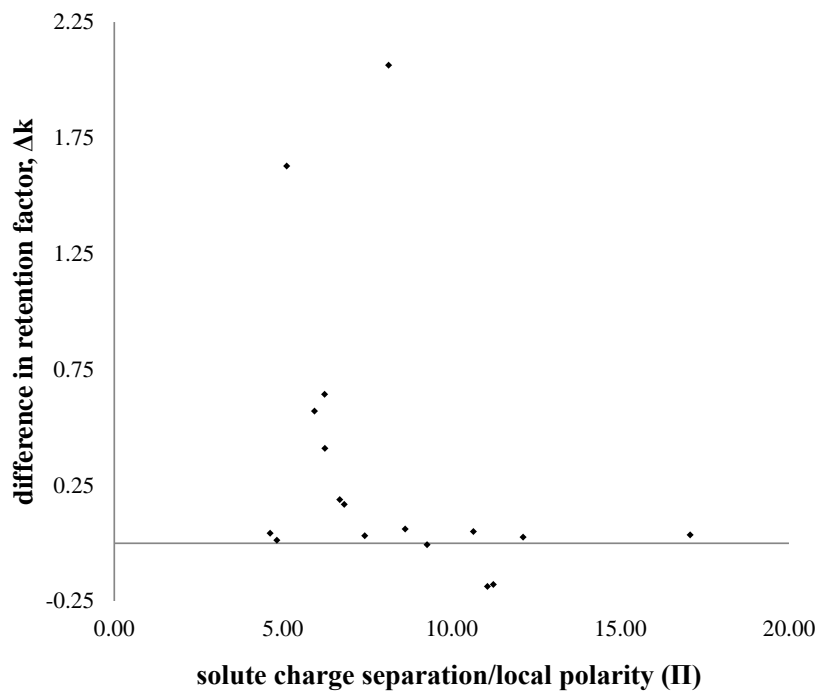
**Figure 5:** Plot of solute charge separation/local polarity ( $\Pi$ ) versus change in  $k$  ( $\Delta k$ ; **Equation 9**) for 18C6 modified SDS PSP.  $\Pi$  values taken from references as detailed in **Figure 4**.



**Solute  $\Pi$  values and  $\Delta k$  data  
35 mM SDS, 25 mM 18C6**

<b>solute</b>	<b><math>\Pi</math></b>	<b><math>\Delta k</math></b>
4-nitrotoluene	11.24	-0.08
3-nitrotoluene	11.07	-0.06
phenylamine	9.28	-0.02
anisole	7.43	0.06
benzene	4.83	0.11
phenol	8.63	0.12
nitrobenzene	12.13	0.12
1,3-dinitrobenzene	17.08	0.19
toluene	4.63	0.22
2-nitrotoluene	10.65	0.24
1,4-dimethylbenzene	6.69	0.48
chlorobenzene	6.25	0.67
1,3-dimethylbenzene	6.83	0.75
bromobenzene	5.94	1.01
1,4-dichlorobenzene	6.24	1.80
naphthalene	5.12	2.70
2-naphthol	8.14	3.84

**Figure 6:** Plot of solute charge separation/local polarity ( $\Pi$ ) versus change in  $k$  ( $\Delta k$ ; **Equation 9**) for 12C4 modified SDS PSP.  $\Pi$  values taken from references as detailed in **Figure 4**.



**Solute II values and  $\Delta k$  data  
35mM SDS, 25mM 12C4**

<b>solute</b>	<b>II</b>	<b><math>\Delta k</math></b>
3-nitrotoluene	11.07	-0.19
4-nitrotoluene	11.24	-0.18
phenylamine	9.28	-0.01
benzene	4.83	0.01
nitrobenzene	12.13	0.03
anisole	7.43	0.03
1,3-dinitrobenzene	17.08	0.04
toluene	4.63	0.04
2-nitrotoluene	10.65	0.05
phenol	8.63	0.06
1,3-dimethylbenzene	6.83	0.17
1,4-dimethylbenzene	6.69	0.19
chlorobenzene	6.25	0.41
bromobenzene	5.94	0.57
1,4-dichlorobenzene	6.24	0.64
naphthalene	5.12	1.63
2-naphthol	8.14	2.06

solutes saw the largest increase in retention in MP modified SDS PSP relative to unmodified SDS PSP. Though this relationship is not 1:1 (i.e. lowest  $\Pi$  values = lowest  $\Delta k$ ), overall  $k$  increased for the more non-polar solutes while a decrease was seen for more polar solutes. The lack of 1:1 correlation is not surprising given the diversity of solutes and the complex nature of interactions leading to partitioning, as the LSER **Equation 3** illustrates.

This solute subset's  $k$  data (pooled in **Table 4**) shows that the addition of a MP leads to a decrease in micelle surface polarity, with 15C5 causing the biggest decrease, followed closely by 18C6, where 12C4 addition provoked the smallest drop. This modulation in polarity is likely brought on by two related “water loss” events. One event correlates to the water associated with  $\text{Na}^+$ . While the entire solvation shell of  $\text{Na}^+$  is not stripped with MP complexation, there is some loss of associated  $\text{H}_2\text{O}$ .<sup>19, 81</sup> The second water loss event involves those  $\text{H}_2\text{O}$  molecules that are generally associated with the micelle, residing in the Stern and Gouy-Chapman layer (**Figure 1**).

Complexation of  $\text{Na}^+$  by an MP, while not affecting the ion's charge, does increase the ion's effective size, with the MP-  $\text{Na}^+$  complex occupying a larger area in the Stern layer.<sup>23, 30</sup> The MP-  $\text{Na}^+$  complex displaces  $\text{H}_2\text{O}$  from the Stern layer and the Gouy-Chapman – Stern layer interface out to the Gouy-Chapman layer and possibly the aqueous bulk phase.<sup>23, 30, 32, 34, 82</sup> Of course this “bullying” behavior is not limited to  $\text{H}_2\text{O}$ , a variety of charged or polar species typically associated with such a highly charged particle in solution (i.e. ionic micelle<sup>76</sup>) are likely subject to “eviction”. This eviction



**Influence of MPs on solute retention correlated to solute  $\Pi$  values**

solute	$\Pi$	35 mM SDS 25	35 mM SDS 25	35 mM SDS 25
		mM 15C5	mM 18C6	mM 12C4
		average change in retention, $\Delta k$		
3-nitrotoluene	11.07	-0.07 [.07]	-0.06 [.12]	-0.19 [.07]
4-nitrotoluene	11.24	-0.05 [.08]	-0.08 [.09]	-0.18 [.06]
phenylamine	9.28	-0.03 [0]	-0.02 [0]	-0.01 [.01]
anisole	7.43	0.06 [.04]	0.06 [.06]	0.03 [.03]
phenol	8.63	0.09 [.01]	0.12 [0]	0.06 [0]
nitrobenzene	12.13	0.10 [.02]	0.12 [.01]	0.03 [.03]
benzene	4.83	0.11 [.01]	0.11 [.01]	0.01 [.02]
1,3-dinitrobenzene	17.08	0.21 [.03]	0.19 [.03]	0.04 [.06]
2-nitrotoluene	10.65	0.22 [.17]	0.24 [.16]	0.05 [.16]
toluene	4.63	0.27 [.04]	0.22 [.03]	0.04 [.06]
1,3-dimethylbenzene	6.83	0.78 [.29]	0.75 [.19]	0.17 [.10]
1,4-dimethylbenzene	6.69	1.02 [.05]	0.48 [.11]	0.19 [.24]
chlorobenzene	6.25	1.11 [.06]	0.67 [.27]	0.41 [.10]
bromobenzene	5.94	1.52 [.10]	1.01 [.26]	0.57 [.01]
1,4-dichlorobenzene	6.24	1.88 [.48]	1.80 [.12]	0.64 [.24]
naphthalene	5.12	4.58 [.62]	2.70 [.36]	1.63 [.52]
2-naphthol	8.14	4.99 [.10]	3.84 [.08]	2.06 [.18]

**Table 4:** Change in  $k$  ( $\Delta k$ ) was calculated using **Equation 9**.  $\Pi$  values taken from references as detailed in **Figure 4**.

results in a decrease in micelle's surface charge density, listed as a MP addition effect in section 4.1.1.

For common ionic surfactants, the ability of the PSP to induce dipole-dipole and dipole-induced dipole interactions ( $s$ ), is typically negative given PSPs are typically less dipolar than water.<sup>60, 61, 72</sup> Consulting **Table 3**, all PSPs studied have negative  $s$  values. Somewhat surprisingly, for both unmodified and MP modified SDS PSP, these values are statistically constant.

As stated above, a variety of charged or polar species typically associated with the SDS micelle are likely subject to eviction from the micelle surface with formation of a MP–Na<sup>+</sup> complex in the Stern layer. The eviction of ions is the cause of the decrease in surface charge density observed for SDS upon the addition of 15C6 or 18C6.<sup>22-33</sup> Of relevance to the H-bonding ability of SDS PSP is the eviction of hydrogen ions, whose concentration at the surface of micelles has been observed to decrease with the addition of 15C5 or 18C6.<sup>32, 76, 82</sup>

For a wide array of surfactants, interactions due to a hydrogen bond acceptor ( $a$ ) or hydrogen bond donor ( $b$ ) are the driving forces of solute partitioning.<sup>49, 55, 60, 61, 72</sup> A slight change in MP modified SDS PSP  $a$  values was observed (**Table 3**), with  $a$  values becoming less negative and following the trend 12C4 < 15C5 < 18C6. Overall, this increase in PSP H-bond acceptor ability is small. The  $a$  values for 15C5 and 18C6 were statistically equivalent, while the  $a$  values for 12C4 and unmodified SDS were statistically equivalent. The change in H-bond donating ability ( $b$ ), however, was more

substantial. Of all the PSP descriptors,  $b$  was affected the most by the addition of MPs to the SDS PSP.

Large negative  $b$  values indicate that the aqueous phase is a better H-bond donor than the PSP. The effect of the aforementioned eviction of hydrogen ions upon the formation of  $\text{MP}^- \text{Na}^+$  complex in the Stern layer is clearly seen in the  $b$  values. Addition of MPs to the SDS PSP gave  $b$  values for each MP modified PSPs that became more negative (**Table 3, Figure 3**). Thus, MP modification caused a decrease in H-bond donating ability of the SDS PSP. For the MPs, the following trend was observed: 12C4 (small negative value) < 18C6 < 15C5 (large negative value). The  $a$  and  $b$  values for 15C5 versus 18C6 were statistically equivalent.

Differences between 15C5 and 18C6 modified SDS PSPs can be found in  $\Delta k$  versus solute H-bond accepting ability ( $B$ ) plots (**Figures 7 - 9**). For each MP, retention generally decreased for solutes with greater H-bond accepting ability (larger  $B$  values), while an increase in retention was seen for those solutes with smaller  $B$  values (**Table 5**). Four solutes that were exceptions to this general trend are easily observed and are highlighted in **Figures 7 - 9**.

The four exceptions were naphthalene, 1-naphthol, 2-naphthol, and diphenylamine. The common feature of these solutes is solute volume ( $V$ ) and excess molar refraction ( $E$ ), with these solutes having the largest  $V$  and  $E$  values in the solute set (**APPENDIX A**). Large solute  $V$  and  $E$  values favor solute partitioning in the micellar phase (**Figure 2**). As detailed earlier, the addition of MPs had little effect on the cohesiveness of the PSP ( $\nu$ ), but did increase the polarizability ( $e$ ) of the micelles. This

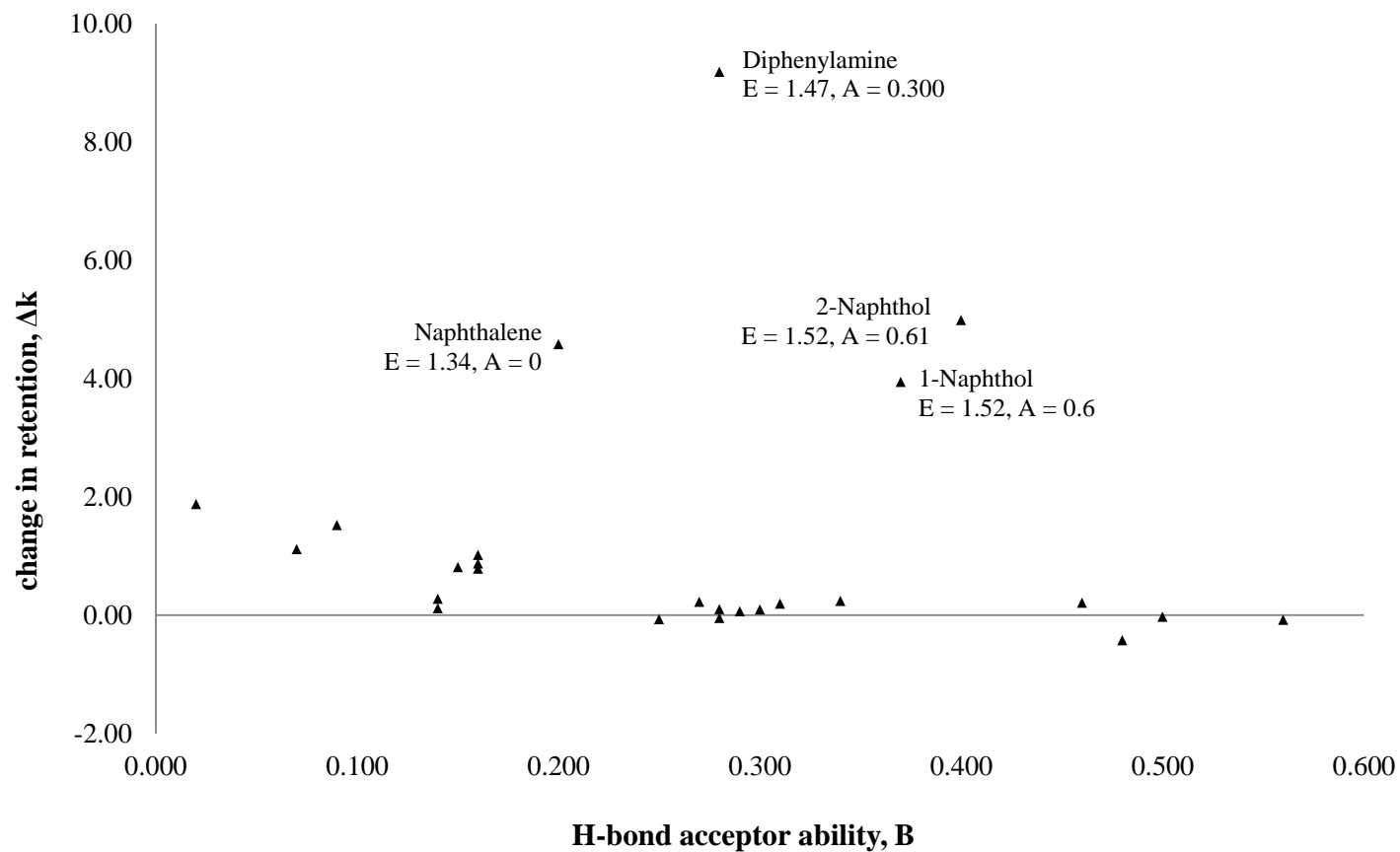


**Figure 7:** Plot of change in  $k$  ( $\Delta k$ ) versus solute H-bond acceptor ability ( $B$ ) for 15C5 modified SDS PSP. Solutes not following the general trend of decreased retention with larger  $B$  values are highlighted, with  $E$  = excess molar refraction and  $A$  = solute H-bond donating ability.

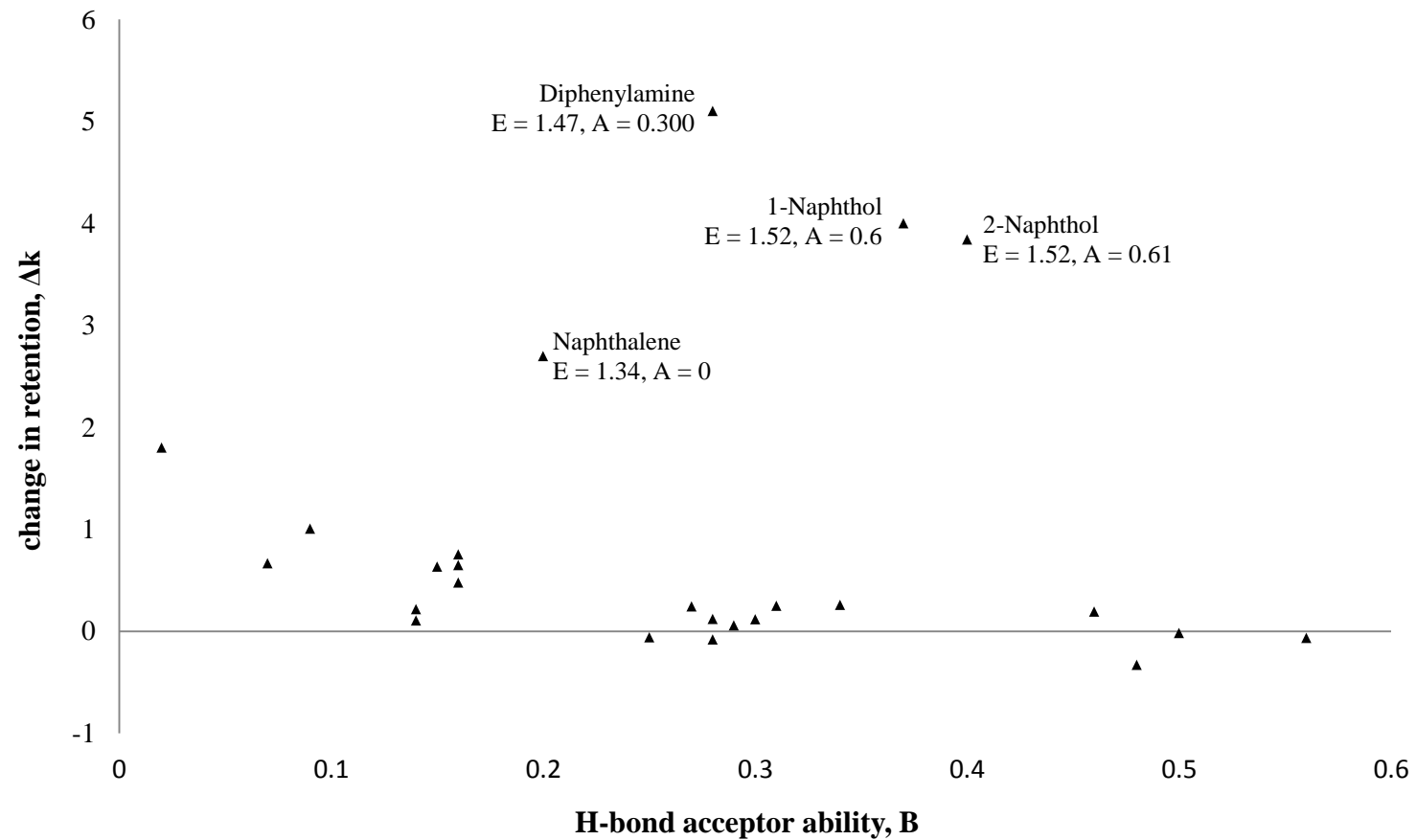


**Figure 8:** Plot of change in  $k$  ( $\Delta k$ ) versus solute H-bond acceptor ability ( $B$ ) for 18C6 modified SDS PSP. Solutes not following the general trend of decreased retention with larger  $B$  values are highlighted, with  $E$  = excess molar refraction and  $A$  = solute H-bond donating ability.

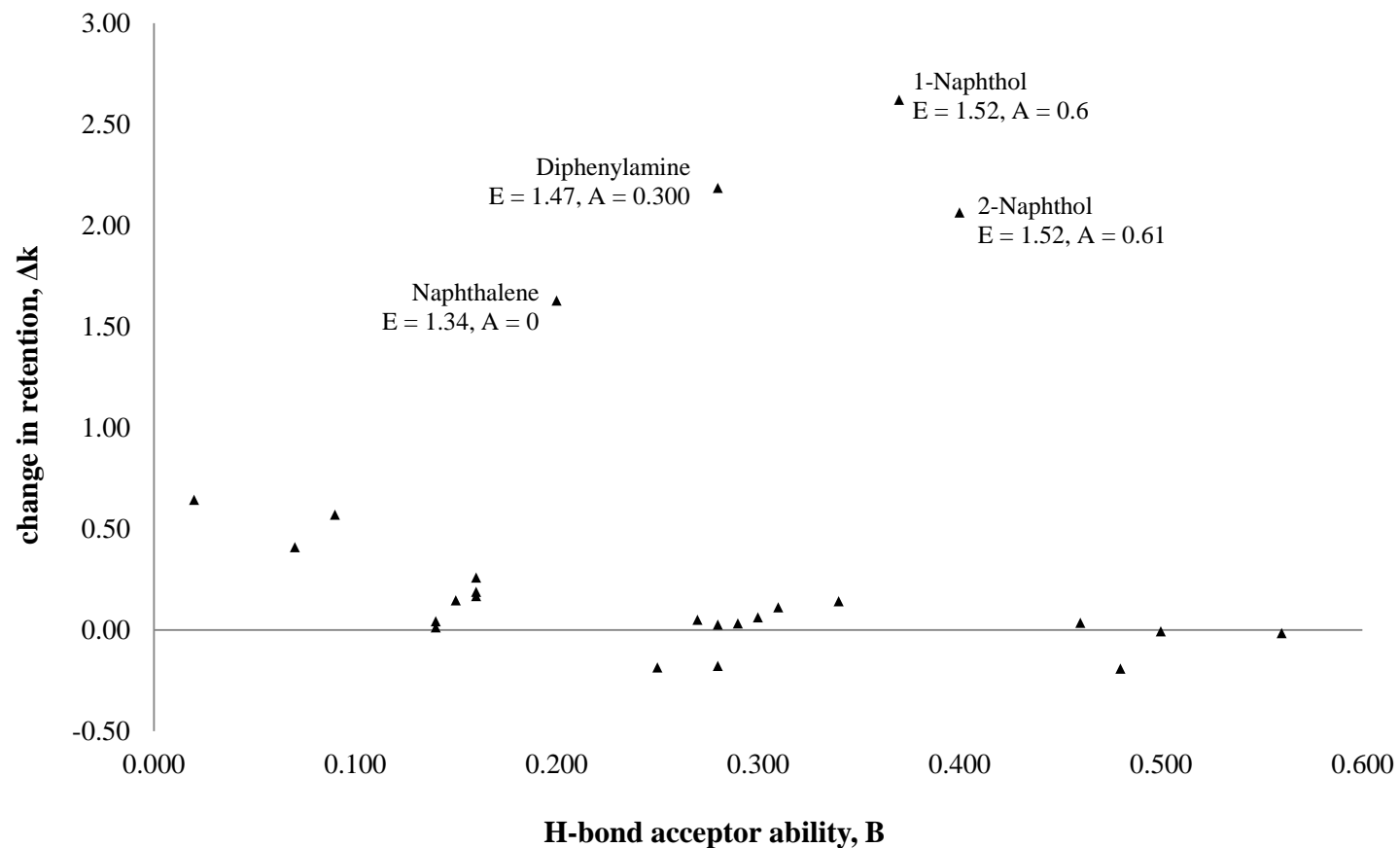


**Figure 9:** Plot of change in  $k$  ( $\Delta k$ ) versus solute H-bond acceptor ability ( $B$ ) for 12C4 modified SDS PSP. Solutes not following the general trend of decreased retention with larger  $B$  values are highlighted,  $E$  = excess molar refraction and  $A$  = solute H-bond donating ability.

Solute	LSER solute descriptors			35 mM SDS 25 mM 15C5	35 mM SDS 25 mM 18C6	35 mM SDS 25 mM 12C4
	B	E	A	average change in retention, $\Delta k$		
acetophenone	0.480	0.818	0	-0.42	-0.33	-0.19
benzyl alcohol	0.560	0.803	0.390	-0.08	-0.07	-0.02
3-nitrotoluene	0.250	0.874	0	-0.07	-0.06	-0.19
4-nitrotoluene	0.280	0.870	0	-0.05	-0.08	-0.18
phenylamine	0.500	0.955	0.260	-0.03	-0.02	-0.01
anisole	0.290	0.710	0	0.06	0.06	0.03
phenol	0.300	0.805	0.600	0.09	0.12	0.06
nitrobenzene	0.280	0.871	0	0.10	0.12	0.03
benzene	0.140	0.610	0	0.11	0.11	0.01
4-methylphenol	0.310	0.820	0.570	0.20	0.25	0.11
1,3-dinitrobenzene	0.460	1.130	0	0.21	0.19	0.04
2-nitrotoluene	0.270	0.866	0	0.22	0.24	0.05
3-methylphenol	0.340	0.840	0.570	0.24	0.26	0.14
toluene	0.140	0.601	0	0.27	0.22	0.04
1,3-dimethylbenzene	0.160	0.623	0	0.78	0.75	0.17
ethylbenzene	0.150	0.613	0	0.81	0.63	0.15
1,2-dimethylbenzene	0.160	0.663	0	0.87	0.65	0.26
1,4-dimethylbenzene	0.160	0.613	0	1.02	0.48	0.19
chlorobenzene	0.070	0.718	0	1.11	0.67	0.41
bromobenzene	0.090	0.882	0	1.52	1.01	0.57
1,4-dichlorobenzene	0.020	0.825	0	1.88	1.80	0.64
1-naphthol	0.370	1.520	0.600	3.94	4.00	2.62
naphthalene	0.200	1.340	0	4.58	2.70	1.63
2-naphthol	0.400	1.520	0.610	4.99	3.84	2.06
diphenylamine	0.280	1.470	0.300	9.18	5.10	2.18

**Table 5:** Influence of MPs on solute retention correlated to B. Where B = H-bond

accepting ability, E= ability of the phases to interact with solute  $n$ - or  $\pi$ -electrons and A =

H-bond donating ability. Change in k ( $\Delta k$ ) was calculated using **Equation 9**.

suggests MP modified SDS PSP's increased ability to interact with the solutes'  $n$ - or  $\pi$ -electrons influenced the aforementioned exception to the trend of decreased retention for solutes with larger B values. For three of the four solute exceptions, a common feature is H-bond donor ability (A). As seen in **Table 5**, 1-naphthol, 2-naphthol, and diphenylamine are three of the eight solutes with H-bond donor ability.

The LSER results, along with careful examination of solute retention data, showed that MPs, in general, increased the SDS PSP ability to interact with solute  $n$ - or  $\pi$ -electrons (polarizability), decreased micellar surface polarity, increased micellar H-bond accepting ability and decreased micellar H-bond donating ability. Some of these effects are differential, with 15C5 and 18C6 causing a greater change than 12C4, which is in good agreement with MP- $\text{Na}^+$  and MP-SDS binding, partitioning and solubilization constants in **Table 2**.

The generally similar effect MPs have on the SDS PSP also translates into statistically equivalent values for the constant  $c$ , representing phase ratio. In chromatography, the phase ratio is defined as the ratio of the volume of the mobile phase (here: bulk aqueous) to that of the stationary phase (here: PSP) in a column/capillary.<sup>83</sup> Under the same experimental conditions (e.g. buffer, temperature, additives), consistent phase ratio values are expected. The observed statistically equivalent values for  $c$  indicate that the addition of MPs did not change the phase ratio. This consistency in phase ratio was previously noted for the addition of these MPs to aqueous solutions of sodium decanoate [ $\text{CH}_3(\text{CH}_2)_8\text{C}(=\text{O})\text{O}^- \text{Na}^+$ ].<sup>37</sup> Another point of consistency for the MPs studied was the  $t_{\text{eo}}/t_{\text{mc}}$  ratio, where  $t_{\text{eo}}$  was migration time of a non-retained solute, which represented electroosmotic force (EOF), and  $t_{\text{mc}}$  was the migration time of the PSP, as



marked by a highly retained compound. As is typical for class I modifiers in CE<sup>8, 14</sup>, addition of MPs was found to have virtually no impact on the ratio  $t_{eo}/t_{mc}$ , which averaged  $0.35 \pm 0.02$  for all experiments.

#### 4.3.2 $\Delta\Delta G_R^\circ$ observations

The general trends observed for MPs revealed by LSER analysis are echoed in solute transfer free energy of functional group  $R$  ( $\Delta\Delta G_R^\circ$ ) values. As stated in 4.2.1,  $\Delta\Delta G_R^\circ$  is the transfer free energy of functional group  $R$  from the aqueous phase to the micellar phase, which can be calculated by using **Equation 6**.

$$\Delta\Delta G_R^\circ = -RT \ln \tau \quad \text{Equation 6}$$

The term  $\tau$  is functional groups selectivity ( $\tau$ ) for a group  $R$ , given by **Equation 5**.

$$\tau = \frac{k_{C_6H_5-R}}{k_{C_6H_6}} \quad \text{Equation 5}$$

From the LSER solute set (see **APPENDIX A**), a subset of mono-substituted aromatic compounds were selected and their calculated  $\Delta\Delta G_R^\circ$  values for each PSP studied are given in (see **APPENDIX D**).

As detailed in section 4.3.1, PSP descriptors  $a$ ,  $b$  and  $e$  were affected by MP addition, along with micellar surface polarity. The most significant effect of MP addition was a decrease in SDS PSP H-bond donating ability ( $b$ ). Plots of the change in  $\Delta\Delta G_R^\circ$  ( $\Delta\Delta\Delta G_R^\circ$ ) versus a solute's H-bond accepting ability ( $B$ ) for each MP modified SDS PSP

are given in **Figures 10 – 12**. The change in  $\Delta\Delta G_R^\circ$  ( $\Delta\Delta\Delta G_R^\circ$ ) was calculated as shown in **Equation 10**.

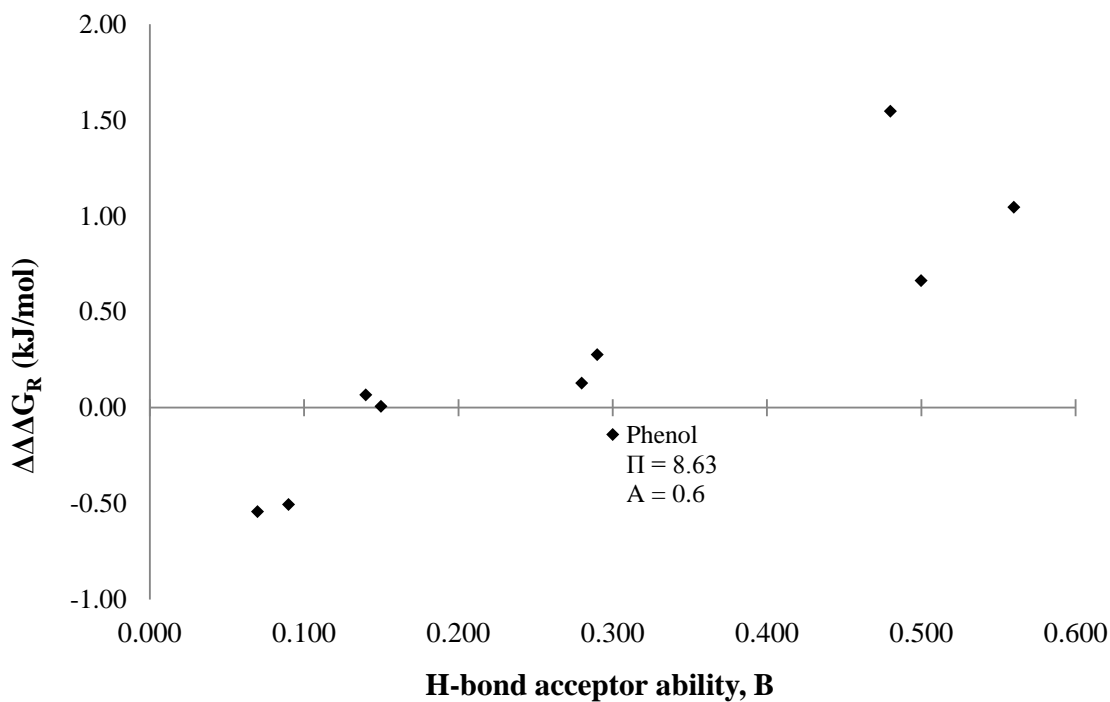
$$\Delta\Delta\Delta G_R^\circ = \Delta\Delta G_{R\text{MP}}^\circ - \Delta\Delta G_{R\text{SDS}}^\circ \quad \text{Equation 10}$$

The term  $\Delta\Delta G_{R\text{SDS}}^\circ$  is the  $\Delta\Delta G_R^\circ$  of a solute in unmodified SDS PSP and  $\Delta\Delta G_{R\text{MP}}^\circ$  is the  $\Delta\Delta G_R^\circ$  of a solute in a MP modified SDS PSP. Positive  $\Delta\Delta\Delta G_R^\circ$  values indicate that the addition of R was not favorable for solute-micelle interactions. Alternatively, favorable solute-micelle interactions are indicated by negative  $\Delta\Delta\Delta G_R^\circ$  values.

LSER analysis showed that for each MP, retention generally decreased for solutes with greater H-bond accepting ability (larger B values), while retention increased for those solutes with smaller B values (**Table 5**). From the  $\Delta\Delta\Delta G_R^\circ$  versus B plots (**Figures 10 – 12**), it can be seen that an addition of a functional group (R) that yielded in a poor H-bond acceptor resulted in more favorable solute-micelle interactions ( $-\Delta\Delta\Delta G_R^\circ$ ). Those R additions that produced strong H-bond acceptors experienced less favorable solute-micelle interactions ( $\Delta\Delta\Delta G_R^\circ$ ).

Also present in **Figures 10 – 12** is  $\Delta\Delta\Delta G_R^\circ$  data correlated to solute descriptors A, B and E, as well as charge separation/local polarity ( $\Pi$ ) values for those solutes for which  $\Pi$  values are known. As seen in earlier analysis, the impact of 15C5 and 18C6 on solute partitioning is more significant than observed for 12C4. As highlighted in **Figures 10 – 12**, a consistent exception to the large B – large  $\Delta\Delta\Delta G_R^\circ$  trend is phenol. However, phenol has the largest A value of this solute subset and is a good H-bond donor. As

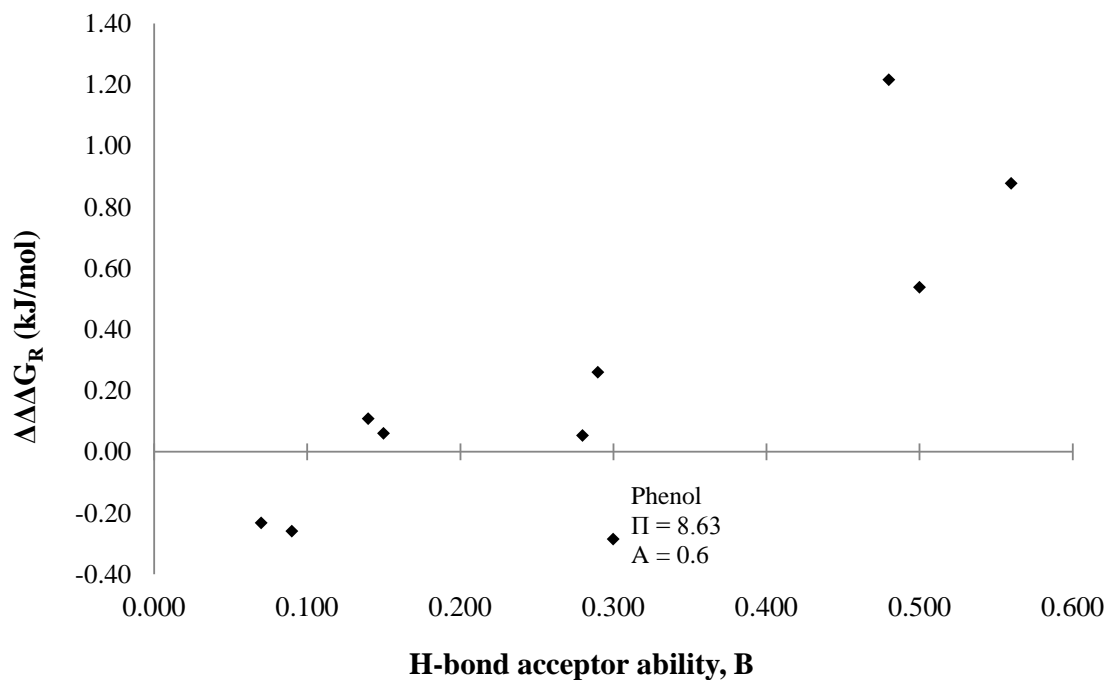
**Figure 10:** Influence of 15C5 on solute transfer free energy of functional group  $R$  ( $\Delta\Delta G_R^\circ$ ; **Equation 6**) values. The change in  $\Delta\Delta G_R^\circ$  ( $\Delta\Delta\Delta G_R^\circ$ ) was calculated using **Equation 10**. For solutes in italics,  $\Delta\Delta G_R^\circ$  values were statistically equivalent to unmodified SDS PSP  $\Delta\Delta G_R^\circ$ . B = H-bond accepting ability, E = ability of the phases to interact with solute  $n$ - or  $\pi$ -electrons, and A = H-bond donating ability. Solute charge separation/local polarity ( $\Pi$ ) values taken from references as detailed in **Figure 4**.



**Influence of MP on  $\Delta\Delta G_R^\circ$  values correlated to select LSER solute descriptors  
35 mM SDS, 25 mM 15C5**

solute	R	A	B	E	$\Pi$	$\Delta\Delta G_R$ (kJ/mol)
chlorobenzene	Cl	0	0.07	0.718	6.25	-0.54
bromobenzene	Br	0	0.09	0.882	5.94	-0.50
phenol	OH	0.6	0.3	0.805	8.63	-0.14
<i>ethylbenzene</i>	<i>CH<sub>2</sub>CH<sub>3</sub></i>	0	0.15	0.613	–	0.01
<i>toluene</i>	<i>CH<sub>3</sub></i>	0	0.14	0.601	4.63	0.07
nitrobenzene	NO <sub>2</sub>	0	0.28	0.871	12.13	0.13
anisole	OCH <sub>3</sub>	0	0.29	0.71	7.43	0.28
phenylamine	NH <sub>2</sub>	0.26	0.5	0.955	9.28	0.66
benzyl alcohol	CH <sub>2</sub> OH	0.39	0.56	0.803	–	1.05
acetophenone	C(=O)CH <sub>3</sub>	0	0.48	0.818	–	1.55

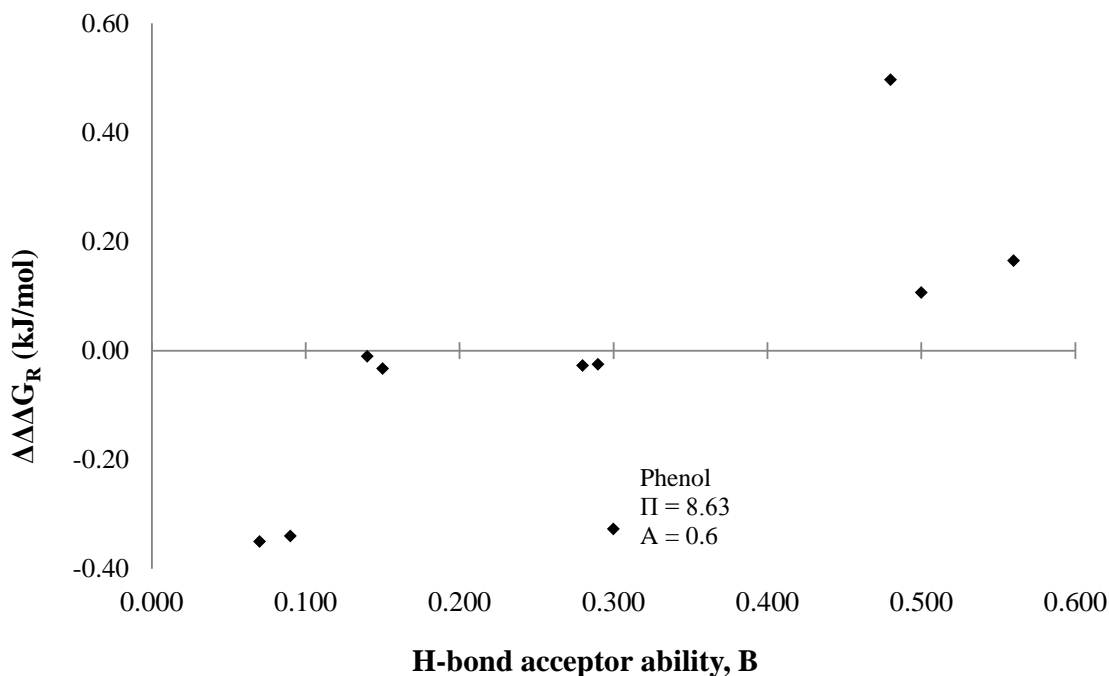
**Figure 11:** Influence of 18C6 on solute transfer free energy of functional group  $R$  ( $\Delta\Delta G_R^\circ$ ; **Equation 6**) values. The change in  $\Delta\Delta G_R^\circ$  ( $\Delta\Delta\Delta G_R^\circ$ ) was calculated using **Equation 10**. For solutes in italics,  $\Delta\Delta G_R^\circ$  values were statistically equivalent to unmodified SDS PSP  $\Delta\Delta G_R^\circ$ . B = H-bond accepting ability, E = ability of the phases to interact with solute  $n$ - or  $\pi$ -electrons, and A = H-bond donating ability. Solute charge separation/local polarity ( $\Pi$ ) values taken from references as detailed in **Figure 4**.



**Influence of MP on  $\Delta\Delta G_R^\circ$  values correlated to select LSER solute descriptors  
 35 mM SDS, 25 mM 18C6**

solute	R	A	B	E	$\Pi$	$\Delta\Delta\Delta G_R$ (kJ/mol)
phenol	OH	0.60	0.300	0.81	8.63	-0.29
bromobenzene	Br	0	0.090	0.88	5.94	-0.26
chlorobenzene	Cl	0	0.070	0.72	6.25	-0.23
nitrobenzene	$NO_2$	0	0.280	0.87	12.13	0.05
ethylbenzene	$CH_2CH_3$	0	0.150	0.61	–	0.06
toluene	$CH_3$	0	0.140	0.60	4.63	0.11
anisole	$OCH_3$	0	0.290	0.71	7.43	0.26
phenylamine	$NH_2$	0.26	0.500	0.96	9.28	0.54
benzyl alcohol	$CH_2OH$	0.39	0.560	0.80	–	0.88
acetophenone	$C(=O)CH_3$	0	0.480	0.82	–	1.22

**Figure 12:** Influence of 12C4 on solute transfer free energy of functional group  $R$  ( $\Delta\Delta G_R^\circ$ ; **Equation 6**) values. The change in  $\Delta\Delta G_R^\circ$  ( $\Delta\Delta\Delta G_R^\circ$ ) was calculated using **Equation 10**. For solutes in italics,  $\Delta\Delta G_R^\circ$  values were statistically equivalent to unmodified SDS PSP  $\Delta\Delta G_R^\circ$ . B = H-bond accepting ability, E = ability of the phases to interact with solute  $n$ - or  $\pi$ -electrons, and A = H-bond donating ability. Solute charge separation/local polarity ( $\Pi$ ) values taken from references as detailed in **Figure 4**.



**Influence of MP on  $\Delta\Delta G_R^\circ$  values correlated to select LSER solute descriptors  
35 mM SDS, 25 mM 12C4**

<b>solute</b>	<b>R</b>	<b>A</b>	<b>B</b>	<b>E</b>	<b>Π</b>	<b><math>\Delta\Delta G_R</math> (kJ/mol)</b>
chlorobenzene	Cl	0	0.07	0.718	6.25	-0.35
bromobenzene	Br	0	0.09	0.882	5.94	-0.34
phenol	OH	0.6	0.3	0.805	8.63	-0.33
<i>ethylbenzene</i>	<i>CH<sub>2</sub>CH<sub>3</sub></i>	0	0.15	0.613	–	-0.03
<i>nitrobenzene</i>	<i>NO<sub>2</sub></i>	0	0.28	0.871	12.13	-0.03
<i>anisole</i>	<i>OCH<sub>3</sub></i>	0	0.29	0.71	7.43	-0.03
<i>toluene</i>	<i>CH<sub>3</sub></i>	0	0.14	0.601	4.63	-0.01
<i>phenylamine</i>	<i>NH<sub>2</sub></i>	0.26	0.5	0.955	9.28	0.11
benzyl alcohol	CH <sub>2</sub> OH	0.39	0.56	0.803	–	0.16
acetophenone	C(=O)CH <sub>3</sub>	0	0.48	0.818	–	0.50



detailed previously, MP addition resulted in a SDS PSP that was a better H-bond acceptor. As the analysis presented here has shown, the partitioning of solutes is the result of several types of solute – micelle interactions.

#### 4.3.3 *Effect of MPs on micelle physicochemical properties*

The effect of each MP on the micelle physicochemical properties of critical micelle concentration (CMC), micellar ionization degrees ( $\beta$ ) and free energy of micellization ( $\Delta G_{MC}^{\circ}$ ) were investigated. CMC values for each PSP studied were determined using a current titration method described in **APPENDIX B**. Typical titration data are shown in **APPENDIX C**. The titration data could also be used to calculate values for  $\beta$  and  $\Delta G_{MC}^{\circ}$ . Values of  $\beta$  were calculated as detailed in section 4.2.5 using **Equation 8**.

$$\beta = \frac{S_{\text{post-CMC}}}{S_{\text{pre-CMC}}} \quad \text{Equation 8}$$

The term  $\beta$  is related to the ratio of the slopes (S) of the two linear segments of the current titration post-CMC and pre-CMC (see **APPENDICES B** and **C**). **Equation 7** was used to calculate  $\Delta G_{MC}^{\circ}$ .

$$\Delta G_M^{\circ} = RT(1 + \beta)\ln\text{CMC} \quad \text{Equation 7}$$

CMC,  $\beta$  and  $\Delta G_{MC}^{\circ}$  values for unmodified SDS and MP modified SDS PSP in aqueous buffer, along with unmodified SDS PSP in water, are given in **Table 6**.

As stated in section 4.1.2, an ionic surfactant's CMC is the result of the interplay between *hydrophobic* and *electrostatic* interactions. Ionic head group repulsion disfavors micelle formation while hydrophobic alkane tail association favors aggregation. As expected from a review of the literature<sup>3, 12, 13, 15, 74, 76</sup>, the CMC of SDS in buffer versus water was lower. The CMC was further depressed for the SDS PSP by the addition of a MP. The CMC values follow the trend  $12C4 < 15C5 < 18C6$ , with values for 12C4 and 15C5 being nearly statistically equivalent. The CMC value for 12C4 is intriguing given the smaller effect this MP had on other partitioning and PSP properties detailed earlier, in addition to the binding, partitioning and solubilization constants given in **Table 2**.

One may think that the addition of MPs to SDS, which via  $Na^{+}$  complexation has been shown to increase  $SO_4^{-}$  head group repulsion for 15C5 and 18C6<sup>22-33</sup>, would cause an increase in CMC. As discussed in section 4.1.1, this is not the case and the CMC decreases. This phenomenon is not adequately addressed in the current, relevant literature. Work by Baglioni<sup>84</sup> offers an explanation to the observed depression of SDS CMC values upon the addition of 15C5 or 18C6. Though MP-  $Na^{+}$  complex formation may cause an initial increase in head group repulsion, the MP-  $Na^{+}$  complex comes to reside in an orientation in which the MP methylenes ( $-CH_2-$ ) intercalate among the  $SO_4^{-}$  head groups. Baglioni<sup>84</sup> suggests that this intercalation, along with the delocalization of sodium's charge over the MP ring, could favor a rearrangement of  $SO_4^{-}$  head groups, which decreases the area per head group. This type of CMC depression via intercalation

Effect of MPs on the CMC, $\beta$ and $\Delta G_{MC}^{\circ}$			
PSP	CMC	$\beta$	$\Delta G_{MC}^{\circ}$ (kJ/mol)
35 mM SDS (water)	8.1 [.05]	0.41 [.05]	7.29 [.12]
35 mM SDS (buffer solution)	4.5 [0.1]	0.48 [.05]	5.51 [.21]
35 mM SDS 25 mM 18C6 (buffer solution)	2.7 [0.1]	0.50 [.02]	3.65 [.04]
35 mM SDS 25 mM 15C5 (buffer solution)	2.3 [0.1]	0.56 [.03]	3.21 [.17]
35 mM SDS 25 mM 12C4 (buffer solution)	2.0 [0.1]	0.49 [.03]	2.64 [.03]

**Table 6:** CMC is the critical micelle concentration,  $\beta$  is micellar ionization degrees and  $\Delta G_{MC}^{\circ}$  is free energy of micellization.

has been noted for alcohol class I modifiers.<sup>3, 7-15</sup> This may explain the CMC depression seen for 12C4.

In a  $(12C4)_2 + Na^+$  complex,  $Na^+$  is coordinated by eight oxygen atoms of two 12C4 molecules, though these associations are weak.<sup>21</sup> The  $(12C4)_2 + Na^+$  complex would be bulky in comparison to the strongly associated  $MP + Na^+$  typically observed in aqueous solutions for both 15C5 and 18C6.<sup>22-33</sup> Perhaps the  $(12C4)_2 + Na^+$  complex is capable of delocalization and intercalation Baglioni<sup>84</sup> posits explains the observed depression of SDS CMC upon addition of a 15C5 and 18C6.

Once the CMC is reached, and upon formation of micelles, a fraction ( $\beta$ ) of an ionic surfactant's counter-ions (here:  $Na^+$ ) are dissociated from the micelles, leaving the micelles charged.<sup>64, 65</sup> The degree of ionization of a micelle is associated with the hydration of the hydrophilic "head" and the association of counter-ions.<sup>64-66</sup> From the data presented thus far, one would expect the  $\beta$  values for all MPs to be similar. As seen in **Table 6**,  $\beta$  values are nearly statistically equivalent. MP complexation keeps sodium ions at the micelle surface and probably in the Stern layer. As with the CMC data, 12C4 showed similar results to 15C5 and 18C6. This indicates that 12C4 is associated with the micelle surface in an  $MP-Na^+$  complex, perhaps in the form  $(12C4)_2 + Na^+$ .

Using CMC and  $\beta$  values, the Gibbs free energy of micellization ( $\Delta G_{MC}^\circ$ ) for each PSP was calculated using **Equation 7**. From **Table 6**, the addition of MPs to the SDS PSP resulted in more favorable transfers of surfactant monomers from the aqueous phase to the PSP (i.e.,  $\Delta G_{MC}^\circ$  values decreased). This decrease followed the trend  $12C4 < 15C5 < 18C6$ . This result for  $\Delta G_{MC}^\circ$ , along with the CMC and  $\beta$  data, suggests that while the

effect of 12C4 on solute partitioning is less than noted for 15C5 and 18C6 (see sections 4.3.1 and 4.3.2), the effect of 12C4 on the process of micellization is on par with 15 and 18C6. Somewhat in contradiction with previously-published work<sup>37, 51, 85</sup> on 12C4–Na<sup>+</sup> and 12C4–sodium counter-ion surfactants, the data presented here suggest 12C4, upon complexation of Na<sup>+</sup>, is well associated with the micelle surface. The weaker nature of this complex, possibly in the form (12C4)<sub>2</sub> + Na<sup>+</sup>, may explain the minimal impact 12C4 has on solute partitioning, as monitored here using retention (k) data.

#### ***4.4 Conclusion and Future Work***

The work presented in **CHAPTER 3** was the first use of a MP as a class I modifier. This chapter represents, to the author's knowledge, the first time MP modification to a pseudophase has been characterized using LSER and  $\Delta\Delta G_R^\circ$  studies. S. Poole and C. Poole in a recent review<sup>60</sup> of the use of quantitative structure-retention relationships (e.g. LSER) to study the effect of organic solvents and additives by MEKC wrote:

The third category is complex-forming compounds such as cyclodextrins or ligands for metal atoms that have a profound affect on the apparent partition coefficients for the analytes with the micellar pseudophase. Complex-forming interactions involve the use of secondary chemical equilibrium in competition with the solute-micelle equilibrium and allow fine tuning of the selectivity factor. This is one of the main successes of MEKC but beyond the scope of this review.

The solvation parameter model contains no terms to account for these specific interactions. [Poole, S. and Poole, C.<sup>60</sup>, page 16]

Based on the work presented here, LSER is well-suited for characterizing the complex-forming additives 15C5, 18C6 and 12C4. While the mode of micelle interaction the MPs engage in is unique among typical PSP additives<sup>60</sup>, the LSER terms currently in common use are more than adequate to allow characterization of effects by MPs on the PSP.

The effects of MPs studied in this chapter are mainly rooted in electrostatics, which manifest in the SDS PSP's increased ability to interact with solute *n*- or *π*-electrons (polarizability), a decreased micellar surface polarity, an increased micellar H-bond accepting ability and decreased micellar H-bond donating ability. As these effects are differential, depending on the desired results, or system of study, one can select a MP to suit their needs.

This work also showed that though SDS PSP modification by 12C4 has a smaller effect on solute partitioning than modification by 15C5 and 18C6, 12C4 affected micellization to a similar level to 15C5 and 18C6. This may indicate the formation of the previously theorized aqueous phase  $(12C4)_2 - Na^+$ .

Future work should include the use of other macrocycles, including polyethers, in MEKC. Izatt et al. have published cation and anion binding data on hundreds of such compounds<sup>16,17</sup>. As this work illustrates, use of LSER, solute retention (*k*) data, solute transfer free energy of functional group *R* ( $\Delta\Delta G_R^\circ$ ), critical micelle concentration (CMC), micellar ionization degrees ( $\beta$ ) and free energy of micellization ( $\Delta G_{MC}^\circ$ ) analysis are more than capable of robustly categorizing macrocycle modified PSPs.

The unique behavior of cation and anion binding macrocycles in micelle solutions could allow for phase interactions to be examined in greater detail. As surfactants are popular mimic systems for cells and soils<sup>12, 13, 15</sup>, MP (or another relevant macrocycle) PSP CE is a tool researchers could use to probe electrostatics in cell membrane interactions. Crown ether effects on ion transport across cell membranes are well known<sup>18, 86-91</sup>, but the influence of their cation binding ability on the partitioning of organic molecules into cells is a relatively unexplored area<sup>86, 92, 93</sup>.

#### 4.5 References

1. Terabe, S.; Otsuka, K.; Ando, T., *Anal. Chem.* **1985**, *57*, 834-841.
2. Terabe, S.; Otsuka, K.; Ichikawa, K.; Tsuchiya, A.; Ando, T., *Anal. Chem.* **1984**, *56*, 111-113.
3. Camilleri, P., *Capillary Electrophoresis*. 2 ed.; CRC Press: Boca Raton, 1997.
4. Landers, J., *Handbook of Capillary Electrophoresis*. CRC Press: Boca Raton, 1993.
5. Quirino, J.; Terabe, S., *J. Chromatogr. A* **1999**, *856*, 465-482.
6. Altria, K., *Capillary Electrophoresis Guidebook*. Humana Press: Totowa, 1996.
7. Allen, D. J.; Wall, W. E.; Denson, K. D.; Smith, J. T., *Electrophoresis* **1999**, *20* (1), 100-10.
8. Wall, W. E.; Allen, D. J.; Denson, K. D.; Love, G. I.; Smith, J. T., *Electrophoresis* **1999**, *20* (12), 2390-9.
9. Katsuta, S.; Saitoh, K., *J. Chromatogr. A* **1997**, *780*, 165-178.
10. Seals, T., *Chromatographia* **2000**, *51*, 669-680.
11. Seifar, R.; Kraak, J.; Kok, W., *Anal. Chem.* **1997**, *69*, 2772-2778.
12. Elworthy, P.; Florence, A.; Macfarlane, C., *Solubilization by Surface-Active Agents*. Chapman and Hall LTD: London, 1968.
13. Zana, R., *Dynamics of Surfactant Self-Assemblies*. Taylor & Francis: Boca Raton, 2005; Vol. 125.
14. Pascoe, R.; Foley, J. P., *Electrophoresis* **2002**, *23* (11), 1618-27.
15. Rosen, M., *Surfactants and Interfacial Phenomena*. 2 ed.; John Wiley and Sons: New York, 1988.



16. Izatt, R.; Pawlak, K.; Jerald, S., *Chem. Rev.* **1995**, *95*, 2529-2586.
17. Izatt, R.; Bradshaw, J. S.; Nielsen, S.; Lamb, J. D.; Christensen, J., *Chem. Rev.* **1985**, *85*, 271-339.
18. Christensen, J.; Eatough, D.; Izatt, R., *Chem. Rev.* **1974**, *74* (3), 351-384.
19. Frensdorff, H. K., *J. Amer. Chem. Soc.* **1971**, *93* (3), 600-606.
20. Katritzky, A. R.; Malhotra, N.; Ramanathan, R.; Kemerait, R. C.; Zimmerman, J. A.; Eyler, J. R., *Rapid Commun. Mass Spectrom.* **1992**, *6* (1), 25-27.
21. Akutagawa, T.; Hasegawa, T.; Nakamura, T.; Takeda, S.; Inabe, T.; Sugiura, K.-i.; Sakata, Y.; Underhill, A. E., *Inorg. Chem.* **2000**, *39* (12), 2645-2651.
22. Baglioni, P.; Kevan, L., *J. Chem. Soc. Faraday Trans.* **1988**, *84*, 467-472.
23. Evans, D.; Evans, J.; Radha, S.; Warr, G., *J. Phys. Chem.* **1988**, *92*, 784-790.
24. Bakshi, M.; Crisantino, R.; Lisi, R.; Milioto, S., *Langmuir* **1994**, *10*, 423-431.
25. Caponetti, E.; Chillura-Martino, D.; Pedone, L., *Langmuir* **2004**, *20*, 3854-3862.
26. Caponetti, E.; Martino, D.; Floriano, M.; Triolo, R.; Wignall, G., *Langmuir* **1995**, *11*, 2464-2470.
27. Crisantino, R.; De Lisi, R.; Milioto, S.; Pellerito, A., *Langmuir* **1996**, *12*, 890-901.
28. Stilbs, P., *J. Colloid Interface Sci.* **1983**, *94*, 463-469
29. Chillura-Martino, D.; Caponetti, E.; Pedone, L., *J. Appl. Cryst.* **2003**, *36*, 562-567.
30. Evans, D.; Sen, R.; Warr, G., *J. Phys. Chem.* **1986**, *90*, 5500-5502.
31. Loginovaa, L.; Samokhina, L.; Mchedlov-Petrosyan, N.; Alekseevab, V.; Savvina, L., *Colloids Surf. A* **2001**, *193*, 207-219.

32. Myassoedova, T.; Grand, D.; Hauteclouque, S., *J. Photochem. Photobiol. A*. **1992**, *64*, 159-169.
33. Stilbs, P., *J. Colloid Interface Sci.* **1982**, *87*, 385-394
34. Baglioni, P.; Kevan, L., *J. Chem. Soc. Faraday Trans.* **1988**, *84*, 467-472.
35. Taillardat-Bertschinger, A.; Carrupt, P. A.; Testa, B., *Eur. J. Pharm. Sci.* **2002**, *15* (2), 225-34.
36. Sprunger, L.; Acree, W.; Abraham, M., *J. Chem. Inf. Model.* **2007** *47*, 1808-1817.
37. Vikingstad, E.; Bakken, J., *J. Colloid Interface Sci.* **1980**, *74*, 8-15.
38. Seno, M.; Namba, T.; Kise, H., *Bull. Chem. Soc. Jpn.* **1981**, *54*, 2841-2842.
39. Hubbard, A. T., *Encyclopedia of Surface and Colloid Science: Inv-Pol.* Marcel Dekker: 2002.
40. Politzer, P.; Murray, J., *Quantitative Treatments of Solute/Solvent Interactions.* Elsevier: Amsterdam, 1994; Vol. 1, p 368.
41. Bailey, D.; Dorsey, J., *J. Chromatogr., A* **2001**, *919*, 181-194.
42. Vitha, M. F.; Dallas, A. J.; Carr, P. W., *J. Colloid Interface Sci.* **1997**, *187* (1), 179-83.
43. Bui, H.; Masquelin, T.; Perun, T.; Castle, T.; Dage, J.; Kuo, M. S., *J. Chromatogr., A* **2008**, *1206* (2), 186-95.
44. Kamlet, M.; Abboud, J.; Abraham, M.; Taft, R., *J. Org. Chem.* **1983**, *48*, 2877-2887.
45. Yang, S.; Khaledi, M. G., *Anal. Chem* **1995**, *67*, 499-510.

46. Chen, N.; Zhang, Y.; Terabe, S.; Nakagawa, T., *J. Chromatogr., A* **1994**, 678, 327-332.
47. Ahmed, H.; Poole, C. F., *J Chromatogr A* **2006**, 1104 (1-2), 82-90.
48. Poole, S.; Poole, C., *Analyst* **1997**, 122, 267-274.
49. Vitha, M.; Weckwerth, J.; Odland, K.; Dema, V.; Carr, P., *J. Phys. Chem.* **1996**, 100, 18823-18828.
50. Taft, R.; Murray, J., Some Effects of Molecular Structure on Hydrogen-Bonding Interactions. Some Macroscopic and Microscopic Views from Experimental and Theoretical Results. In *Quantitative Treatments of Solute/Solvent Interactions*, Politzer, P.; Murray, J., Eds. Elsevier: Amsterdam, 1994; Vol. 1.
51. Sprunger, L.; Acree, W. E., Jr.; Abraham, M. H., *J. Chem. Inf. Model.* **2007**, 47 (5), 1808-17.
52. Dongbin, W.; Aiqian, Z.; Zhongbo, W.; Shuokui, H.; Liansheng, W., *Ecotoxicol. Environ. Saf.* **2002**, 52, 143-149.
53. Apostoluk, W.; Drzymala, J., *J. Colloid Interface Sci.* **2003**, 262, 483-488.
54. Hickey, J.; Passino-Reader, D., *Environ. Sci. Technol.* **1991**, 25, 1753-1760.
55. Abraham, M.; Chadha, H.; Dixon, J.; Rafols, C.; Treiner, C., *J. Chem. Soc., Perkin Trans. 2* **1995**, 887-894.
56. Abraham, M.; Chadha, H.; Whiting, G.; Mitchell, R., *J. Pharm. Sci.* **1994**, 83, 1085-1100.
57. Abraham, M.; McGowan, J., *Chromatographia* **1987**, 23, 243-246.
58. Koehler, M.; Grigoras, S.; Dunn, W., *Quant. Struct. Act. Relat.* **1988**, 7, 150-159.

59. Hagelin, H.; Murray, J.; Brinck, T.; Berthelot, M.; Politzer, P., *Can. J. Chem.* **1995**, *73*, 483-488.
60. Poole, S.; Poole, C., *J. Chromatogr., A* **2008**, *1182*, 1-24.
61. Fuguet, E.; Ràfols, C.; Bosch, E.; Abraham, M. H.; Rosés, M., *J. Chromatogr. A* **2002**, *942* (1-2), 237-248.
62. Trone, M. D.; Leonard, M. S.; Khaledi, M. G., *Anal. Chem.* **2000**, *72* (6), 1228-1235.
63. Kelly, K. A.; Burns, S. T.; Khaledi, M. G., *Anal. Chem.* **2001**, *73* (24), 6057-6062.
64. Rodríguez, A.; Graciani, M. d. M.; Muñoz, M.; Moyá, M. L., *Langmuir* **2003**, *19* (18), 7206-7213.
65. Bales, B. L., *J. Phys. Chem., B* **2001**, *105* (29), 6798-6804.
66. Evans, H. C., *J. Chem. Soc* **1956**, 579-586.
67. Zana, R., *Langmuir* **1996**, *12* (5), 1208-1211.
68. Burns, S. T.; Khaledi, M. G., *Anal. Chem.* **2004**, *76* (18), 5451-8.
69. Werlich, S.; Andersson, J., *Fresenius J. Anal. Chem.* **1999**, *364*, 3-14.
70. Kelly, K. A.; Burns, S. T.; Khaledi, M. G., *Anal. Chem.* **2001**, *73* (24), 6057-62.
71. Berthod, A.; Mitchell, C. R.; Armstrong, D. W., *J. Chromatogr., A* **2007**, *1166* (1-2), 61-9.
72. Abraham, M., New solute descriptors for linear free energy relationships and quantitative structure-activity relationships. In *Quantitative Treatments of Solute/Solvent Interactions*, Politzer, P.; Murray, J., Eds. Elsevier: Amsterdam, 1994; Vol. 1, pp 83-134.

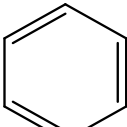
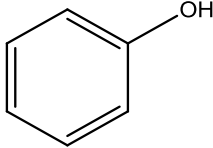
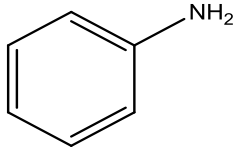
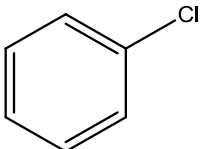
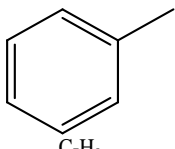
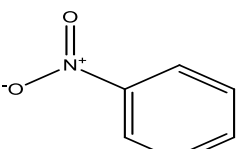
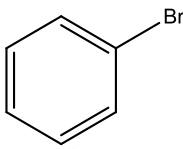
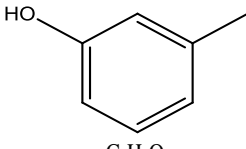
73. Fuguet, E.; Rafols, C.; Bosch, E.; Roses, M., *Electrophoresis* **2002**, *23* (1), 56-66.
74. Cifuentes, A.; Bernal, J.; Diez-Masa, J., *Anal. Chem.* **1997**, *69*, 4271-4274.
75. Rahman, A.; Brown, C., *J. Appl. Polym. Sci.* **1982**, *28*, 1331-1334.
76. Hsiao, C. C.; Wang, T. Y.; Tsao, H. K., *J. Chem. Phys.* **2005**, *122* (14), 144702.
77. Murray, J. S.; Brinck, T.; Politzer, P., *Chem. Phys.* **1996**, *204* (2-3), 289-299.
78. Murray, J. S.; Brinck, T.; Politzer, P., *J. Chem. Phys.* **1993**, *97* (51), 13807-13809.
79. Murray, J. S.; Brinck, T.; Lane, P.; Paulsen, K.; Politzer, P., *J. Mol. Struct.* **1994**, *307*, 55-64.
80. Zou, J.; Yu, Q.; Shang, Z., *J. Chem. Soc., Perkin Trans 2* **2001**, (8), 1439-1443.
81. Tossell, J. A., *J. Chem. Phys., B* **2001**, *105* (45), 11060-11066.
82. Loginovaa, L.; Samokhina, L.; Mchedlov-Petrossyan, N.; Alekseevab, V.; Savvina, L., *Colloids Surf. A* **2001**, *193*, 207-219.
83. McNaught, A. D.; Wilkinson, A., *IUPAC Compendium of Chemical Terminology*. 2 ed.; International Union of Pure and Applied Chemists: Hoboken, 1997.
84. Baglioni, P.; Kevan, L., *J. Chem. Soc., Faraday Trans. 1* **1988**, *84* (2), 467-472.
85. Stilbs, P., *J. Colloid Interface Sci.* **1982**, *87*, 385-394.
86. Boojar, M.; Goodarzi, F., *Clin. Chim. Acta* **2006**, *364*, 321-327.
87. Izatt, R.; Bruening, R.; Clark, G.; Lamb, J.; Christensen, J., *J. Membr. Sci.* **1986**, *28*, 77-86.
88. Arenaz, P.; Bitticks, L.; Pannell, K.; Garcia, S., *Mutagenesis* **1989**, *4*, 437-438.
89. Arenaz, P.; Bitticks, L.; Pannell, K.; Garcia, S., *Mutat. Res.* **1992**, *280*, 109-115.
90. He, G.; Kurita, M.; Ishii, I.; Wada, F.; Matsuda, T., *J. Membr. Sci.* **1992**, *69*, 61-74.

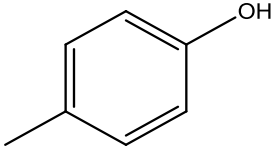
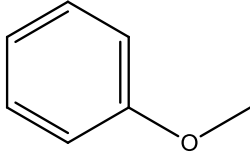
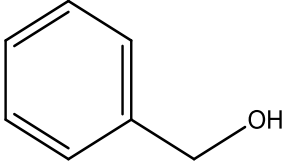
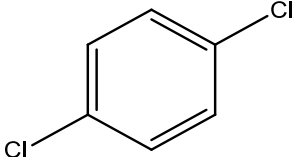
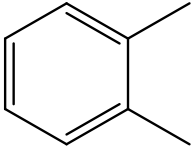
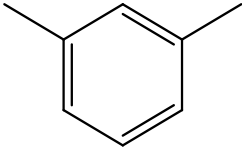
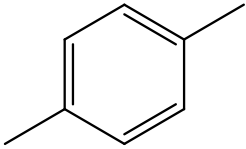
91. Kudo, Y.; Takeda, Y.; Matsuda, H., *J. Electroanal. Chem.* **1995**, 396, 333-338.
92. Darwish, I.; Uchegbu, I., *Int. J. Pharm.* **1997**, 159, 207-213.
93. Muzzalupo, R.; Nicoletta, F.; Trombino, S.; Cassano, R.; Iemma, F.; Picci, N., *Colloids Surf., B* **2007**, 58, 197-202.
94. Lin, C. E., *J. Chromatogr. A* **2004**, 1037 (1-2), 467-78.
95. Lu, Y.; Stellwagen, E.; Stellwagen, N., *Anal. Biochem.* **2004**, 332, 191-192.
96. Nesmerak, K.; Nemcova, I., *Anal. Lett.* **2006**, 39, 1023-1040.
97. Coury, L., *Curr. Sep.* **1999**, 18, 91-96.
98. Evans, H., *J. Chem. Soc.* **1956**, 579 - 586.

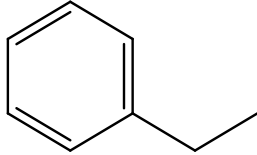
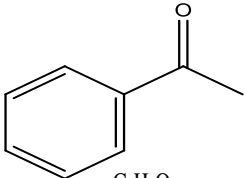
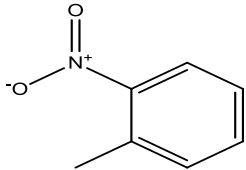
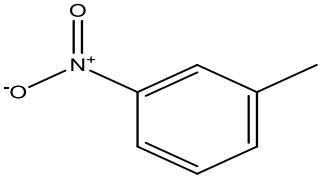
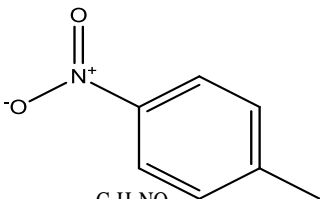
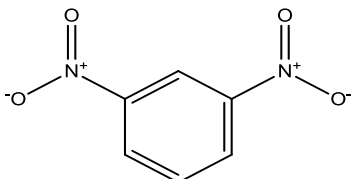
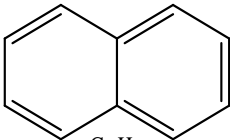
**APPENDIX A**  
**LSEr Solute Descriptors**

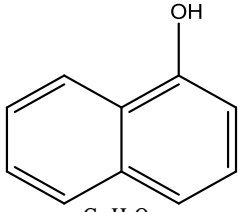
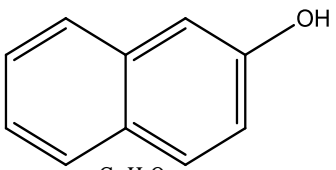
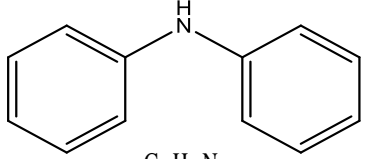
LSER solute descriptors listed in the preceding table were taken from the sources listed in section 4.2.2.



Solute	Structure	Solute descriptors				
		V	S	A	B	E
benzene	 C <sub>6</sub> H <sub>6</sub>	0.716	0.520	0	0.140	0.610
phenol	 C <sub>6</sub> H <sub>6</sub> O	0.775	0.890	0.600	0.300	0.805
phenylamine	 C <sub>6</sub> H <sub>7</sub> N	0.816	0.960	0.260	0.500	0.955
chlorobenzene	 C <sub>6</sub> H <sub>5</sub> Cl	0.839	0.650	0	0.070	0.718
toluene	 C <sub>7</sub> H <sub>8</sub>	0.857	0.520	0	0.140	0.601
nitrobenzene	 C <sub>6</sub> H <sub>5</sub> NO <sub>2</sub>	0.891	1.110	0	0.280	0.871
bromobenzene	 C <sub>6</sub> H <sub>5</sub> Br	0.891	0.730	0	0.090	0.882
3-methylphenol	 C <sub>7</sub> H <sub>8</sub> O	0.916	0.880	0.570	0.340	0.840

Solute	Structure	<i>Solute descriptors</i>				
		V	S	A	B	E
4-methylphenol	 $C_7H_8O$	0.916	0.870	0.570	0.310	0.820
anisole	 $C_7H_8O$	0.916	0.750	0	0.290	0.710
benzyl alcohol	 $C_7H_8O$	0.916	0.870	0.390	0.560	0.803
1,4-dichlorobenzene	 $C_6H_4Cl_2$	0.961	0.750	0	0.020	0.825
1,2-dimethylbenzene	 $C_8H_{10}$	0.998	0.560	0	0.160	0.663
1,3-dimethylbenzene	 $C_8H_{10}$	0.998	0.520	0	0.160	0.623
1,4-dimethylbenzene	 $C_8H_{10}$	0.998	0.520	0	0.160	0.613

Solute	Structure	Solute descriptors				
		V	S	A	B	E
ethylbenzene	 C <sub>8</sub> H <sub>10</sub>	0.998	0.510	0	0.150	0.613
acetophenone	 C <sub>8</sub> H <sub>8</sub> O	1.014	1.010	0	0.480	0.818
2-nitrotoluene	 C <sub>7</sub> H <sub>7</sub> NO <sub>2</sub>	1.032	1.110	0	0.270	0.866
3-nitrotoluene	 C <sub>7</sub> H <sub>7</sub> NO <sub>2</sub>	1.032	1.100	0	0.250	0.874
4-nitrotoluene	 C <sub>7</sub> H <sub>7</sub> NO <sub>2</sub>	1.032	1.110	0	0.280	0.870
1,3-dinitrobenzene	 C <sub>6</sub> H <sub>4</sub> N <sub>2</sub> O <sub>4</sub>	1.060	1.630	0	0.460	1.130
naphthalene	 C <sub>10</sub> H <sub>8</sub>	1.085	0.920	0	0.200	1.340

Solute	Structure	Solute descriptors				
		V	S	A	B	E
1-naphthol	 <chem>Oc1ccc2ccccc12</chem> $C_{10}H_8O$	1.144	1.050	0.600	0.370	1.520
2-naphthol	 <chem>Oc1ccc2ccccc12</chem> $C_{10}H_8O$	1.144	1.080	0.610	0.400	1.520
diphenylamine	 <chem>Nc1ccccc1c2ccccc2</chem> $C_{12}H_{11}N$	1.424	1.320	0.300	0.280	1.470

## **APPENDIX B**

### **Current titration method for the determination of CMC**

In a capillary electrophoresis (CE), the magnitude of the current observed obeys Ohm's Law<sup>4, 74, 94-96</sup>, as given in **Equation 1**.

$$V=IR \quad \text{Equation 1}$$

The term V is the applied voltage, I is the measured current, and R is the resistance of the solution between the inlet and outlet electrodes. The reciprocal of R, conductance, is given by **Equation 2**<sup>95, 97</sup>.

$$\frac{1}{R} = \kappa \frac{\pi r^2}{L_t} \quad \text{Equation 2}$$

Conductivity is denoted by  $\kappa$ , the total length of the capillary is given by  $L_t$ , and r is the radius of the capillary. Combining **Equations 1** and **2** gives **Equation 3**.

$$I = \kappa \frac{V\pi r^2}{l} \quad \text{Equation 3}$$

In CE,  $V/l$  denotes electric field strength<sup>3, 4</sup>, E (V/cm), allowing **Equation 3** to be written as **Equation 3a**.

$$I = \kappa E \pi r^2 \quad \text{Equation 3a}$$

Molar conductivity,  $\Lambda$ , is the solution conductivity ( $\kappa$ ) normalized by the total ionic concentration (C)<sup>97</sup> and is given by **Equation 4**.

$$\Lambda = \frac{\kappa}{C} \quad \text{Equation 4}$$

Substituting **Equation 4** into **Equation 3a** gives **Equation 5**.

$$I = E \Lambda \pi r^2 C \quad \text{Equation 5}$$

For an SDS solution of concentration [SDS], **Equation 5** can be written as **Equation 5a**.

$$I_{\text{SDS soln}} = E\Lambda_{\text{SDS soln}}\pi r^2[\text{SDS}] \quad \text{Equation 5a}$$

Considering **Equation 4**, the molar conductivity of a SDS solution,  $\Lambda_{\text{SDS soln}}$ , can be written as **Equation 6**.

$$\Lambda_{\text{SDS soln}} = \frac{\kappa_{\text{SDS solution}}}{[\text{SDS}]} \quad \text{Equation 6}$$

The conductivity of the SDS solution,  $\kappa_{\text{SDS}}$ , is equal to the sum of conductivity values of relevant species in solution<sup>74, 98</sup>, as illustrated by **Equation 7**.

$$\kappa_{\text{SDS soln}} = \kappa_{\text{monomer}} + \kappa_{\text{Na}^+} + \kappa_{\text{micelle}} \quad \text{Equation 7}$$

Thus, **Equation 6** can be written as **Equation 6a**.

$$\Lambda_{\text{SDS soln}} = \frac{\kappa_{\text{monomer}}}{[\text{SDS}]} + \frac{\kappa_{\text{Na}^+}}{[\text{SDS}]} + \frac{\kappa_{\text{micelle}}}{[\text{SDS}]} \quad \text{Equation 6a}$$

Inserting **Equation 6a** into **Equation 5a** produces the following expression for  $I_{\text{SDS soln}}$  (**Equation 5b**).

$$I_{\text{SDS soln}} = E \left( \frac{\kappa_{\text{monomer}}}{[\text{SDS}]} + \frac{\kappa_{\text{Na}^+}}{[\text{SDS}]} + \frac{\kappa_{\text{micelle}}}{[\text{SDS}]} \right) \pi r^2 [\text{SDS}] \quad \text{Equation 5b}$$

At [SDS] below the critical micelle concentration (CMC), the contribution of the term  $\frac{\kappa_{\text{micelle}}}{[\text{SDS}]}$  to  $I_{\text{SDS soln}}$  is very small<sup>74, 98</sup> and **Equation 5b** can be written as **Equation 5c**.

$$I_{\text{SDS solution}} = E \left( \frac{\kappa_{\text{monomer}}}{[\text{SDS}]} + \frac{\kappa_{\text{Na}^+}}{[\text{SDS}]} \right) \pi r^2 [\text{SDS}] = I_{\text{pre-CMC}} \quad \text{Equation 5c}$$

Alternatively, above the CMC, the contribution of  $\left(\frac{\kappa_{\text{monomer}}}{[\text{SDS}]} + \frac{\kappa_{\text{Na}^+}}{[\text{SDS}]}\right)$  is very small<sup>74, 98</sup>

and  $I_{\text{SDS soln}}$  can be written as **Equation 5d**.

$$I_{\text{SDS soln}} = E \left( \frac{\kappa_{\text{micelle}}}{[\text{SDS}]} \right) \pi r^2 [\text{SDS}] = I_{\text{post-CMC}} \quad \text{Equation 5d}$$

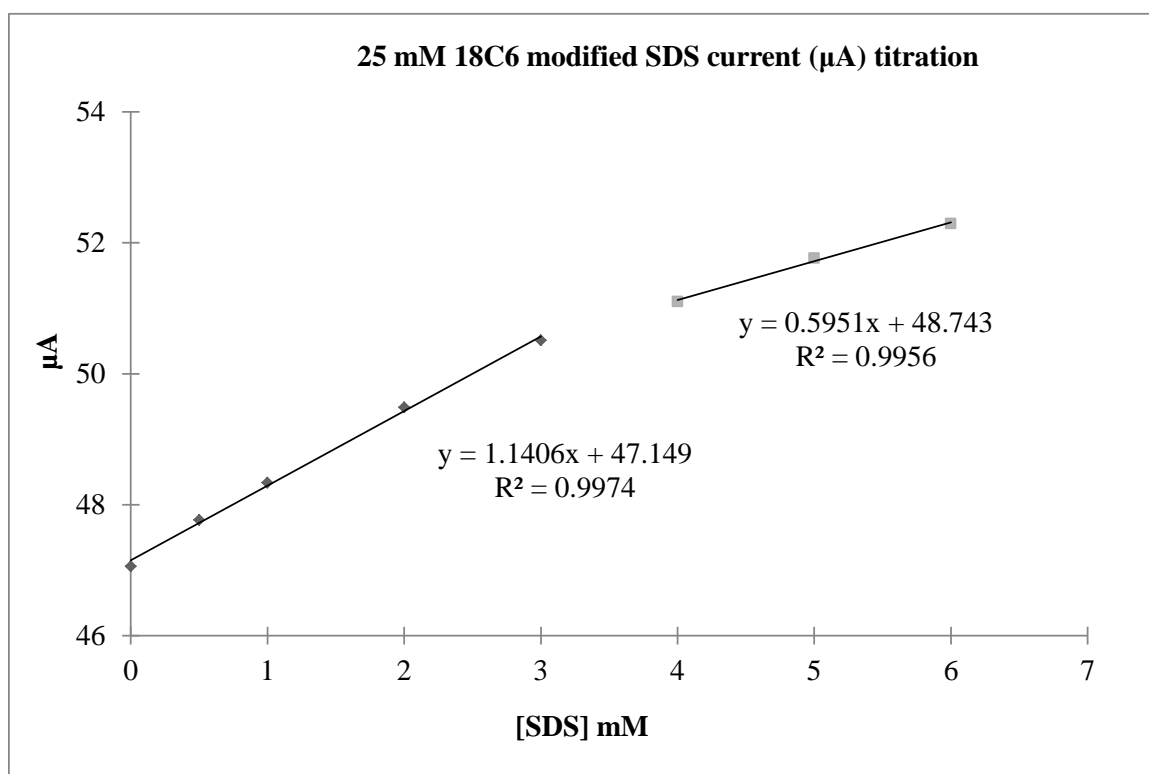
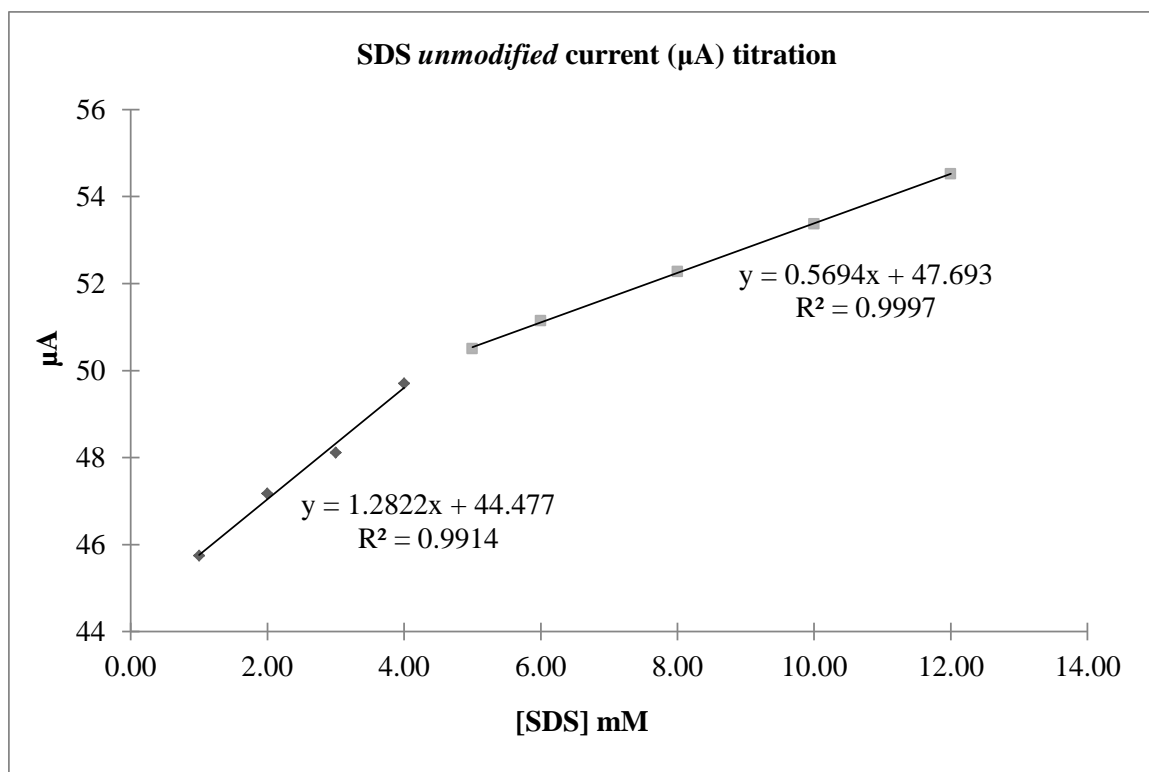
In practice, plotting  $I_{\text{SDS soln}}$  vs.  $[\text{SDS}]$  reveals a sharply increasing slope up to the CMC and a “slower” increasing slope after the CMC due to changes in conductivity with  $[\text{SDS}]$ . The conductivity of a SDS solution pre-CMC increases over the  $[\text{SDS}]_{<\text{CMC}}$  range yet decreases over the range  $[\text{SDS}]_{>\text{CMC}}$  such that the slope of  $I_{\text{pre-cmc}}$  vs.  $[\text{SDS}]_{<\text{CMC}}$  is greater than  $I_{\text{post-CMC}}$  vs.  $[\text{SDS}]_{>\text{CMC}}$ . The ordered structure of the anionic micelle, where approximately half of the surfactants counterions (e.g.  $\text{Na}^+$ ) are localized to the Stern layer and the other half distributed in the Gouy-Chapman region, translates into an increased resistance to migration by the micelle explaining the conductivity decrease for SDS solutions above the CMC<sup>74, 96, 98</sup>.

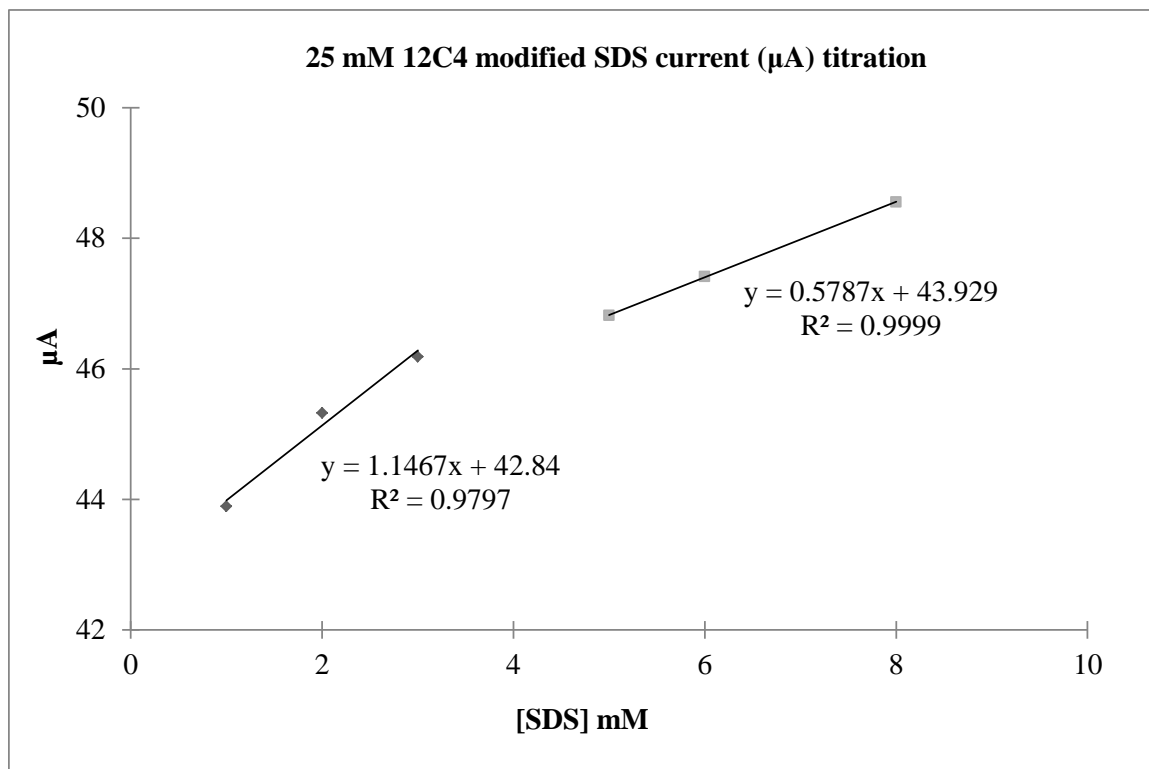
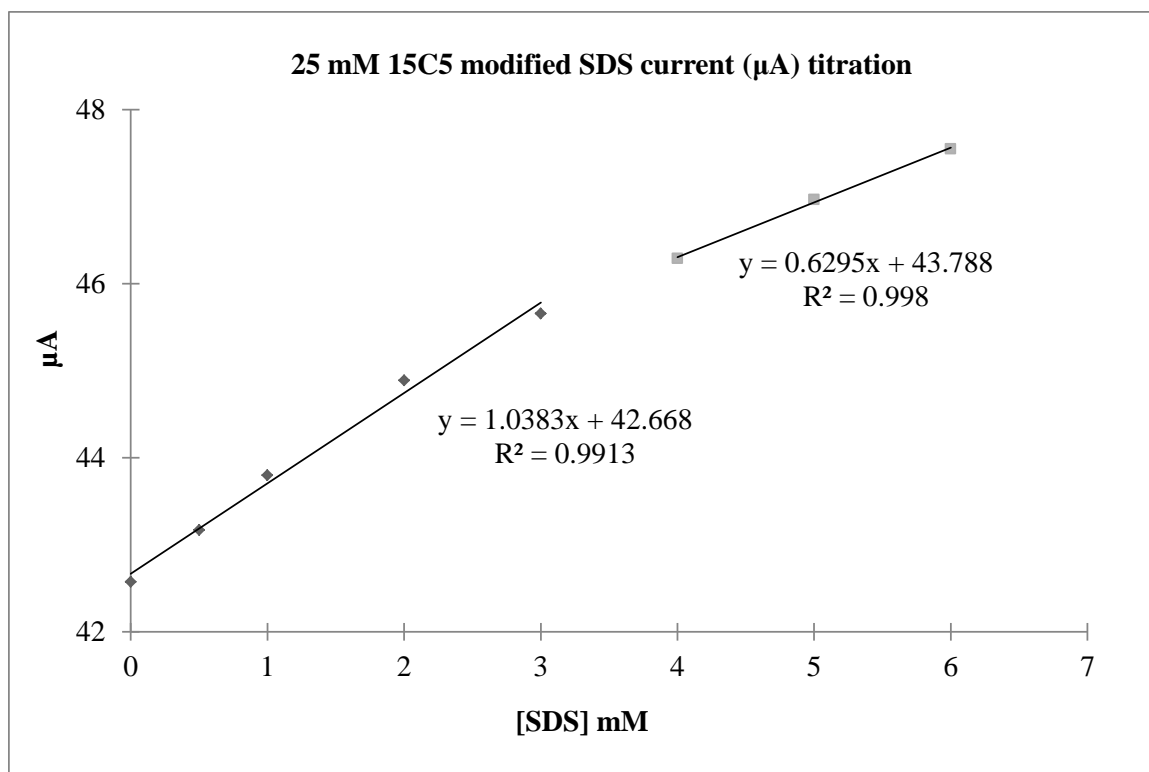
Conductivity has been utilized for nearly 100 years to study surfactant solution behavior<sup>12, 15, 98</sup>, with simple  $[\text{surfactant}]$  vs.  $\kappa$  or  $I$  plots readily revealing the monomer-to-micelle transition region.<sup>74</sup> This region is called, somewhat erroneously, *the CMC*<sup>12, 13, 15, 98</sup>. As detailed above, two linear curves of different slopes are easily seen in  $[\text{surfactant}]$  vs.  $\kappa$  or  $I$  plots when the  $[\text{surfactant}]$  range encompassing several points above and below the CMC. To determine the CMC, the linear trend line equations are determined for both curves. The intersection of these two lines gives the CMC.



## **APPENDIX C**

### **Current titration data for the determination of CMC**





**APPENDIX D****Influence of MPs on  $\Delta\Delta G_R^\circ$**

Influence of MPs on solute $\Delta\Delta G_R^\circ$ values						
Solute	<i>R</i>	$\Delta\Delta G_R$ (kJ/mol)				
		35 mM SDS <i>unmodified</i>	35 mM SDS 25 mM 18C6	35 mM SDS 25 mM 15C5	35 mM SDS 25 mM 12C4	
phenylamine	NH <sub>2</sub>	1.86 [.03]	2.40 [.05]	2.53 [.04]	1.97 [.10]	
toluene	CH <sub>3</sub>	-2.63 [.04]	-2.52 [.05]	-2.56 [.05]	-2.64 [.11]	
ethylbenzene	CH <sub>2</sub> CH <sub>3</sub>	-4.89 [.02]	-4.83 [.04]	-4.88 [.04]	-4.92 [.09]	
nitrobenzene	NO <sub>2</sub>	-0.70 [.03]	-0.65 [.05]	-0.58 [.06]	-0.73 [.12]	
phenol	OH	1.27 [.02]	0.98 [.05]	1.13 [.08]	0.94 [.10]	
anisole	OCH <sub>3</sub>	-1.39 [.03]	-1.13 [.13]	-1.11 [.08]	-1.41 [.11]	
acetophenone	C(=O)CH <sub>3</sub>	-1.52 [.02]	-0.30 [.06]	0.03 [.06]	-1.02 [0.15]	
benzyl alcohol	CH <sub>2</sub> OH	1.35 [.02]	2.23 [.22]	2.40 [.04]	1.52 [.09]	
bromobenzene	Br	-4.18 [.02]	-4.44 [.16]	-4.68 [.06]	-4.52 [.09]	
chlorobenzene	Cl	-3.28 [.03]	-3.52 [.22]	-3.82 [.05]	-3.63 [.13]	

Table 1: The term  $\Delta\Delta G_R^\circ$  is the solute transfer free energy of functional group *R*, calculated using **Equation 6**.. Beneath each  $\Delta\Delta G_R^\circ$  value is the calculated standard deviation in brackets.

## CHAPTER 5

### CURRENT TRENDS PEROXIDE-BASED EXPLOSIVES DETECTION

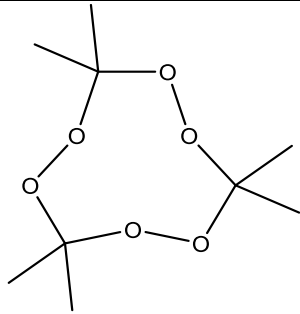
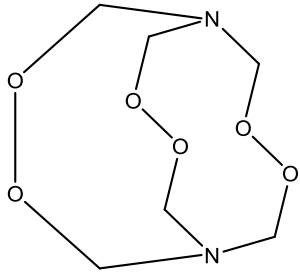
#### *5.1 Introduction*

Triacetone triperoxide (TATP) and hexamethylene triperoxide diamine (HMTD) were first synthesized in the 1880s using simple recipes calling for just three ingredients – hydrogen peroxide, an acid, and acetone (TATP) or hexamine (HMTD).<sup>1-6</sup> In the intervening years, these peroxide-based explosives (PBEs) have seen little-to-no military or civilian use due to their extreme sensitivity to mechanical stress, limited stability, high volatility and lower explosive power compared to easier-to-handle nitro-based explosives.<sup>3, 5, 7-14</sup> Nitro-based explosives such as trinitrotoluene (TNT) may be more powerful, but the intensity of PBE explosions is substantial and destructive.<sup>7, 8</sup> Their power, along with their simple synthesis from readily available materials, has led to the increased use of PBEs in improvised explosive devices (IEDs) for criminal and terrorist activities.

Terrorist attacks using PBEs first occurred in Israel in 1980.<sup>15</sup> However, PBE detection methods have received little attention prior to a series of high-profile terrorist plots in the last decade. These plots included an attempt on American Airlines transatlantic flight 63 using a PBE IED, the Casablanca explosions in 2003, the 2005 London public transportation attacks and a UK transatlantic flight bombing attempt in

2006. These events made the fast and reliable detection of PBEs and their precursors a research priority.<sup>8, 16-20</sup> Designing a detection scheme for PBEs is no easy task given their sensitivity to mechanical stress and low stability, lack of UV absorbance or fluorescence, and limited solubility.<sup>2, 5, 7, 8, 12, 21, 22</sup> These challenges have been recently overcome; today there is an array of techniques for the quick and reliable detection of PBEs, their precursors and degradation products.<sup>8, 9, 18, 23-26</sup>

The journal of *Analytical and Bioanalytical Chemistry* (ABC) reviewed PBE detection in 2006<sup>8</sup>, providing an excellent overview of established and new methods. This chapter, recently published in ABC as a review article, focuses on PBE detection trends that have appeared over the last three years or work that was not included in the journal's previous review. This chapter is organized by detection mode and includes work focused on the two most commonly encountered PBEs (i.e., TATP and HMTD) along with their precursors and degradation products. The structures of TATP and HMTD, along with key properties of these explosives, are given in **Table 1**. Select methods targeting hydrogen peroxide in explosives have also been included because hydrogen peroxide is a precursor and degradation product for TATP and HMTD and is also used in IEDs.<sup>15</sup> **Table 2** summarizes the PBE detection techniques that are highlighted in this review.

		
	TATP	HMTD
Formula	$C_9 H_{18} O_6$	$C_6 H_{12} N_2 O_6$
F.W. (g/mol)	222.24	208.17
<sup>a</sup> Melting point (°C)	96	148
<sup>a</sup> Density (g mL <sup>-1</sup> )	1.2	1.6
<sup>b</sup> Vapor Pressure (Pa)	7.87	*
<sup>b</sup> Enthalpy of sublimation (kJ mol <sup>-1</sup> )	73	*
<sup>a</sup> Detonation velocity (km s <sup>-1</sup> )	5.3	5.1
<sup>a</sup> TNT equivalence	88%	60%
<sup>c</sup> TNT Vapor Pressure (Pa)	0.00173	-

**Table 1:** Key physical and chemical properties of TATP and HMTD. <sup>a</sup>The melting points, densities, detonation velocities, and TNT equivalence data were taken from Ref. [7]. TNT equivalence compares blast over pressure or impulse of the explosive of interest to a similar amount of TNT. <sup>b</sup>TATP vapor pressure and enthalpy of sublimation were acquired from [76]. (\*)From Ref. 76, the authors found these values for HMTD could “not determined, due to reduced thermal stability and vapor phase decomposition.”



**Table 2:** Detection methods highlighted in this chapter. <sup>a</sup>Method references. <sup>b</sup>A check mark in the PBE column denotes the method directly monitors PBEs. <sup>c</sup>In the H<sub>2</sub>O<sub>2</sub> column, a check mark corresponds to simple H<sub>2</sub>O<sub>2</sub> monitoring. <sup>c</sup>A check mark with notation indicates the method indirectly directs PBE by first producing H<sub>2</sub>O<sub>2</sub> by photodecomposition ( $\checkmark_{UV}$  or  $\checkmark_{laser}$ ), PBE acid digest ( $\checkmark_{H^+}$ ) or low pH ( $\checkmark_{pH}$ ).

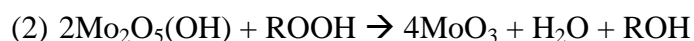
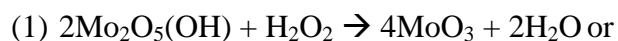
<sup>a</sup> Method	<sup>b</sup> PBE	<sup>c</sup> H <sub>2</sub> O <sub>2</sub>	Detection scheme	LOD
<i>Luminescence</i>				
[27]		√	LG/PVA $\xrightarrow{\text{H}_2\text{O}_2}$ LGDP/PVA	< 1% wt H <sub>2</sub> O <sub>2(g)</sub>
[28]	√	√	6Mo <sub>2</sub> O <sub>5</sub> (OH) $\xrightarrow{\text{TATP}}$ 12MoO <sub>3</sub> + 3H <sub>2</sub> O + (CH <sub>3</sub> ) <sub>2</sub> CO	Qualitative 300 ppm (10 min) H <sub>2</sub> O <sub>2(g)</sub>
[29]		√	PolyF – 1 $\xrightarrow{\text{H}_2\text{O}_2}$ fluorescein	30 ppm (30 sec) H <sub>2</sub> O <sub>2(l)</sub> 1 ppm (5 min) H <sub>2</sub> O <sub>2(l)</sub>
[30]		√ <sub>H<sup>+</sup></sub>	H <sub>2</sub> (Salen) $\xrightarrow{\text{H}_2\text{O}_2, \text{Zn}^{\text{II}}}$ Zn(Salen)	10 nM TATP
[31]		√ <sub>UV</sub>	pyrene sulfoxides $\xrightarrow{\text{H}_2\text{O}_2}$ pyrene sulfones	100 nmol TATP
[32]	√	√	trimeric SID $\xrightarrow{\text{H}_2\text{O}_2}$ 3 fluophore reporters	1 μM H <sub>2</sub> O <sub>2</sub> ~ μg TATP
[33]		√	nano – CRET $\xrightarrow{\text{H}_2\text{O}_2}$ nano – CRET + λ	qualitative
<i>IR and Raman Spectroscopy</i>				
[37]		√	Gas phase FTIR with PLS-DA	qualitative
[35]		√	FTIR, GC-FTIR and Raman microscopy	qualitative
[43]		√	hollow fiber MIR QCL gas sensor	240 ng TATP
[42]			hollow fiber or open path MIR QCL gas sensor	TATP low ng (fiber) 5 ppm per meter (open)
[17, 44]		√	MIR QCL device (walkthrough portal)	15 ppb H <sub>2</sub> O <sub>2</sub>
[41]		√	fiber coupled MIR QCL device (handheld)	qualitative
[45]		√	IR QCL-PAS	18 ppb TATP 3 ppb acetone
[47]		√	Raman field portable device (FirstDefender, Ahura Scientific)	qualitative
[50]		√	Raman microscopy	qualitative
[52]		√	SERS	1 pg HMTD

<i>Mass spectrometry</i>			
[57]	√	IMS (ItemiserFX, General Electric)	1.9 μg TATP (E-mode) 0.8 μg TATP (N-mode)
[58]	√	<i>aspiration</i> IMS (ChemPro100i, Environics)	low mg m <sup>-3</sup> TATP
[19]	√	headspace GC-MS	< 0.1 ng TATP
[59]	√	SPME GC-MS	5 ng TATP
[60]	√	CH <sub>4(g)</sub> and NH <sub>3(g)</sub> GC/PICI-MS or GC/NICI-MS, EI-MS	50 pg – 2 ng TATP
[53]	√	Na <sup>+</sup> adduct ESI-MS	62.5 ng TATP
[63]	√	Alkali metal adduct $\left\{ \begin{array}{l} \text{DESI-MS} \\ \text{DAPCI-MS} \end{array} \right.$	low ng TATP or HMTD
[64]	√	API TOF MS (AccuTOF DART, JEOL USA)	qualitative
[65]	√	<i>laser</i> TOF MS	qualitative
[66]	√	<i>laser</i> SPI TOF MS	low ppb TATP
<i>Electrochemical</i>			
[68, 70]	√ <sub>UV</sub> √ <sub>laser</sub> √ <sub>H<sup>+</sup></sub>	H <sub>2</sub> O <sub>2</sub> $\xrightarrow{\text{PB-electrode}}$ 2HO <sup>-</sup>	250 nM TATP (UV) 300 nM HMTD (UV) 50 nM TATP (laser) 55 nM TATP (H <sup>+</sup> )
[16, 71]	√ <sub>H<sup>+</sup></sub> √ <sub>pH</sub>	H <sub>2</sub> O <sub>2</sub> /ROOH $\xrightarrow[\text{GC-Electrode}]{\text{Fe}^{\text{II/III}}\text{EDTA}}$ HO <sup>-</sup> /RO <sup>-</sup> + HO <sup>•</sup>	890 nM TATP (H <sup>+</sup> ) 30 μM HMTD (pH)
[72]	√	MPC chemiresistor	50 ppb – 40.1 ppm H <sub>2</sub> O <sub>2</sub>
<i>Other Methods</i>			
[73]	√	HPLC-IR	1 mM TATP 0.5 mM HMTD
[74]	√	field portable GC (zNose, Electronic Sensor Technology)	low pptz TATP
[75]	√	differential scanning μCal	qualitative

## 5.2 Luminescence Methods

Presumptive tests based on changes in color, fluorescence changes or chemiluminescence can provide quick and reliable results for a variety of target analytes. Such luminescence-based methods were reviewed previously in this journal for explosives detection<sup>9</sup>. The methods presented here were recently introduced and targeted PBEs and/or the precursor hydrogen peroxide ( $\text{H}_2\text{O}_2$ ). Seeking to easily detect  $\text{H}_2\text{O}_2$  through a simple color test, Mills et al. encapsulated the triarylmethane dye lissamine green (LG) in polyvinyl alcohol (PVA) to monitor the bleaching of LG by  $\text{H}_2\text{O}_2$ .<sup>27</sup> Experiments in solution showed that  $\text{H}_2\text{O}_2$  bleaching of LG through rapid oxidative degradation is slow at pH values significantly below the  $\text{pK}_a$  of  $\text{H}_2\text{O}_2$  (11.75). However, by placing LG in a largely neutral polymeric environment, this dye is made particularly vulnerable to oxidative bleaching by  $\text{H}_2\text{O}_2$  vapor. When blue-green LG/PVA films cast on glass discs were placed above 50% (w/w) aqueous  $\text{H}_2\text{O}_2$  solutions, significant bleaching was observed in less than 5 min. Adjusting the film thickness did allow bleaching of LG/PVA by vapors above a 1% (w/w)  $\text{H}_2\text{O}_2$  solution. While the exact bleaching mechanism is unknown, it is known that the bleaching is due to degradation of LG and the mechanism is probably similar to the  $\text{H}_2\text{O}_2$  induced oxidative degradation of another triarylmethane dye, phenolphthalein. Specificity was a problem with LG/PVA films, as researchers noted other volatile strong oxidizing agents such as ozone, chlorine and nitrogen dioxide all produced bleaching. The authors stated that though this trait is undesirable, LG/PVA films were found to be rapid sensors for strong oxidizing agents with applications to PBE detection.<sup>27</sup>

In an interesting use of nanomaterials for PBE detection, Apblett et al. used molybdenum hydrogen bronze (MoHB) to detect and deactivate TATP.<sup>28</sup> Due to its high acidity and metallic properties, MoHB (formula,  $2\text{Mo}_2\text{O}_5(\text{OH})$ ) is capable of shuttling electrons and protons to peroxide- and nitro-based explosives, leading to their decomposition to non-explosive compounds. Researchers added a suspension of MoHB in butanol, which was dark blue in color, to solid TATP, TATP in toluene, or water. The reaction between TATP and MoHB was found to lead to the disappearance of the suspension's blue color. Excess TATP resulted in a yellow color due to the formation of peroxo complexes of molybdenum. This reaction and its accompanying color changes were dramatic enough to run as a titration, with a persistent blue color of the sample solution marking the endpoint. Researchers also made test strips using this reaction, noting that exposure to either TATP or  $\text{H}_2\text{O}_2$  vapors rapidly bleached the blue color. This reaction was noted to be general in nature, occurring between  $\text{H}_2\text{O}_2$  or ROOH and MoHB as detailed in Eqns (1) and (2).



Concerning the specific reactions between MoHB and TATP, analysis by gas chromatography-mass spectrometry (GC-MS) of the headspace above the reaction mixture confirmed that the main ROH species formed was acetone. Given the common response of this method using either  $\text{H}_2\text{O}_2$  or TATP, along with clear indication that other organic peroxides can produce the same color change, there is a clear possibility of false

positives in this approach. The limit of detection (LOD) for this method was also not addressed.<sup>28</sup>

Another assay easily integrated into a test strip format is the fluorimetric method introduced by Sanchez and Trogler.<sup>29</sup> This method targeted H<sub>2</sub>O<sub>2</sub> vapor and liquid because it was noted that residual H<sub>2</sub>O<sub>2</sub> may be present in bulk TATP and HMTD, with H<sub>2</sub>O<sub>2</sub> being both a PBE precursor and degradation product. After synthesizing the polymer poly-3',6'-bis(1,3,2-dioxaborinane)fluoran (PolyF-1), thin films were fabricated by drop-casting the polymer onto thin sheets of filter paper (4 cm<sup>2</sup>). Exposure of PolyF-1 to H<sub>2</sub>O<sub>2</sub> led to oxidation of the polymer and formation of fluorescein for use in detection, as shown in **Figure 1**. This method had a LOD for H<sub>2</sub>O<sub>2</sub> vapors of 300 ppm with a 10 min PolyF-1 exposure time (note: the LOD dropped with increased exposure time). For liquid H<sub>2</sub>O<sub>2</sub>, a 30 sec Poly-1 exposure time gave an LOD of 30 ppm, and 5 min of exposure gave an LOD of 1 ppm. It was stated in this report that the specificity of boronic esters toward H<sub>2</sub>O<sub>2</sub> oxidation makes PolyF-1 a highly sensitive and selective sensor for H<sub>2</sub>O<sub>2</sub>. The use of PolyF-1 under ambient conditions and under UV light showed little response by PolyF-1 to radical oxygen species and other oxidants found in the atmosphere or generated by a UV lamp ( $\lambda = 302$  nm). The authors suggested that the lower vapor pressure of organic peroxides relative to H<sub>2</sub>O<sub>2</sub> precludes their possible interference. Previous solution phase studies also showed little to no response resulted from exposure to liquid interferents.<sup>29</sup>

A fluorescence detection method by Germain and Knapp also targeted H<sub>2</sub>O<sub>2</sub> by using a chelator formed by reaction with hydrogen peroxide.<sup>30</sup> Taking advantage of the ability of H<sub>2</sub>O<sub>2</sub> to convert C-B bonds to C-O bonds, these researchers designed a

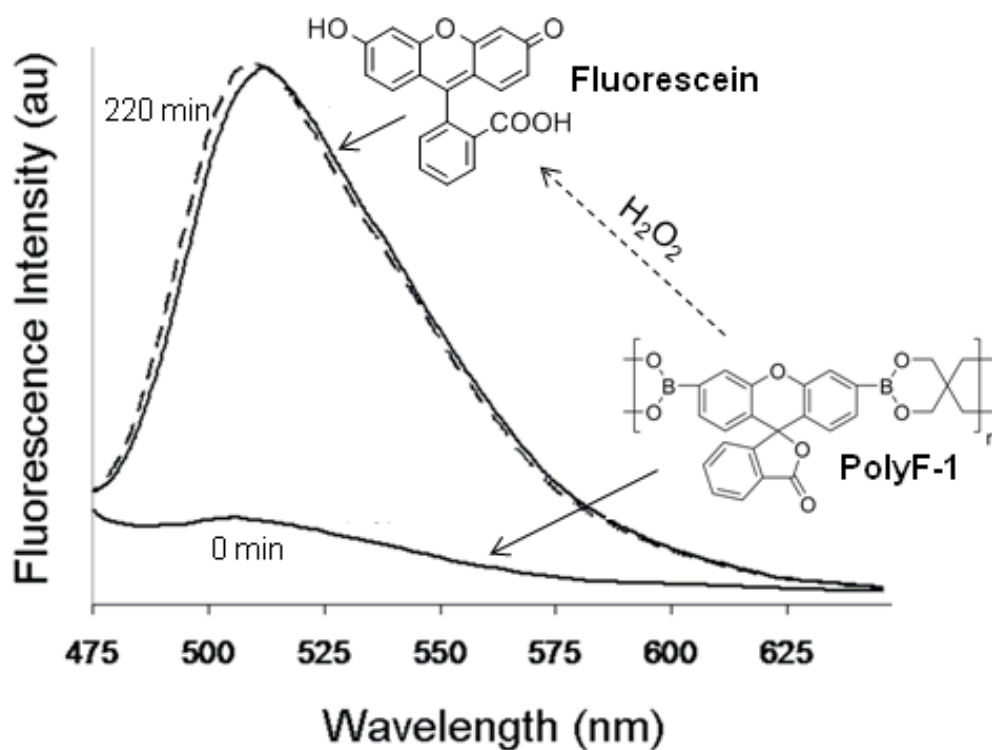


**Figure 1** Polymer based H<sub>2</sub>O<sub>2</sub> sensor [29]. Fluorescence response of a 10  $\mu\text{g cm}^{-2}$  film of PolyF-1 to 2.9 ppm H<sub>2</sub>O<sub>2</sub> vapor. Solid line at 0 min represents the baseline fluorescence intensity of the PolyF-1 film. The dashed line represents the fluorescence emission of 10  $\mu\text{g cm}^{-2}$ . Figure provided by W. Trogler

boronated prochelator that is easily converted to the chelator H<sub>2</sub>Salen [*N,N'*-ethylenebis(salicylaldehyde)] by means of H<sub>2</sub>O<sub>2</sub> deboration. This reaction is easily monitored; the addition of H<sub>2</sub>O<sub>2</sub> to a methanol solution of prochelator and Zn(acetate)<sub>2</sub> results in a fluorescence signal with maximum emission at 440 nm. The LOD for H<sub>2</sub>O<sub>2</sub> in this method was below 10 nM. Substituting benzoyl peroxide for H<sub>2</sub>O<sub>2</sub> gave a similar fluorescence response. TATP solicited no such response, indicating TATP could not deborate the prochelator. TATP was also subjected to acid digest using 1 M acetic acid to produce H<sub>2</sub>O<sub>2</sub>, giving an 80-fold increase in fluorescence signal relative to the standard prochelator/Zn<sup>2+</sup> solution. The authors suggested that benzoyl peroxide was hydrolyzed by the low levels of water present in the reaction mixture but that, overall, organic peroxides would not result in fluorescence for this method.<sup>30</sup>

Malashikhin and Finney also took advantage of fluorescence detection by investigating the use of various sulfur-containing pyrene derivatives in the presence of methyltrioxorhenium as visual sensors for TATP.<sup>31</sup> These researchers settled on the oxidation of pyrene sulfoxides to sulfones, based on their observation that these reactions gave the greatest fluorescence signal compared to other sulfur oxidation reactions. TATP did not react directly with the pyrene sulfoxide profluorophores that were tested, but rapid oxidation was achieved using the H<sub>2</sub>O<sub>2</sub> produced through UV irradiation of TATP. The resulting pyrene sulfones displayed a 5-fold increase in fluorescence after 15 min of reaction relative to the profluorophores. A 90 min reaction gives a fluorescent signal visible to the naked eye for 100 nmol TATP that had been subjected to UV irradiation. It was noted that oxidants such as tert-butyl hydroperoxide, NaOCl, LiClO<sub>4</sub>, K<sub>2</sub>Cr<sub>2</sub>O<sub>7</sub> and air did not appreciably react with their profluorophores while KMnO<sub>4</sub> did undergo such a



reaction. While the profluorophores were stable in visible light, they were not stable with prolonged exposure to UV irradiation.

A shift in fluorescence, rather than the generation of fluorescence, was used in a  $\text{H}_2\text{O}_2$  method employing self-immolative dendrimers (SID) that was designed by Sella and Shabat.<sup>32</sup> SIDs are unique molecules that upon a single activation event will self-eliminate their end-groups; this process leads to complete dissociation of the dendrimer into separate building blocks. A fluorescent trimeric SID was synthesized that contained an aryl borate ester, a functionality that reacts with  $\text{H}_2\text{O}_2$  under mild alkaline conditions ( $\text{NaHCO}_3$ , pH 8.3). Such a reaction begins a series of self-elimination events that causes the trimeric SID to release three “reporter” units. The release of reporter units red-shifts the fluorescence signal of the SID from a maximum emission of 450 nm to 510 nm. An LOD of 1  $\mu\text{M}$  was reported for  $\text{H}_2\text{O}_2$  when using this approach. These SID probes were also reactive with TATP under alkaline conditions, with detection being possible in the  $\mu\text{g}$  range. Reaction times ranged from 90 min (for  $\text{H}_2\text{O}_2$ ) to 120 min (for TATP).

A second  $\text{H}_2\text{O}_2$  assay employing nanomaterials was a chemiluminescent nanoreactor (nano-CRET) method introduced by Wingert and colleagues.<sup>33</sup> Hollow calcium phosphate (CaP) nanoshells were fabricated by coating a phospholipid liposome with a nanometers-thick layer of CaP. Encapsulated inside these nanoshells was a fluorescein-enhanced chemiluminescent luminol system with haematin. Incoming  $\text{H}_2\text{O}_2$  reacted with luminol, generating excited intermediates. A portion of these intermediates produced chemiluminescence at 425 nm, while others engaged in Förster resonance energy transfer (FRET) with fluorescein molecules and produced fluorescence that was observed at 525 nm. Compared to the same chemiluminescent reaction in bulk solution,

the efficiency of light production was increased by using the nano-CRET method due to the improved proximity of reactive species. Use of simple micelles and liposomes gave a similar improvement in light production efficiency; however, the researchers sought to limit interferences by organic molecules by restricting entry into their liposome through the use of a CaP shell. The assay time was not explicitly stated in this report and the authors stated that quantitative determination of LODs is currently underway.<sup>33</sup> A new luminol chemiluminescence based assay for the indirect detection of PBEs is presented in **CHAPTER 6**. This assay uses the Radziszewski reaction to generate singlet oxygen from acetonitrile and H<sub>2</sub>O<sub>2</sub> produced via acid digest of PBE. Singlet oxygen reacts with luminol, producing light easily seen by the naked eye at low concentrations of H<sub>2</sub>O<sub>2</sub> (µg/mL) and small milligram amounts of PBEs (≤ 10 mg).

### ***5.3 Infrared and Raman Spectroscopy***

One of the first analytical methods used to characterize and detect TATP or HMTD was IR spectroscopy.<sup>4,8</sup> IR and Raman spectroscopy are classic tools for the analysis of “unknowns”, in spite of the challenges presented by mixtures. Both IR and Raman have been used to identify and characterize PBEs, along with related compounds.<sup>2, 8, 22, 34-36</sup> Gas phase IR and Raman spectroscopy is especially well-suited to PBE detection given the relatively high vapor pressure of PBEs (**Table 1**), which often means no sample preparation is required for this type of analysis. Hernández-Rivera and colleagues used IR and Raman spectroscopy to study PBEs, their precursors and by-products, as well as structurally-similar compounds.<sup>24, 35, 37-40</sup> Recently, an IR spectra

pattern recognition process was created based on partial least squares regression with discriminant analysis (PLS-DA).<sup>37</sup> In-flow gas phase IR was used to generate spectra for TATP and select nitro-based explosives in the near-IR (NIR) and mid-IR (MIR). Solid explosives, ranging  $100 - 300 \mu\text{g cm}^{-2}$ , were deposited in a chamber subject to air flow ranging from  $80 - 120 \text{ mL min}^{-1}$  and various temperatures. Researchers found that the NIR region offered statistically significant differences for identifying explosives in air. No LODs were explicitly stated.

GC/FTIR, FTIR and Raman microscopy were used to characterize and differentiate a collection of cyclic organic peroxides.<sup>35</sup> TATP, diacetone diperoxide (DADP), tetracetone tetraperoxide (TRARP), were synthesized in-house and analyzed to determine IR and Raman differences for such similar peroxides. Differences were found in Raman and IR spectroscopy for the  $\nu(\text{O-O})$ ,  $\nu(\text{C-O})$ ,  $\delta(\text{CH}_3\text{-C})$  and  $\delta(\text{C-O})$  bands. Though all cycloperoxides studied had a Raman signature with the  $\nu(\text{O-O})$  vibration, researchers found that this band could be used to determine if a dimer or trimer of a peroxide (e.g. DADP vs. TATP) was present. LOD values were not reported in this paper.<sup>35</sup>

Oxley et al. sought to identify IR or Raman spectral lines of high intensity in regions clear of peaks resulting of atmospheric species.<sup>34</sup> This research identified such clear “windows” at  $909 - 1333$ ,  $2083 - 2273$  and  $2381 - 2630 \text{ cm}^{-1}$  and set out to explore PBE and related compound vibrations in these areas. Researchers found that for these windows, there are no unique spectral features allowing for PBE differentiation with a broad spectral region required to make reliable PBE identifications. This work was qualitative in nature with no LOD explicitly stated.<sup>34</sup>

Focus on the MIR region and use of quantum cascade lasers (QCLs) has resulted in collection methods for trace detection of PBE vapor. Explosives show strong and distinct absorption bands in the MIR region of 5 -10  $\mu\text{m}$  (or 2000 – 1000  $\text{cm}^{-1}$ ); this feature makes quick and sensitive probing of PBEs possible through the use of QCLs.<sup>41, 42</sup> Lambrecht and colleagues used hollow fibers as compact infrared gas sensors and monitored the QCL MIR light absorption by TATP.<sup>43</sup> This analysis took only seconds to conduct and gave an LOD of approximately 10 g/L or 240 ng. Recently, this group extended its investigation of hollow fiber-QCL for standoff and extractive TATP detection, in addition to open path QCL.<sup>42</sup> For hollow fiber detection, the LOD was in the low nanogram range. A LOD of 5 ppm per meter was achieved for open path experiments in a laboratory setting, but it was noted that a lower LOD would be required for realistic standoff measurements. QCL based systems are making impressive gains in the area of PBE detection in high traffic areas such as airports and train stations. Ongoing research at Cascade Technologies (Stirling, Scotland) has focused on a walkthrough portal using a quasi-continuous wave (CW) intra-pulse QCL regime for the fast and reliable detection of explosive precursors such as ammonia and  $\text{H}_2\text{O}_2$ .<sup>17, 44</sup> This portal has fans to create air flow across the walkway and IR spectra are collected in milliseconds. Researchers reported an LOD of 15 ppb for  $\text{H}_2\text{O}_2$  in this approach.

For close-up monitoring of suspicious materials, Schade et al. designed a handheld sensor employing a fiber coupled CW distributed feedback (DFB) – QCL ( $\lambda = 1235.1$  and  $1245.3 \text{ cm}^{-1}$ ). This sensor, shown in **Figure 2**, was utilized for the detection of TATP in ambient air.<sup>41</sup> This sensor was placed about 1 cm above a few milligrams of TATP under ambient air conditions and gave distinctive and reproducible spectra. The

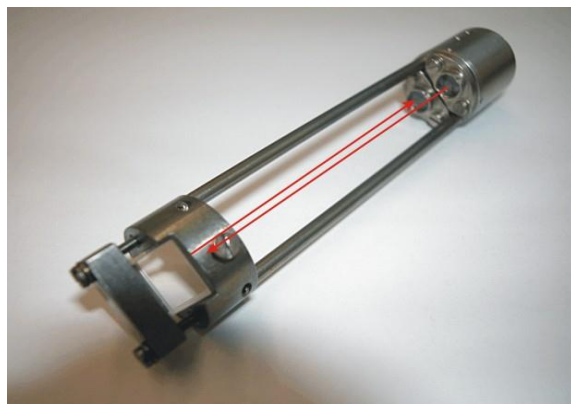
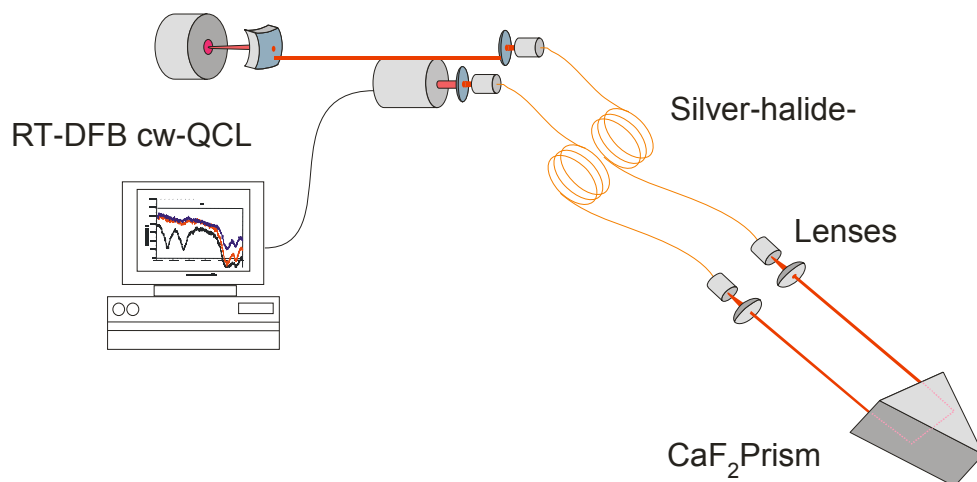


**Figure 2** QCL based handheld sensor device [41]. (a) general sensor set-up and (b) photograph of sensor head. Figure provided by C. Bauer.

researchers identified unique spectral features when they compared TATP and its precursor acetone. TATP and its precursor acetone were also the target of a QCL photoacoustic spectroscopy (PAS) technique designed by Patel et al.<sup>45</sup> These researchers used an array of wavelengths (dubbed a “smart grid”) to bypass the interference of water vapor under ambient conditions. Distinct spectra were collected for TATP, acetone and TNT, with LODs of 18 ppb for TATP and 3 ppb for acetone. Integration of this technique with walkthrough portal devices may be possible in the future.

Raman-based systems for the field analysis of explosives and other compounds of forensic interest are commercially available and have been described previously.<sup>46</sup> A study of the Ahura Scientific (Wilmington, MA) portable Raman device, FirstDefender™, has been recently presented.<sup>47</sup> FirstDefender™, introduced by Ahura Scientific in 2005<sup>48</sup>, incorporates a dispersive Raman spectrograph that included a 785 nm laser and charge coupled device (CCD) detector along with a database of over 4000 compounds and mixtures for vapor monitoring. This device is designed to allow rapid identification of suspect material through transparent containers such as plastic or glass bottles. The study of this device found that discrimination is possible between TATP, HMTD and organic peroxides such as methylenethylketone peroxide; however, LOD values were not reported. Offering many of the same features of FirstDefender™, Ahura Scientific’s TruDefender™ is a FTIR based handheld device. TruDefender™ was introduced in 2008<sup>49</sup>, likely explaining the lack of literature available from peer reviewed journals.

Given the urgent need of portable and/or stand-off detection ready devices, it is not surprising such devices are the focus of much research. For stand-off screening of

bottles for liquid explosives precursors (e.g.,  $\text{H}_2\text{O}_2$  for PBEs), Stokes et al. used Raman microscopy.<sup>50</sup> These researchers used a Raman microscope with a long working distance lens and found that closed plastic bottles could be reliably screened for 30%  $\text{H}_2\text{O}_2$  with an analysis time of 100 ms. At the same time, the liquid explosive combination of  $\text{H}_2\text{O}_2$  / water/ ethanol<sup>50, 51</sup> could also be detected with component differentiation.

An approach for pushing the boundaries of Raman detection limits is surface-enhanced Raman scattering (SERS). The metal surfaces employed in this technique enhance the Raman signal via the large electromagnetic fields present on the small gaps between metal nanoparticles.<sup>52</sup> Taking advantage of the additional waveguide ability of a cylindrical SERS substrate, Tsukruk et al. designed a substrate of alumina nanopores containing gold nanoparticle clusters for the detection of explosives that included HMTD.<sup>52</sup> Fabrication of their substrate is illustrated in **Figure 3(a)**. After fabrication of a porous alumina membrane, the surface of these pores was modified with polyethylenimine (PEI), with its amine groups providing a convenient way to attach the cetyltrimethylammonium bromide (CTAB) capped gold nanoparticles. **Figure 3(b)** shows the Raman spectra of HMTD at several concentrations on the SERS substrate. This approach gave a LOD of approximately 1 pg for HMTD precipitated on the substrate.

#### ***5.4 Ion Mobility and Mass Spectrometry***

Along with IR and Raman spectroscopy, mass spectrometry (MS) was one of the first techniques used to analyze PBEs and related compounds<sup>4, 8</sup>. TATP synthesis by-products<sup>53, 54</sup> and acid degradation products<sup>55</sup>, along with the thermal decomposition of

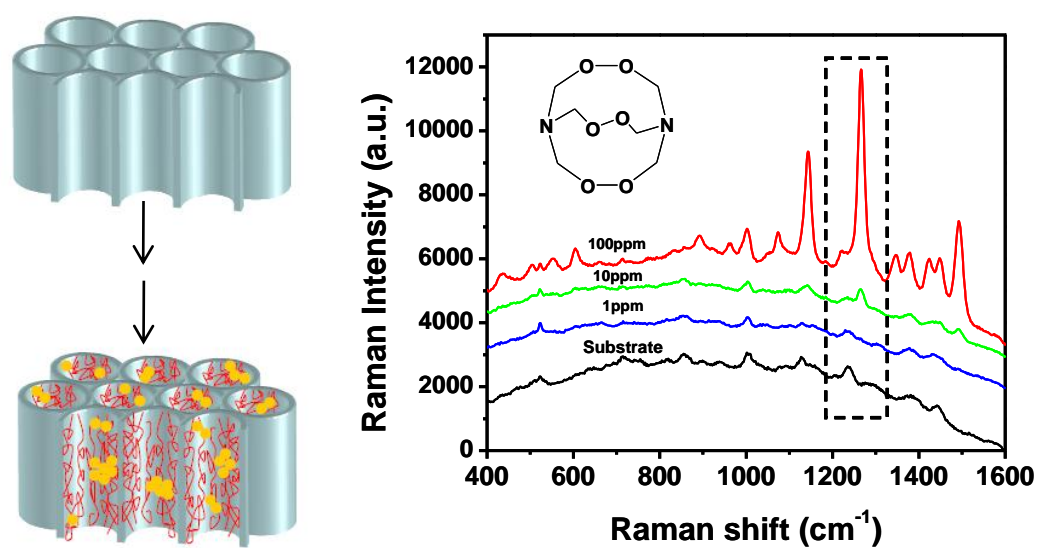


**Figure 3** SERS detection of HMTD [52]. (a) SERS substrate fabrication (see text for details) and (b) SERS spectra of HMTD; characteristic signature peaks are marked.

Figure provided by V. Tsukruk



TATP<sup>56</sup> and HMTD<sup>5</sup>, have all been studied using MS techniques. These methods have seen wide application in the field monitoring of explosives and narcotics, especially through the use of ion mobility spectrometry (IMS). Because they offer suitable sensitivity, reliability and easy operation, IMS instruments are often found in airports, government buildings and border crossings.<sup>8, 57, 58</sup> Studies of two commercially-available IMS field-friendly instruments have recently been published.<sup>57, 58</sup>

Using General Electric's Itemiser<sup>®</sup>FX, Oxley et al. developed a method to detect explosives in hair.<sup>57</sup> This instrument is geared toward detecting narcotics and explosives and can be operating in both positive and negative ion modes. As most narcotics have a positive ion affinity, the detection of positive ions by this device is called the "N-mode", while negative "E-mode" is used for nitro-based explosives that have a negative ion affinity. Experiments were run in both modes to test their use for nitro-based explosives and TATP. The high vapor pressure of TATP proved to be an experimental challenge due to its quick desorption from hair. Longer TATP exposure times and amounts, in addition to larger hair samples, were required to detect this analyte in hair. LODs of 0.8 µg (N-mode) and 1.9 µg (E-mode) were reported. Another field ready IMS instrument was studied by Räsänen et al. for its first-time use in TATP detection.<sup>58</sup> An aspiration-type IMS has been integrated with semiconductor gas sensors in a handheld device called ChemPro100i from Environics (Toronto, ON). TATP vapor was measured under ambient conditions with this device and gave a LOD in the low mg m<sup>-3</sup> region, as verified by gas chromatography GC-MS. However, the detection of TATP in complex matrices when using this device was not reported.

The high vapor pressure of TATP has been a boon for the application of headspace GC-MS in detecting this explosive. Stambouli et al. designed a headspace GC-MS technique targeted at detecting trace TATP in post-explosion debris.<sup>19</sup> For this study, debris was collected from the 2003 Casablanca explosion by the forensic laboratory of Moroccan Gendarmerie Royale. Both TATP and its by-product DADP were easily detected though extensive decomposition and/or fragmentation results from thermal degradation and MS ionization. Characteristic ion peaks were present for both TATP and DADP. The developed method then examined post-blast debris had been collected in glass containers and hermetically sealed. Final procedure included heating the glass sample container for 30 min followed by sampling 1 mL the headspace vapor for analysis. A LOD of 0.1 ng was reported for TATP, but the LOD of DADP was not provided.

GC-MS was combined with solid phase micro-extraction (SPME) by Kende and colleagues for trace analysis of TATP.<sup>59</sup> These researchers used polydimethyl siloxane fibers to trap TATP vapor in the headspace of sample containers, followed by transfer of fibers to the injector of a GC system kept at 160 °C. Maximum signal was achieved when the fiber-to-TATP exposure time was 20 min. Electron impact (EI) MS was used with a trio of indicative ion peaks for compound identification, including the parent ion. Researchers examined a variety of model pre- and post-blast samples, such as TATP contaminated soil, with favorable results. An LOD of 5 ng for TATP was reported.

Sigman and colleagues have used a variety of MS modes to detect and characterize the fragmentation of TATP and its synthesis by-products when these chemicals are subjected to collision-induced dissociation (CID).<sup>53, 54, 60</sup> Low nanogram

LODs were achieved for the GC-MS analysis of TATP using ammonia or methane positive ion chemical ionization (PICI) and negative ion chemical ionization (NICI) along with EI.<sup>60</sup> Researchers found ammonia PICI to be the best overall method, as a diagnostic adduct  $[\text{TATP} + \text{NH}_4]^+$  was consistently detected and gave LOD values of 0.5 ng (ion trap) or 0.1 ng (quadrupole). Sigman et al. next used ESI-MS to monitor both ammonia and sodium adducts of TATP and its oligoperoxide by-products.<sup>53, 54</sup> Sodium adducts for TATP, previously seen using desorption ionization electrospray (DESI) MS<sup>61</sup>, were observed along with a new series of ions corresponding to  $[\text{oligoperoxides} + \text{Na}]^+$ .<sup>53</sup> An LOD of 62.5 ng was reported for TATP. This sodium adduct technique was used to analyze TATP synthesis products in post-blast samples, with trace amounts of TATP and oligoperoxides being detected after detonation. TATP synthesis reaction mixtures, which include a variety of oligoperoxide by-products, received more attention in a recent article<sup>54</sup> in which detailed CID mechanisms of sodiated and ammonium adducts were determined using deuterium isotopic labeling tandem MS experiments. The CID mechanisms differed for the sodiated and ammonium adducts; smaller oligoperoxide ammonium adducts formed cyclic peroxides while sodium adducts did not. Both adduct forms underwent extensive fragmentation, as seen for ammonium adduct CID in **Figure 4**. Notice in this example that the 314  $m/z$  peak corresponding to tetracetone tetraperoxide (TRARP)  $[\text{TRARP} + \text{NH}_4]^+$  is quite abundant, as is the 240  $m/z$  peak for  $[\text{TATP} + \text{NH}_4]^+$ . Studies of various synthetic TATP batches revealed a variation in oligoperoxide distribution between batches, a feature that could prove useful in forensic analysis. Distribution of oligoperoxides shifted in pre- and post-blast samples, an effect that was likely due to thermal decomposition.

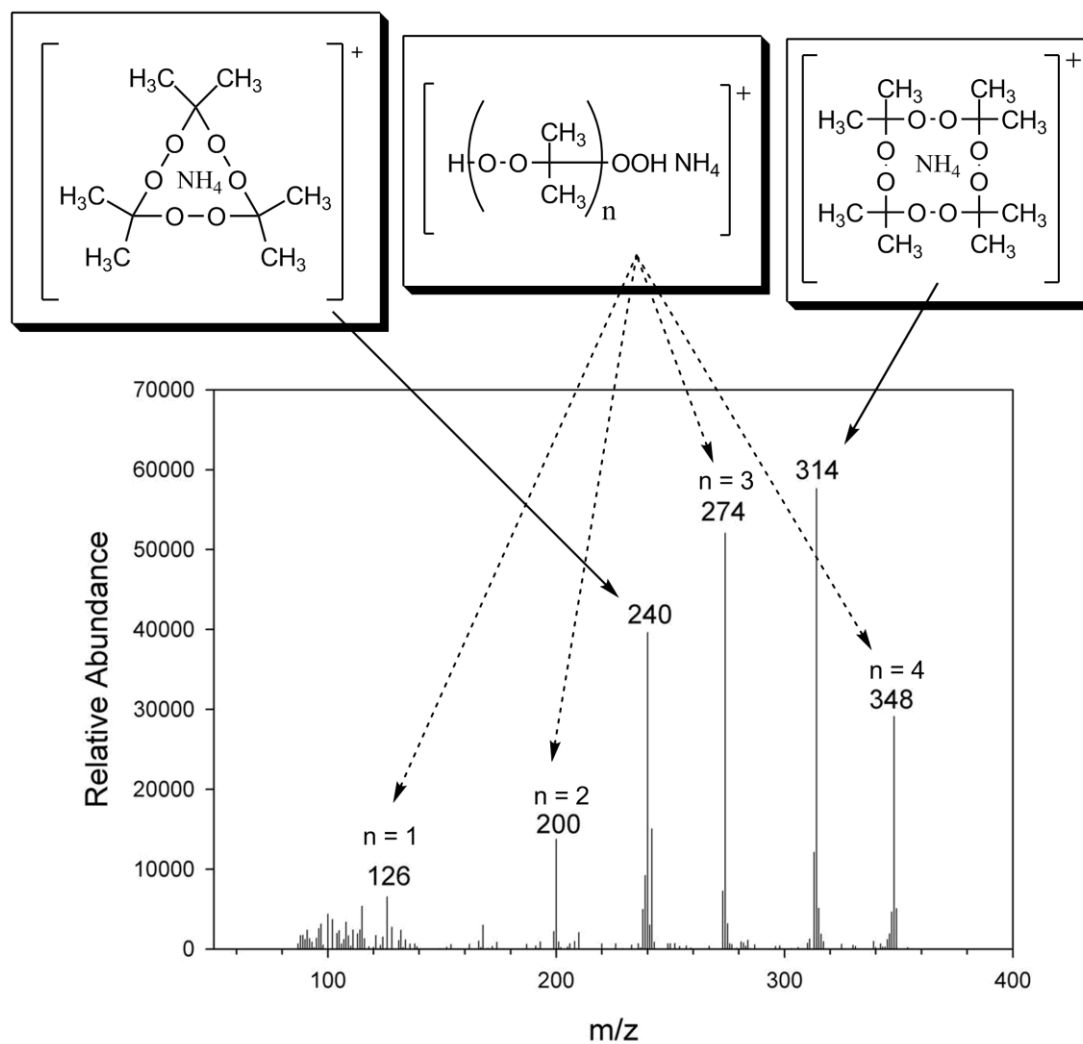


**Figure 4** Analysis of oligomeric peroxides in synthetic TATP samples by ESI-MS [54].

Product ion spectrum obtained from CID of  $m/z$  348  $[\text{H}(\text{OOC}(\text{CH}_3)_2)_4\text{OOH} + \text{NH}_4]^+$ .

Major  $m/z$  peak are identified. Figure provided by M. Sigman.

Detection of sodiated and ammonium adducts of TATP was introduced by Cooks et al.<sup>61, 62</sup> Their DESI MS technique was discussed in detail in a previous review.<sup>8</sup> These same researchers recently presented a DESI MS method for the rapid detection of trace amounts of TATP, TRARP and HMTD directly from ambient surfaces with no sample preparation.<sup>63</sup> In addition to sodium and ammonium, this group also investigated the use of potassium and lithium for complex formation. Positive ion DESI spectra of TATP and HMTD are shown in **Figure 5**. Rapid (< 5 sec) detection of target PBEs in complex matrixes (e.g., diesel fuel) was achieved using single or multiple cation additives and gave LODs in the low nanogram range. The use of desorption atmospheric pressure chemical ionization (DAPCI) MS was also explored for the detection of TATP and HMTD. Trace amounts of HMTD were easily detected by DAPCI by using methanol vapor in nitrogen but gave insufficient ionization for TATP. This effect was attributed to the lower proton affinity of TATP relative to HMTD. The higher proton affinity of HMTD is due to its two basic amine groups. For TATP detection, ammonium acetate was added to the DAPCI gas so that ammonium adducts could be monitored. Favorable results led to modification of the HMTD DAPCI regime to also include ammonium acetate. LODs for all experiments were in the low nanogram range.

Ammonia hydroxide-treated TATP, HMTD and tetramethylene diperoxide dicarbamide (TMDD) were analyzed by Peña-Quevedo et al. using an AccuTOF DART instrument (JEOL USA, Peabody, MA).<sup>64</sup> DART (direct analysis in real time) is the sampling component which is coupled to an atmospheric pressure ionization (API) time-of-flight (TOF) MS. Compounds were synthesized in-house and characterized by Raman and IR. Reaction mixtures were subjected to minimal purification prior to MS analysis.

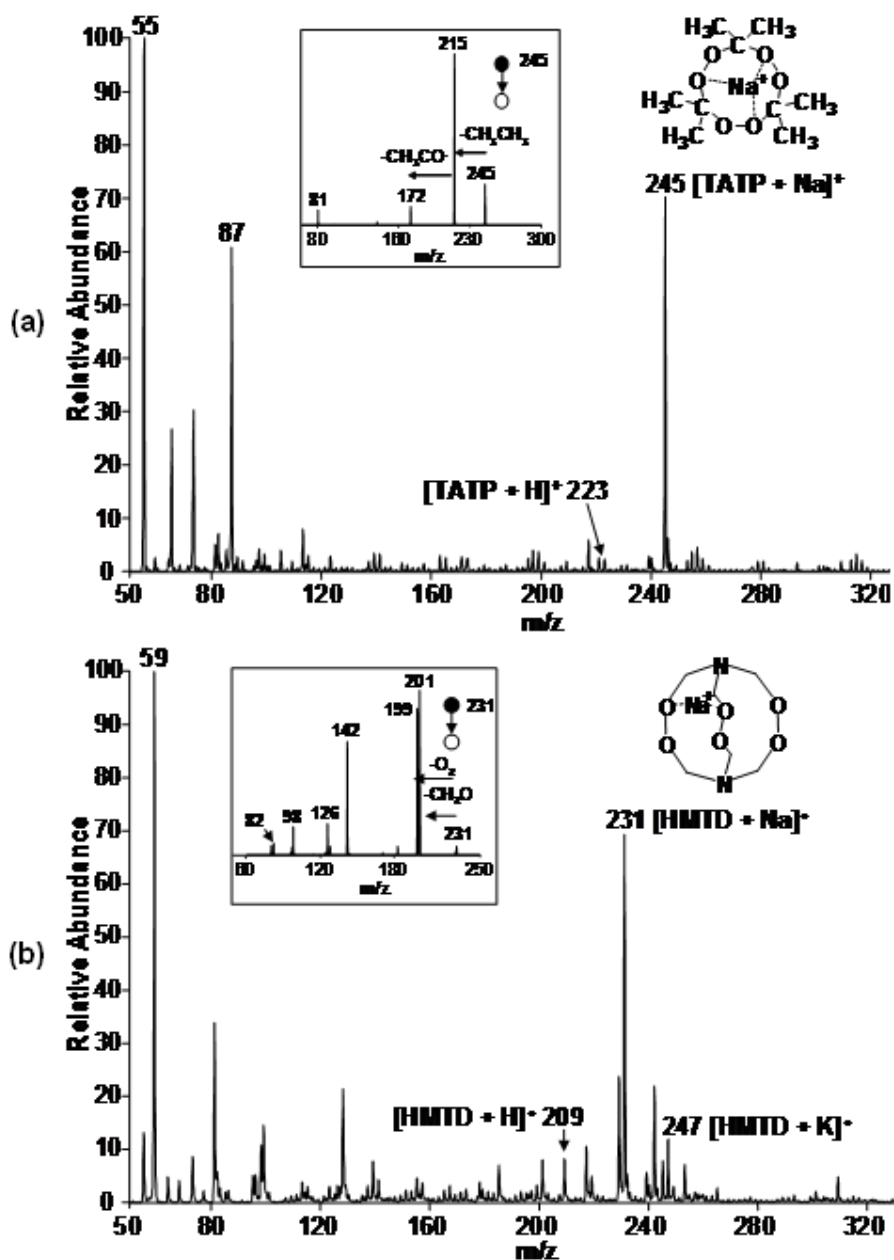


**Figure 5** DESI-MS detection of TATP and HMTD [63]. Positive ion DESI mass spectrum of 10 ng TATP (a) or HMTD (b) deposited on paper in an area of 1 cm<sup>2</sup>. Methanol/water (70:30) doped with 10 mM NaCl was used as spray solvent. Product ion MS/MS spectrum of (PBE + Na)<sup>+</sup> complex (insets). Figure provided by R. Cooks.

Positive ammonia adducts were detected for all PBEs. For HMTD, the parent ion peak  $[\text{HMTD} + \text{H}]^+$  was more abundant than the ammonia adduct, while for TATP the ammonia adduct  $[\text{TATP} + \text{NH}_4]^+$  was the only peak present. To explain the lack of a fragmentation pattern for TATP, the author suggests that TATP is stabilized by ammonia. For TMDD, the  $[\text{TMDD} + \text{NH}_4]^+$  peak was more abundant than the peak for the parent ion,  $[\text{TMDD} + \text{H}]^+$ . It was reported that trace PBE analysis could be performed by this approach, although LOD values were not provided.

Oser et al. used laser photoionization for MS studies of TATP.<sup>65, 66</sup> When comparing femtosecond (fs) and nanosecond (ns) laser pulses for the analysis of TATP vapor by TOF MS<sup>65</sup>, researchers noted that a parent ion peak was only present in fs laser pulse spectra. This shorter pulse provided “softer” ionization and yielded more abundant acetone ion peaks compared to previously published GC-MS analysis data for TATP. Single photo ionization (SPI) TOF MS was next used to detect a variety of explosives and related compounds in the gas phase.<sup>66</sup> In SPI MS, the parent molecule was directly ionized using a vacuum ultraviolet (VUV) photon. A single VUV photon was absorbed by a molecule and, if the photon energy was higher than the molecule’s ionization potential (IP), an electron was removed. The limited ionization energy of VUV photons can efficiently ionize organic compounds but not bulk gases such as nitrogen, oxygen, and water because these gases have relatively high ionization potentials.<sup>66, 67</sup> A diagram of this SPI TOF MS system is shown in **Figure 6(a)**. As can be seen in **Figure 6(b)**, TATP underwent extensive fragmentation, with the acetyl ion (43 m/z) being the most abundant such ion, although the parent ion was also visible at 222 m/z. For TATP, an LOD in the low ppb range was achieved. To increase the application of SPI MS in the

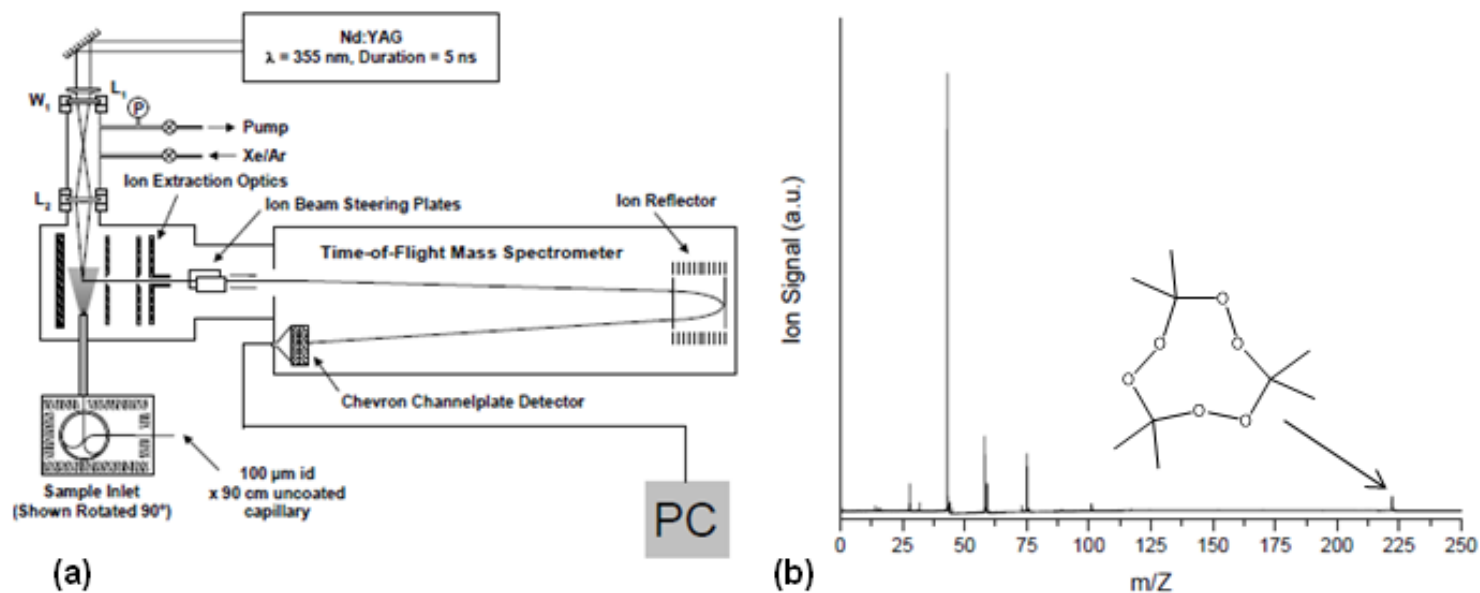


**Figure 6** TATP detection by SPI-TOFMS [66]. (a) Diagram of the SPI – TOFMS instrument and (b) SPI mass spectrum of TATP; parent molecular ion (222 amu) and a number of photodissociative products including acetyl ion (43 amu), acetone ion (58 amu),  $C_3H_7O^+$  (59 amu),  $C_3H_7O_2^+$  (75 amu),  $C_3H_6O_4^+$  (106 amu), diacetone diperoxide (DADP)  $C_3H_6O_5^+$  (122 amu), . Figure provided by H. Oser.



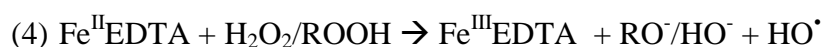
detection of explosives and narcotics, Zimmermann and colleagues determined the ionization potentials of several such compounds<sup>67</sup> using monochromatized synchrotron radiation from BESSY (i.e., Berliner Elektronenspeicherring-Gesellschaft für Synchrotronstrahlung). This latter work was qualitative, aimed at providing IPs for an array of forensically important compounds.

### ***5.5 Electrochemical Methods***

Explosives detection by electrochemical means was comprehensively reviewed by Wang in 2007.<sup>25</sup> This review focused on sensors for commercial and homemade explosives, with portability and disposability major goals of current electrochemical detection research. Though nitro-based explosives are the most popular target analyte, PBEs are receiving greater attention. Wang's lab has made significant contributions to the field with their use of Prussian-blue (PB) modified glassy carbon disk electrodes. These electrodes were used to detect H<sub>2</sub>O<sub>2</sub> that was generated from UV lamp or laser treatment of TATP and HMTD.<sup>68</sup> The preferential electrocatalytic activity of PB towards H<sub>2</sub>O<sub>2</sub> has led to PB being called an "artificial enzyme peroxidase".<sup>25, 68, 69</sup> For TATP that was treated with a short burst laser, a LOD of 50 nM was observed by this electrochemical method. When using UV irradiation, the LOD for TATP was 250 nM and the LOD was 300 nM for HMTD. Researchers next monitored H<sub>2</sub>O<sub>2</sub> produced from acid treatment of TATP with and without neutralization steps.<sup>70</sup> An LOD of 55 nM TATP was observed when a TATP acid solution was neutralized prior to amperometric measurements of stirred solutions. In the same report, a simplified experimental design

was presented based on the fabrication of single-use PB-modified screen-printed electrodes and elimination of the neutralization step. An LOD of 18 mM was achieved using this one-step method. This higher LOD is likely the result of both the elimination of the neutralization step and the direct chronoamperometric monitoring of a non-stirred reaction solution. This approach with screen-printed electrodes required low reaction volumes (~20  $\mu$ L) and a 1 min assay time. HMTD was tested as well, but results for this analyte were not provided.

Acid treatment of TATP was also used in an electrochemical method introduced by Cheng's lab.<sup>16</sup> This approach was based on the reactions in Eqns. (3) and (4). Fe<sup>II</sup>ethylenediaminetetraacetate (EDTA) was produced at a glassy carbon electrode by the reduction of Fe<sup>III</sup>EDTA, as given in Eqn. (3). Next, Fe<sup>II</sup>EDTA electrocatalytically reduces H<sub>2</sub>O<sub>2</sub> and/or hydroperoxides that have been released by acid treatment of TATP, as shown in Eqn. (4).



An LOD of 890 nM for TATP was achieved in this technique. Later work with HMTD<sup>71</sup> indicated a separate acid digest step was not required. HMTD added to a pH 2.1 Fe<sup>II/III</sup>EDTA solution spontaneously hydrolyzed to form simpler peroxides, including H<sub>2</sub>O<sub>2</sub>, and provided a similar sensor response (see **Figure 7**). A slightly higher LOD of 30  $\mu$ M was seen for HMTD in this modified method.

The ability of H<sub>2</sub>O<sub>2</sub> to induce current changes in phthalocyanine p-type semiconductors was employed in a method designed by Trogler et al.<sup>72</sup> In this report,

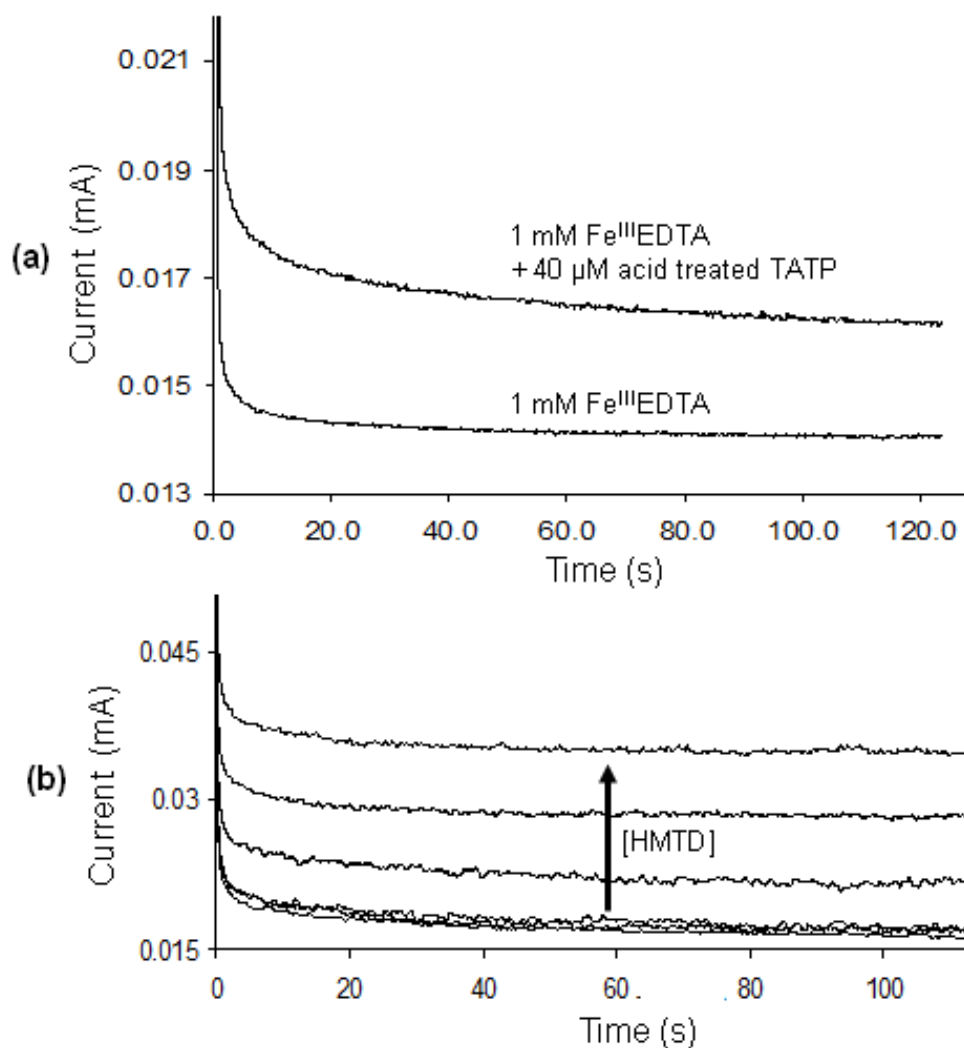


**Figure 7** Electrochemical detection of TATP and HMTD using a Fe<sup>II/III</sup>EDTA reaction [16, 71]. Chronoamperograms of (a) acid treated TATP in 1 mM Fe<sup>III</sup>EDTA and (b) increasing concentrations of HMTD added to a pH 2.1 Fe<sup>II/III</sup>EDTA solution. Chronoamperograms were obtained by stepping to -400 mV (vs. Ag/AgCl). Figure provide by F. Cheng.

50 nm thick films were made of phthalocyanines (MPcs), both metalated and metal-free, forming chemiresistors for use as H<sub>2</sub>O<sub>2</sub> vapor sensors. A host of MPcs (M = Co, Ni, Cu or H<sub>2</sub>) were tested, with H<sub>2</sub>O<sub>2</sub> causing current losses in CoPc and current gains in NiPc, CuPc and H<sub>2</sub>Pc. Other strong oxidants all caused current gains in all MPcs; only H<sub>2</sub>O<sub>2</sub> showed a differential response. This was the first example of contrasting analyte redox behavior dependent on M, the metal center in the chemiresistor. Using all or just a combination of MPcs with opposite responses (e.g. CoPc and CuPc), gave a catalytic redox sensor array for the selective detection of H<sub>2</sub>O<sub>2</sub>. It was suggested that a MPc sensor array could be used to detect PBEs after conversion to H<sub>2</sub>O<sub>2</sub> using UV irradiation. The maximum response time was 10 min for all MPcs and the current response was constant even when changes in humidity occurred. The LOD depended on the MPc that was tested. CoPc, the most potent catalyst for H<sub>2</sub>O<sub>2</sub> redox, had a LOD of 50 ppb. For NiPc, CuPc and H<sub>2</sub>Pc, the LODs were 40.1, 12.2, and 11.7 ppm, respectively.

### ***5.6 Other Methods***

A variety of techniques making use of HPLC have been developed for the detection of PBEs. Both HPLC-MS and HPLC with electrochemical detection have used to monitor TATP, DADP and HMTD.<sup>8</sup> For the detection of TATP and HMTD, Lendl and colleagues developed a reversed phase HPLC method with online IR detection using a CaF<sub>2</sub> flow cell.<sup>73</sup> TATP and HMTD were well resolved in this approach and gave LODs of 1 mM for TATP and 0.5 mM for HMTD. Spiked soil samples gave similar results.

GC is another method that is often used in PBE detection and characterization. A commercially available handheld GC device called zNose (Electronic Sensor Technology, Newbury Park, CA) has been studied for the detection of vapors from explosives.<sup>74</sup> This “electronic nose” contains a solid-state sensor that provides LODs in the low parts-per-trillion range for a variety of explosives, including TATP. For possible future integration into a portable explosives detector, Zuck et al. recently fabricated a microcalorimetry ( $\mu$ Cal) device.<sup>75</sup> This differential scanning device was used to analyze 30 – 100  $\mu$ m size explosives particles in addition to non-explosive material such as sugar and sea sand. The thermograms obtained were sufficiently unique to allow for differential detection. An LOD for TATP was not provided in this report, but the authors stated that work is on-going in the creation of a portable unit.

## ***5.7 Conclusion***

The continued and increased use of PBEs in terrorist activities has made the development of detection methods for the explosives a research priority. In a previous review, method requirements for such work were outlined and it was noted that a variety of techniques would be needed to meet the desired goals of unambiguous identification, portability, easy operation, minimal analysis times, and low LODs in a variety of sample matrices.<sup>8</sup> As can be seen in this current review of recent developments in PBE detection, progress has been made to meet these goals, through the use of a variety of new assays and variations of more established methods. These methods have included techniques based on luminescence and fluorescence measurements, IR or Raman

spectroscopy, mass spectrometry, electrochemical methods, and separation techniques such as HPLC and GC.

Several trends have emerged since the previous review published in ABC. First, there has been an emphasis on field measurements. This work has included methods involving commercially-available portable instruments and the design of devices or assays that have the promise of being portable, such as a QCL handheld sensor<sup>41</sup>, a QCL-based walkthrough portal<sup>17, 44</sup>, and luminescence techniques based on PVA/LG films<sup>27</sup> or MoHB nanoparticles<sup>28</sup> for use in test strips or badges. Clearly, given the high security and high traffic areas in which PBE detection is used, continued advancements in portability is still needed. Another trend has been an increase in the use of IR spectroscopy and mass spectrometry for PBE analysis. For instance, a number of researchers have identified IR regions that can be used to identify PBEs identifying IR regions or elucidated PBE fragmentation pathways for their detection by GC MS<sup>60</sup>, ESI MS<sup>53, 54</sup> or DESI MS<sup>61-63</sup>. This type of work should allow analysts at forensic facilities to more easily integrate new methods, as they can employ their qualified instruments. TATP still appears to be the focus in the development of many of these methods, although HMTD has received increased attention in the last few years.

## 5.8 References

1. Woffenstein, R., *Chem. Ber.* **1895**, 28, 2265-2269.
2. McKay, G., *Kayaku Gakkaishi* **2002**, 63, 323-329.
3. Yeager, K., Dangerous innovations. In *Trace Chemical Sensing of Explosives*, Woodfin, R., Ed. Wiley-Interscience: Hoboken, 2007.
4. Evans, H.; Tulleners, A.; Sanchez, B.; Rasmussen, C., *J. Forensic. Sci.* **1986**, 31, 1119-1125.
5. Oxley, J.; Smith, J.; Chen, H.; Cioffi, E., *Thermochim. Acta* **2002**, 338, 215-225.
6. Legler, L., *Chem. Ber.* **1881**, 14, 602-604.
7. Oxley, J., Peroxide Explosives. In *Detection and disposal of improvised devices*, Schubert, H.; Kuznetson, A., Eds. Springer: New York, 2006.
8. Schulte-Ladbeck, R.; Vogel, M.; Karst, U., *Anal. Bioanal. Chem.* **2006**, 386, 559-565.
9. Meaney, M.; McGuffin, V., *Anal. Bioanal. Chem.* **2008**, 391, 2557-2576.
10. Schulte-Ladbeck, R.; Kolla, P.; Karst, U., *Anal. Chem.* **2003**, 75, 731-735.
11. van Duin, A.; Zeiri, Y.; Dubnikova, F.; Kosloff, R.; Goddard, W., *J. Am. Chem. Soc.* **2005**, 127, 11053-11062.
12. Dubnikova, F.; Kosloff, R.; Almog, J.; Zeiri, Y.; Boese, R.; Itzhaky, H.; Alt, A.; Keinan, E., *J. Am. Chem. Soc.* **2005**, 127, 1146-1159.
13. Widmer, L.; Watson, S.; Schlatter, K.; Crowson, A., *Analyst* **2002**, 127, 1627-1632.
14. Muller, D.; Levy, A.; Shelef, R.; Abramovich-Bar, S.; Sonenfeld, D.; Tamiri, T., *J. Forensic. Sci.* **2004**, 49, 935-938.

15. Oxley, J., What's special about liquid explosives. In *Detection of Liquid Explosives and Flammable Agents in Connection with Terrorism*, Schubert, H.; Kuznetson, A., Eds. Springer: Dordrecht, 2008; pp 27-38.
16. Laine, D.; Roske, C.; Cheng, F., *Anal. Chim. Acta* **2008**, *608*, 56-60.
17. Lindley, R.; Normand, E.; McCulloch, M.; Black, P.; Howieson, I.; Lewis, C.; Foulger, B., *Proc. SPIE - Int. Soc. Opt. Eng* **2008**, *7119*, 71190K-1 - 71190K-11.
18. Pumera, M., *Electrophoresis* **2008**, *29*, 269-273.
19. Stambouli, A.; El Bouri, A.; Bouayoun, T.; Bellimam, M., *Forensic Sci. Int.* **2004**, *146S*, S191-S194.
20. Coucil, N. R. *Existing and potential standoff explosives detection techniques*; The National Academies Press: Washington, DC, 2004.
21. Wilson, P.; Prince, B.; McEwan, M., *Anal. Chem.* **2006**, *78*, 575-579.
22. Bellamy, A., *J. Forensic. Sci.* **1999**, *44*, 603-608.
23. Pumera, M., *Electrophoresis* **2006**, *27*, 244-256.
24. Pacheco-Londono, L.; Primera, O.; Ramirez, M.; Ruiz, O.; Hernandez-Rivera, S., *Proc. SPIE - Int. Soc. Opt. Eng* **2005**, *5778*, 317-326.
25. Wang, J., *Electroanalysis* **2007**, *19*, 415-423.
26. Moore, D., *Sens. Imaging* **2007**, *8*, 9-38.
27. Mills, A.; Grosshans, P.; Snadden, E., *Sens. Actuators, B* **2009**, *136*, 458-463.
28. Apblett, A.; Kiran, B.; Malka, S.; Materer, N.; Piquette, A., *Ceram. Trans.* **2005**, *172*, 29-35.
29. Sanchez, J.; Trogler, W., *J. Mater. Chem.* **2008**, *18*, 5134-5141.
30. Germain, M.; Knapp, M., *Inorg. Chem.* **2008**, *47*, 9748-9750.



31. Malashikhin, S.; Finney, N., *J. Am. Chem. Soc.* **2008**, *130*, 12846-12847.
32. Sella, E.; Shabat, D., *Chem. Comm.* **2008**, 5701-5703.
33. Wingert, P.; Mizukami, H.; Ostafin, A., *Nanotechnology* **2007**, *18*, 1-7.
34. Oxley, J.; Smith, J.; Brady, J.; Dubnikova, F.; Kosloff, R.; Zeiri, L., *Appl. Spectrosc.* **2008**, *62*, 906-915.
35. Pena, A.; Pacheco-Londono, L.; Figueroa, J.; Rivera-Montalvo, L.; Roman-Velazquez, F.; Hernandez-Rivera, S., *Proc. SPIE - Int. Soc. Opt. Eng* **2005**, *5778*, 347358.
36. Hiyoshi, R.; Nakamura, J., *Propell. Explos. Pyrot.* **2007**, *32*, 127-134.
37. Pacheco-Londono, L.; Primera-Pedrozo, O.; de la Torre, L.; Hernandez-Rivera, S., *Proc. SPIE - Int. Soc. Opt. Eng* **2005**, *5816*, 180-185.
38. Pacheco-Londono, L. C.; Pena, A. J.; Primera-Pedrozo, O. M.; Hernandez-Rivera, S. P.; Mina, N.; Garcia, R.; Chamberlain, R. T.; Lareau, R. T., *Proc. SPIE - Int. Soc. Opt. Eng* **2004**, *5403* (Pt. 1, Sensors, and Command, Control Communications, and Intelligence (C31) Technologies for Homeland Security and Homeland Defense III), 279-287.
39. Primera, O. M.; Pacheco, L.; De la Torre, L. F.; Hernandez, S. P.; Chamberlain, R. T.; Lareau, R. T., *Abstracts of Papers, 227th ACS National Meeting, Anaheim, CA, United States, March 28-April 1, 2004* **2004**, PHYS-405.
40. Primera-Pedrozo, O. M.; Pacheco-Londono, L. C.; De la Torre-Quintana, L. F.; Hernandez-Rivera, S. P.; Chamberlain, R. T.; Lareau, R. T., *Proc. SPIE - Int. Soc. Opt. Eng* **2004**, *5403* (Pt. 1, Sensors, and Command, Control Communications,

- and Intelligence (C31) Technologies for Homeland Security and Homeland Defense III), 237-245.
41. Bauer, C.; Sharma, A.; Willer, U.; Burgmeier, J.; Braunschweig, B.; Schade, W.; Blaser, S.; Hvozdar, L.; Muller, A.; Holl, G., *Appl. Phys. B* **2008**, *92*, 327-333.
  42. Hildenbrand, J.; Herbst, J.; Wollenstein, J.; Lambrecht, A., *Proc. SPIE - Int. Soc. Opt. Eng* **2009**, *7222*, 72220B-1 - 72220B-12.
  43. Lambrecht, A.; Hartwig, S.; Herbst, J.; Wollenstein, J., *Proc. SPIE - Int. Soc. Opt. Eng* **2008**, *6901*, 69010V-1 - 69010V-11.
  44. Lindley, R.; Normand, E.; Howieson, I.; McCulloch, M.; Black, P.; Lewis, C.; Foulger, B., *Proc. SPIE - Int. Soc. Opt. Eng* **2007**, *6741*, 67410P-1 - 67410P-12.
  45. Dunayevskiy, I.; Tsekoun, A.; Prasanna, M.; Go, R.; Patel, K., *Appl. Optics* **2007**, *46*, 6397-6404.
  46. Eckenrode, B.; Bartick, E.; Harvey, S.; Vucelick, M.; Wright, B.; Huff, R., *Forensic Sci. Comm.* **2001**, *3* (4).
  47. Santillan, J.; Brown, C.; Jalenak, W., *Proc. SPIE - Int. Soc. Opt. Eng* **2007**, *6540*, 65400P-1 - 65400P-8.
  48. N.A. First Defender – Breakthrough Rugged, Handheld Chemical Identification System Available to First Responders. (accessed June 15).
  49. N.A. Ahura Scientific Launches FTIR Platform with Introduction of TruDefender FT. <http://www.ahurascientific.com/about-ahura/press-releases/pr20080131.php> (accessed June 15).
  50. Stokes, R.; Smith, W.; Foulger, B.; Lewis, C., *Proc. SPIE - Int. Soc. Opt. Eng* **2008**, *7119*, 71190I-1 - 71190I-9.

51. Mostak, P., Chemistry and properties of liquid explosives. In *Detection of Liquid Explosives and Flammable Agents in Connection with Terrorism*, Schubert, H.; Kuznetson, A., Eds. Springer: Dordrecht, 2008; pp 15-25.
52. Ko, H.; Chang, S.; Tsukruk, V., *ACS NANO* **2009**, *3*, 181-188.
53. Sigman, M.; Clark, C.; Caiano, T.; Mullen, R., *Rapid Commun. Mass Spectrom.* **2008**, *22*, 84-90.
54. Sigman, M.; Clark, C.; Painter, K.; Milton, C.; Simatos, E.; Frisch, J.; McCormick, M.; Bitter, J., *Rapid Commun. Mass Spectrom.* **2009**, *23*, 349-356.
55. Armitt, D.; Zimmermann, P.; Ellis-Steinborner, S., *Rapid Commun. Mass Spectrom.* **2008**, *22*, 950-958.
56. Oxley, J.; Smith, J.; Chen, H., *Propell. Explos. Pyrot.* **2002**, *27*, 209-216.
57. Oxley, J.; Smith, J.; Kirschenbaum, L.; Marimnganti, S.; Vadlamannati, S., *J. Forensic. Sci.* **2008**, *53*, 690-693.
58. Rasanen, R.; Nousiainen, M.; Perakorpi, K.; Sillanpaa, M.; Polari, L.; Anttalainen, O.; Utriainen, M., *Anal. Chim. Acta* **2008**, *623*, 59-65.
59. Kende, A.; Lebies, F.; Eke, Z.; Torkos, K., *Microchem. Acta* **2008**, *163*, 335-338.
60. Sigman, M.; Clark, C.; Fidler, R.; Geiger, C.; Clausen, C., *Rapid Commun. Mass Spectrom.* **2006**, *20*, 2851-2857.
61. Cotte-Rodriquez, I.; Chen, H.; Cooks, R., *Chem. Comm.* **2006**, 953-955.
62. Cotte-Rodriquez, I.; Cooks, R., *Chem. Comm.* **2006**, 2968-2970.
63. Cotte-Rodriquez, I.; Hernandez-Soto, H.; Chen, H.; Cooks, R., *Anal. Chem.* **2008**, *80*, 1512-1519.

64. Pena-Quevedo, A.; Cody, R.; Mina-Camilde, N.; Ramos, M.; Hernandez-Rivera, S., *Proc. SPIE - Int. Soc. Opt. Eng* **2007**, 6538, 653828-1 - 653828-12.
65. Mullen, C.; Huestis, D.; Coggiola, M.; Oser, H., *Inter. J. Mass. Spec.* **2006**, 252, 69-72.
66. Mullen, C.; Irwin, A.; Pond, B.; Huestis, D.; Coggiola, M.; Oser, H., *Anal. Chem.* **2006**, 78, 3807-3814.
67. Schramm, E.; Muhlberger, F.; Mitschke, S.; Reichardt, G.; Schulte-Ladbeck, R.; Putz, M.; Zimmermann, R., *Appl. Spectrosc.* **2008**, 62, 238-247.
68. Lu, D.; Cagan, A.; Munoz, R.; Tangkuaram, T.; Wang, J., *Analyst* **2006**, 131, 1279-1281.
69. Karyakin, A.; Gorton, L., *Anal. Chem.* **2000**, 72, 1720-1723.
70. Munoz, R.; Lu, D.; Cagan, A.; Wang, J., *Analyst* **2007**, 132, 560-565.
71. Laine, D.; Cheng, F., *Microchem. J.* **2009**, 91, 125-128.
72. Bohrer, F.; Colesniuc, C.; Park, J.; Schuller, I.; Kummel, A.; Trogler, W., *J. Am. Chem. Soc.* **2008**, 130, 3712-3713.
73. Schulte-Ladbeck, R.; Edelmann, A.; Quintas, G.; Lendl, B.; Karst, U., *Anal. Chem.* **2006**, 78, 8150-8155.
74. Staples, E., Detecting chemical vapours from explosives using the zNose<sup>(R)</sup>, an ultra-high speed gas chromatograph. In *Electronic Noses & Sensors for the Detection of Explosives*, Gardner, J.; Yinon, J., Eds. Kluwer Academic Publishers: Dordrecht, 2004.
75. Zuck, A.; Greenblatt, J.; Zifman, A.; Zaltsma, A.; Kendler, S.; Frishman, G.; Meltzer, S.; Fisher, I., *J. Ener. Mat.* **2008**, 26, 163-180.

76. Oxley J.; Smith J.; Lou W.; Brady J. *Propell. Explos. Pyrot.* **2009**, *34*, **539 - 543**

## CHAPTER 6

### **PRESUMPTIVE ASSAY FOR PEROXIDE-BASED EXPLOSIVES USING THE HYDROGEN PEROXIDE - ACETONITRILE - LUMINOL CHEMILUMINESCENCE REACTION**

#### ***6.1 Introduction***

Easy-to-monitor colorimetric, fluorimetric or chemiluminescent assays are routinely used by forensic scientists, law enforcement and military personnel to screen for drugs of abuse<sup>1-3</sup> and explosives<sup>4-6</sup>. For both nitro- and peroxide-based explosives, reactions producing fluorescent or chemiluminescent species have been successfully incorporated into detection schemes.<sup>5</sup> For peroxide-based explosives (PBEs), luminescence detection schemes are usually indirect and monitor hydrogen peroxide, a precursor and degradation product of PBEs.<sup>7</sup> These schemes often employ peroxidase to yield radical hydrogen peroxide degradation products, which serve as reactants in a variety of luminescent reactions.<sup>7,8</sup> The peroxidase-catalyzed chemiluminescence (CL) reaction between hydrogen peroxide ( $\text{H}_2\text{O}_2$ ) and luminol has been used in a variety of fields, displaying long-lasting luminescence at trace levels of  $\text{H}_2\text{O}_2$ .<sup>8</sup>

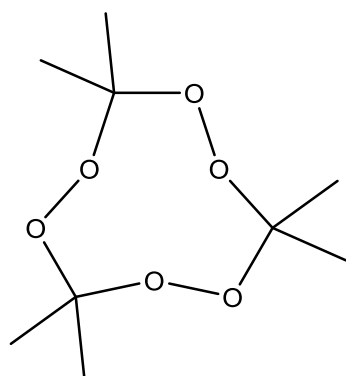
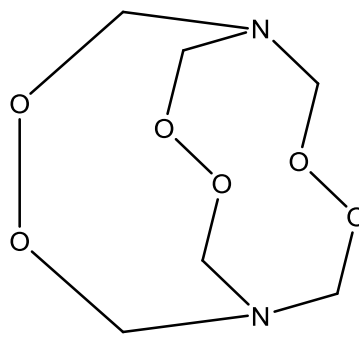
As with most enzyme-based methods, peroxidase methods have operational challenges that are related to the use of enzymes, including the need for special handling/storage and potentially high costs for single-use applications.<sup>8-10</sup> For CL

reactions utilizing singlet molecular oxygen ( $O_2^{\bullet}$ ), such as select luminol CL pathways<sup>11-15</sup>, there is an attractive peroxidase alternative based on nitriles (e.g. acetonitrile). Under alkaline conditions,  $O_2^{\bullet}$  is produced by reacting  $H_2O_2$  with nitriles.<sup>16-18</sup> Because it is a weakly chemiluminescent species,  $O_2^{\bullet}$  can mediate a number of photochemical processes, including stronger secondary CL reactions that are suitable for detection in analytical applications.<sup>16-19</sup>

### 6.1.1 HPAL reaction

Lu et al. first applied the hydrogen peroxide – acetonitrile – luminol (HPAL) reaction to the analytical sciences by using luminol and related conjugates for an application involving high-performance liquid chromatography.<sup>8</sup> This chapter describes the use of an HPAL CL presumptive assay for visual detection of the most commonly encountered PBEs, triacetoneperoxide (TATP) and hexamethylene triperoxide diamine (HMTD) (**Figure 1**), along with liquid  $H_2O_2$ . This is the first use of the HPAL reaction for both a wet chemical presumptive assay and the indirect detection of PBEs.

In addition to acting as a CL assay, this HPAL presumptive test also acts as a color test for low concentrations of  $H_2O_2$  ( $\mu\text{g/mL}$ ) and small amounts of PBEs ( $\leq 10$  mg). Reaction solutions in this assay changed from colorless or white to yellow. This change indicated the presence of the luminol CL reaction degradation product, 3-aminophthalate anion (3-AP), or a closely structurally related side product.<sup>20-22</sup>

**TATP****HMTD****Figure 1:** Structure of target PBEs.



The focus of the research presented in this chapter is the design of a simple wet chemical assay for the presumptive detection of PBEs. The ultimate goal is integration of this assay into a commercial kit for law enforcement and military applications. The design would be similar to the QuickCheck™ Narcotics Identification Kits that is manufactured by the Lynn Peavey Company.<sup>23</sup> These kits are “all-inclusive”, providing reagents in a testing pouch for a single use assay. To meet the limitations imposed by such a design, an assay should not involve any instrumentation, be inexpensive, use easy-to-handle reagents and produce an intense signal for direct visual detection. These needs are met by indirectly detecting PBEs via the production of H<sub>2</sub>O<sub>2</sub> and by employing the HPAL reaction.

## ***6.2 Experimental***

### *6.2.1 Instruments and Consumables*

TATP and HMTD stock solutions (100 µg/mL in acetonitrile) were purchased from AccuStandard (New Haven, CT). TATP and HMTD samples that were synthesized in-house were donated from the laboratories of J. Redepinning and G. Harbinson, respectively, both located in the Chemistry Department at the University of Nebraska-Lincoln (Lincoln, NE). Solid PBE samples that had been synthesized in-house (hereafter referred to as “<sup>ih</sup>PBE”) were used in “visual” detection experiments to fine tune the HPAL assay and evaluate this assay for use with “real world” PBE samples. All other chemicals were obtained from Sigma-Aldrich (St. Louis, MO). All aqueous solutions

were made using water obtained from a Millipore NANOpure system (Bedford, MA). An Optocomp I luminometer (MGM Instrument, Inc.; Hamden, CT) was used to monitor CL for select experiments. A Shimadzu UV-2401 UV-VIS spectrophotometer was used to collect spectra for some select reaction mixtures.

### *6.2.2 General assay procedure*

For PBE detection, the assay developed in this project can be divided into two parts: (1) PBE degradation to  $\text{H}_2\text{O}_2$  and (2)  $\text{H}_2\text{O}_2$  detection using HPAL. Each part was optimized independently and as sequential steps. Initial work focused on HPAL detection of liquid  $\text{H}_2\text{O}_2$  for two main reasons: (1) to establish the minimal amount of  $\text{H}_2\text{O}_2$  required to yield easy-to-see luminescence, and (2) to fine tune the amounts and ratios of HPAL reagents so that the production of luminescence would be maximized.

### *6.2.3 Analysis of $\text{H}_2\text{O}_2$*

This wet chemical assay is based on the high-performance liquid chromatography HPAL method developed by Lu et al.<sup>8</sup> Required reagents include a stock solution of 11.85 mM luminol in 100 mM, pH 11.5  $\text{Na}_2\text{CO}_3$  and acetonitrile (ACN). The assay procedure is as follows: (1) 20  $\mu\text{L}$   $\text{H}_2\text{O}_2$  (or the sample solution) is added to a disposable test tube or vial; (2) 20  $\mu\text{L}$  ACN is added to the test tube and the solution is mixed by for 15 s; (3) the test room is darkened to monitor any luminescence; and (4) 100  $\mu\text{L}$  luminol stock solution is added, solution is mixed, the test room is darkened and the

luminescence is monitored. To determine a limit of detection (LOD) for visual detection, a series of H<sub>2</sub>O<sub>2</sub> solutions were made using a 30% H<sub>2</sub>O<sub>2</sub> stock solution, giving an LOD test set concentration range of 3.4 mg/mL down to 2.7 µg/mL.

#### 6.2.4 PBE sample analysis

Analysis of PBE samples required the decomposition of TATP and HMTD to H<sub>2</sub>O<sub>2</sub>. A comprehensive survey of literature in this area (see **Chapter 5**) indicated that the most common PBE degradation technique is exposure to UV light for ≤ 15 min. A limited study was conducted using UV degradation, but attention was primarily focused on acid degradation for strict adherence to a “wet chemical” requirement for the final assay. In 2007, Munoz et al. used acid treatment of PBEs for the electrochemical sensing of H<sub>2</sub>O<sub>2</sub> with great success.<sup>24</sup> This treatment was modified for use in the HPAL assay described in this chapter.

The HPAL assay procedure outlined in 6.2.2 (steps 1 – 4) was modified to include two additional steps at the beginning: an acid digest step to decompose PBEs to H<sub>2</sub>O<sub>2</sub>, and a neutralization-alkalinization step. Initial experiments used 100 µg/mL PBE standard solutions, where an aliquot of the standard solution was put into a clean vial, to which an equal volume of 6 M HCl was added and the resulting solution was mixed for around 15 s. This solution was neutralized by adding an equal volume of 3 M KOH and mixing for roughly 15 s. An aliquot of this neutralized solution was added to a vial, followed by a five times larger volume of the stock luminol solution (see previous section). The resulting solution was mixed and the pH was checked and adjusted to pH >

11 as needed. These adjustments in pH were made by adding additional KOH. Visually observable luminescence of this mixture was checked in a dark room, followed by the addition of an aliquot of ACN. Visually observable luminescence was checked a second time. This procedure was repeated when a luminometer was used, with luminescence then being recorded by this instrument. The reagent and PBE standard solution volumes were adjusted to yield intense luminescence, but visual detection was not achieved for either PBE standard solutions or  $^{10}\text{PBE}$  samples (see 6.3.2).

For visual detection of the  $^{10}\text{PBE}$  samples, the concentrations of HCl, KOH and luminol were adjusted, along with starting amount of the PBE sample. Both acid and base concentrations were increased to 12.4 M HCl and 15.5 M KOH for visually observable luminescence. Increasing the luminol concentration to around 36 mM maximized the luminescence intensity determined by visual detection. These experimental modifications did not allow for visual detection of PBE in standard solutions (see 6.3.2). All solid  $^{10}\text{PBE}$  samples analyzed were in the low milligram (< 10 mg) range. For these PBE samples, the optimized “one-pot” assay was as follows: (1)  $\leq 5$  mg PBE was placed in a vial; (2) 60  $\mu\text{L}$  12.4 M HCl was added to the vial with mixing; (3) 70  $\mu\text{L}$  of 15.5 M KOH was added to the vial with mixing; (4) 130  $\mu\text{L}$  36 mM luminol solution was added to the vial with mixing; (5) the chemiluminescence was observed; (6) 100  $\mu\text{L}$  of ACN was added to vial with mixing; and (7) the chemiluminescence was observed a second time. Mixing after each step was done for roughly 15 s and the observation of chemiluminescence in steps 5 and 7 refers to visually inspecting the reaction mixture for luminescence in a dark room. For PBE samples  $\leq 5$  mg, the reagent volumes were increased slightly.

### 6.2.5 UV spectra collection

As mentioned in the 6.1.1, the color change of the HPAL reaction mixture from colorless or white to yellow indicates the presence of luminol's CL reaction degradation product, 3-AP, or a structurally-related side product. UV spectra of representative liquid H<sub>2</sub>O<sub>2</sub> and <sup>ih</sup>PBE reaction solutions were collected to compare absorbance data to known  $\lambda_{\max}$  values of 3-AP and related compounds.

## 6.3 Results and Discussion

Luminol luminescence is perhaps the most studied CL reaction.<sup>22, 25</sup> The accepted general reaction for this process is oxidation of luminol to 3-AP, with some amount of 3-AP going into an excited state (3-AP<sup>\*</sup>) and undergoing subsequent relaxation to emit light.<sup>8, 13, 14, 22, 26-34</sup> This general reaction scheme is given in **Figure 2**. There are a variety of mechanistic routes possible in going from luminol to 3-AP. There are multiple pathways operating during a single reaction, depending mainly on the reaction medium and oxidizing agent(s).<sup>8, 13, 14, 22, 26-34</sup> Elucidation of luminol CL mechanisms continues to be an area of active research, as evidenced by the references included in this chapter.

Besides the formation of 3-AP and the emission of light from the relaxation of 3-AP<sup>\*</sup>, another hallmark of luminol CL reactions is the evolution of N<sub>2(g)</sub>.<sup>8, 13, 14, 22, 26-34</sup> In addition, 3-AP and structurally-related side products are yellow.<sup>20-22</sup> Thus, light emission, the formation of bubbles and a yellow reaction solution are all marks of a “successful” luminol reaction. For this presumptive detection assay, these criteria were

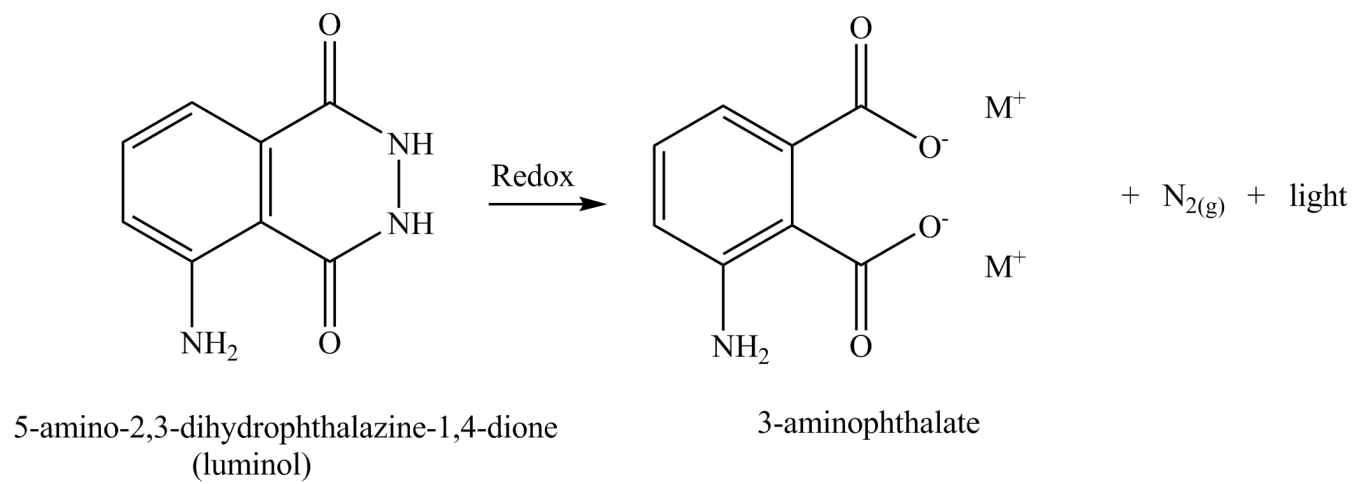


**Figure 2:** General luminol reaction.

used as an indication that a particular set of luminol oxidation conditions were successful in giving the desired response.

The oxidizing agent used in this HPAL assay was  $O_2^{\bullet}$ , as produced via the Radziszewski reaction that involves nucleophilic attack to the nitrile carbon by a peroxide anion<sup>16-18,35</sup>. The Radziszewski reaction, like the luminol reaction, continues to be an area of active research.<sup>8, 18, 35</sup> The general Radziszewski reaction between ACN and  $H_2O_2$ , formulated by Brauer et al. through careful kinetic studies<sup>35</sup>, is shown in **Figure 3**. Elucidation of definitive mechanisms for  $O_2^{\bullet}$  production and  $O_2^{\bullet}$  oxidation of luminol in this process is beyond the scope of this current project.

### 6.3.1 Observations from $H_2O_2$ analysis

Initial work in this study focused on the HPAL detection of liquid  $H_2O_2$ . This work enabled a determination of the minimal amount of  $H_2O_2$  that was needed to produce easy-to-see light in a dark room and made it possible to optimize the HPAL reagents to maximize the perceived intensity of emitted light. Initial HPAL assay experiments examined liquid  $H_2O_2$  samples ranging in concentration from 2.7  $\mu\text{g/mL}$  to 3.4  $\text{mg/mL}$ . As expected, light intensity appeared to increase with an increase in  $H_2O_2$  concentration. The lowest concentration of  $H_2O_2$  that enabled visual detection was approximately 4  $\mu\text{g/mL}$ . Analysis of  $H_2O_2$  below this concentration required the use of a luminometer. **Figure 4** shows luminescence that was detected for  $H_2O_2$  samples with concentrations of  $\leq 4 \mu\text{g/mL}$ , with the luminescence increasing as the  $H_2O_2$  concentration increased, as

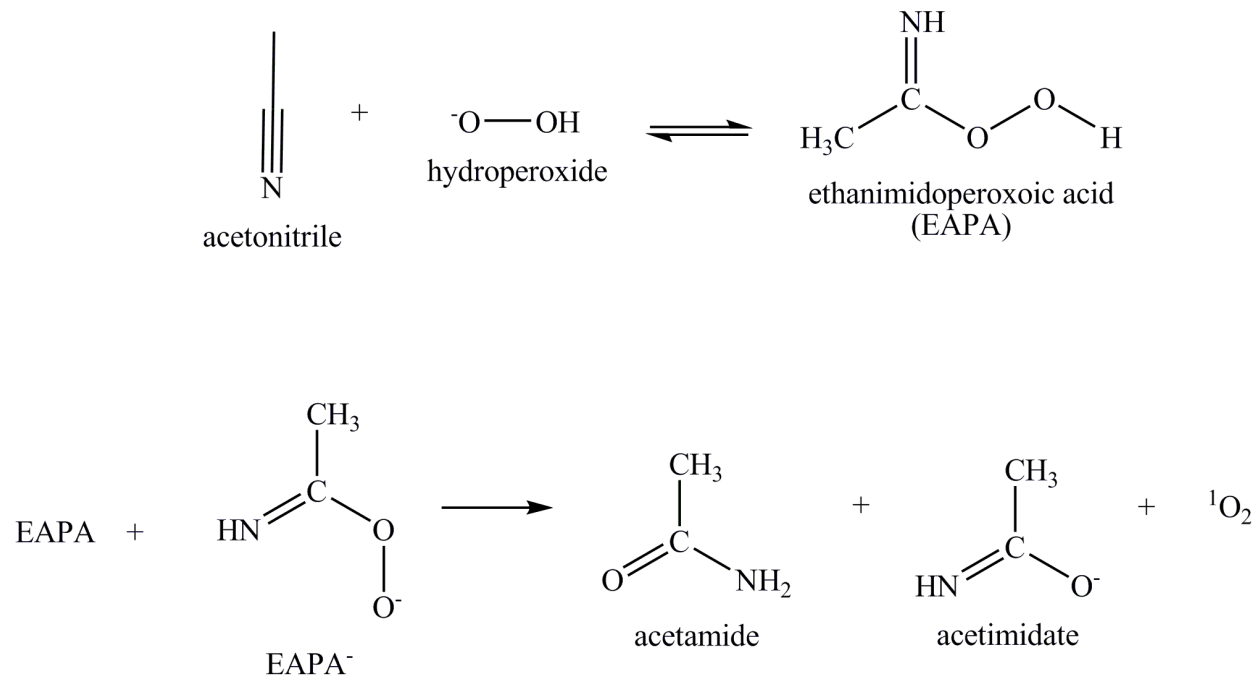


**Figure 3:** The Radziszewski reaction, as proposed by Brauer et al.<sup>35</sup>



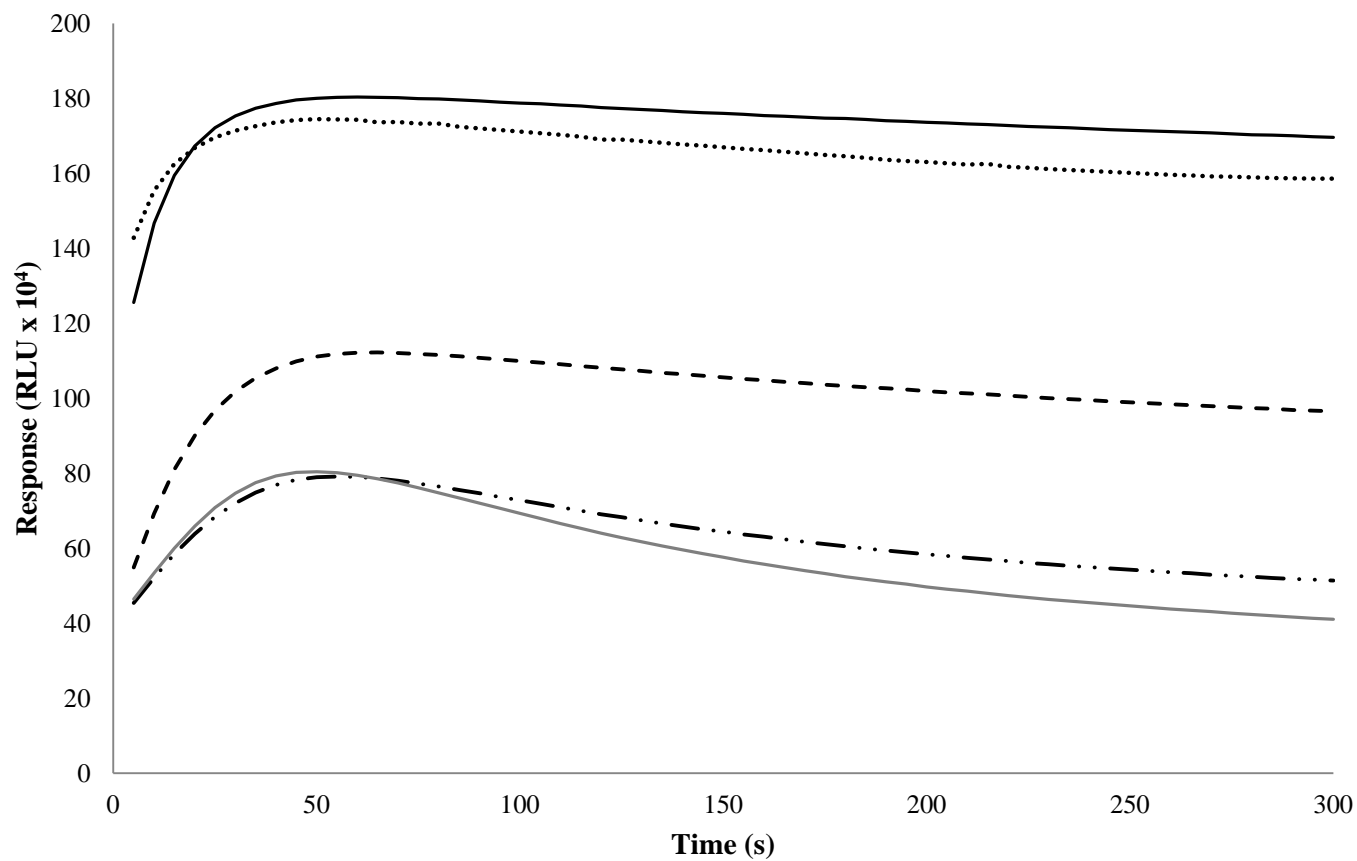


**Figure 4:** HPAL assay of H<sub>2</sub>O<sub>2</sub> liquid samples, as monitored by a luminometer; the concentrations of H<sub>2</sub>O<sub>2</sub> in these samples were (—) 3.3 µg/mL, (···) 2.4 µg/mL, (- - -) 1.6 µg/mL, (- · ·) 0.81 µg/mL, and (—) 3.3 µg/mL.

noted visually for samples  $\geq 4 \mu\text{g/mL}$ . These experiments with liquid  $\text{H}_2\text{O}_2$  samples indicated that the minimum  $\text{H}_2\text{O}_2$  concentration need for visual detection be  $\geq 4 \mu\text{g/mL}$ .

Experiments with liquid  $\text{H}_2\text{O}_2$  samples were also used for preliminary assay optimization of the HPAL reaction to maximize luminescence. In regards to reagents, work done by Lu et al.<sup>8</sup> has shown (a) maximum luminescence intensity is achieved when using around 25% v/v ACN; (b) with an increase in % ACN, the concentration of luminol required to achieve maximum luminescence intensity decreases; and (c) for sodium borate buffer, maximum luminescence intensity is achieved at a pH of 11 or greater. These findings were used to tailor reagent amounts in this study, with the findings being in agreement with those of Lu et al.<sup>8</sup> Both this work and that of Lu et al. indicate that for concentrations greater than 25% v/v the level of luminescence seems to plateau rather than decrease.

### 6.3.2 *Observations from PBE sample analysis*

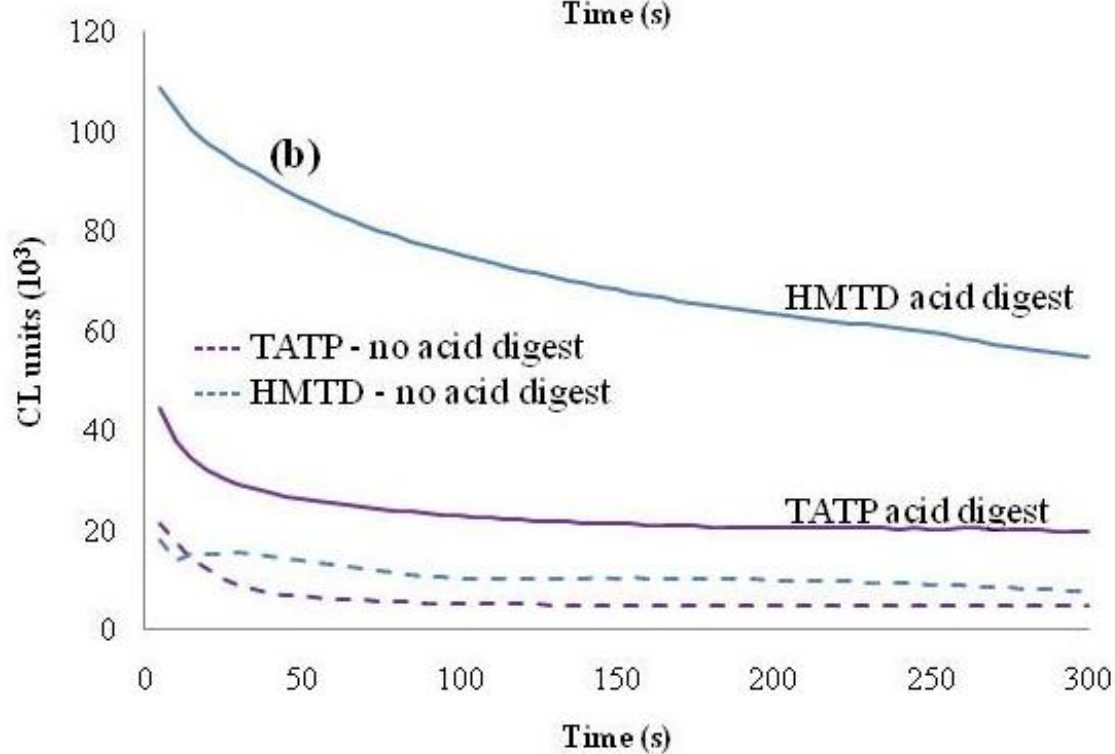
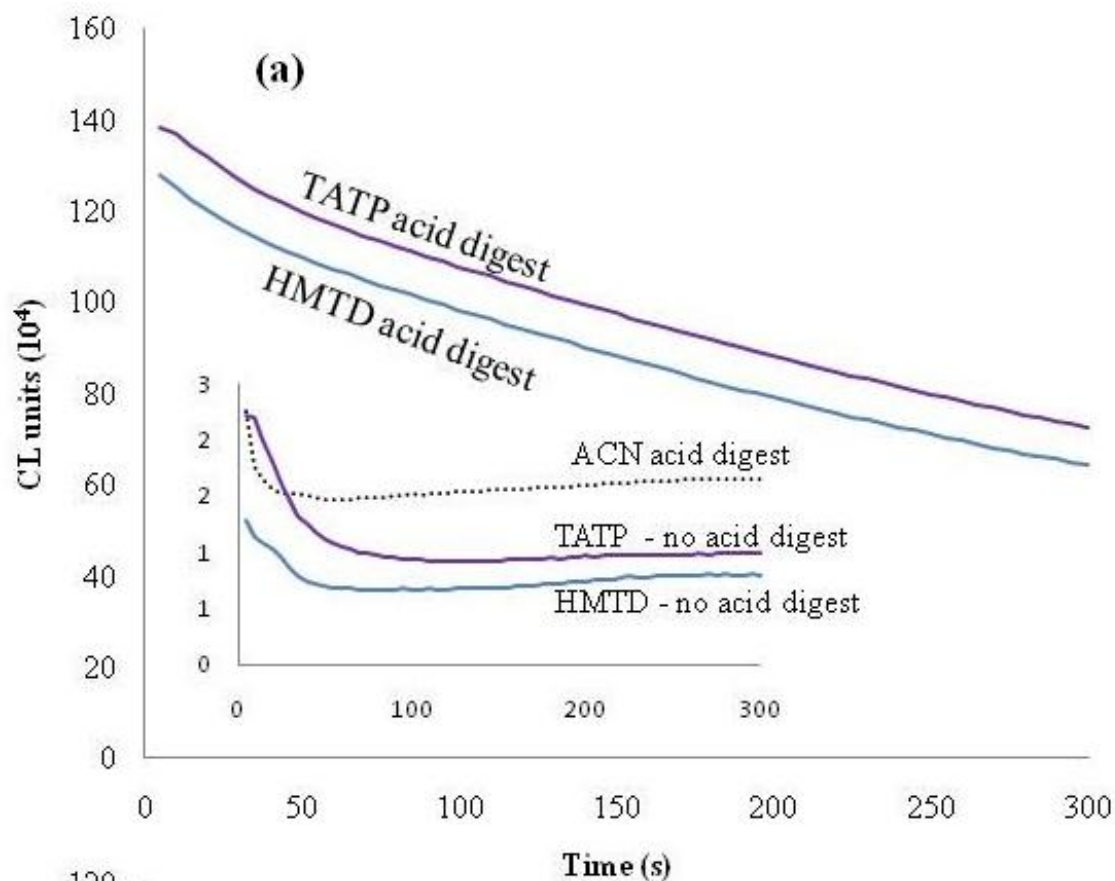
Moving from experiments with liquid  $\text{H}_2\text{O}_2$  samples to the analysis of PBEs required the addition of an assay step to decompose PBEs to  $\text{H}_2\text{O}_2$ . Based on the experiments with liquid  $\text{H}_2\text{O}_2$  samples, it was suggested that the minimum concentration of  $\text{H}_2\text{O}_2$  required to yield adequate amounts of visible light was equal to the visual LOD of around  $4 \mu\text{g/mL}$ . Using PBE standard solutions, experimental modifications (e.g., adjustments in the reagent and standard solution volumes, acid and base concentrations) did not allow for visual detection. This result was likely due to the limited  $\text{H}_2\text{O}_2$

production that was created by the low PBE concentration ( $< 25 \mu\text{g/mL}$ ) that was present in the reaction solution.

While PBE standard solutions were not concentrated enough to yield light production that was visible to the naked eye, this assay did appear to be successful when using a luminometer for detection. **Figure 5(a)** shows the luminescence that was produced for an assay of 20  $\mu\text{L}$  aliquots of 100  $\mu\text{g/mL}$  PBE standard solutions. For comparison,  $^{13}\text{C}$ -PBE 100  $\mu\text{g/mL}$  solutions were analyzed and also monitored for their luminescence, as shown in **Figure 5 (b)**. A one minute acid digest using 6 M HCl, followed by neutralization-alkalinization using 3 M KOH was employed. When comparing the results for the PBE standard and  $^{13}\text{C}$ -PBE solutions, RLU values for the standard solutions were greater than those for the  $^{13}\text{C}$ -PBE solutions by an approximately an order of magnitude. The solubility of PBEs in ACN is minimal<sup>36</sup>. Even though the  $^{13}\text{C}$ -PBE solutions were stirred for 24 h prior to use, it is possible that greater time was required for full dissolution. For PBE standard solutions, assays of TATP and HMTD gave similar results, as indicated in **Figure 5 (a)**. However, for  $^{13}\text{C}$ -PBE solutions, the HMTD solution luminescence was greater than it was for TATP, as shown in **Figure 5 (b)**.

Increasing both the acid and PBE concentration proved crucial in achieving visual detection. Easy-to-see luminescence was achieved for  $^{13}\text{C}$ -PBEs when using 12.4 M HCl and 15.5 M KOH and when the initial amount of PBE in the sample was in the low milligram range (i.e., 2 to 10 mg). This result supports the earlier assertion that low  $\text{H}_2\text{O}_2$  production from the acid digest of PBE standard solutions hampers visual detection. Using low milligram  $^{13}\text{C}$ -PBE samples, a “one-pot” assay (see *Experimental PBE samples*)

**Figure 5** (following page): HPAL assay of **(a)** PBE standards and **(b)** <sup>ih</sup>PBE solutions, as monitored by a luminometer.



was performed, which gave luminescence that was visible from 30 s to several minutes, depending on the initial mass of PBE in the sample.

Similar to the results that were obtained for <sup>ih</sup>PBE solutions (**Figure 5(b)**), the luminescence observed for <sup>ih</sup>PBE HMTD was greater than that of TATP samples of the same mass when using a 1 min acid digest time (**Figure 6**). This difference may be due to the higher proton affinity of HMTD compared to TATP, as a result of HMTD's two basic amine groups.<sup>37</sup> By doubling the acid digest time, the TATP samples also produced intense and long lasting (> 5 min) luminescence, as seen in **Figure 7**.

As mentioned in the 6.1.1, the HPAL presumptive CL assay examined in this chapter can also act as a color test for low concentrations of H<sub>2</sub>O<sub>2</sub> (μg/mL) and small amounts of PBEs (≤ 10 mg). During this assay, the reaction solutions went from colorless or white to yellow. This color change indicated the presence of luminol's CL reaction product, 3-AP, or structurally-similar side products.<sup>37</sup> **Figure 8** shows reaction solutions for the <sup>ih</sup>PBE samples and H<sub>2</sub>O<sub>2</sub>, with a yellow solution easily observed for TATP and H<sub>2</sub>O<sub>2</sub>. The HMTD sample may appear in **Figure 8** to be nearly colorless, like the sodium carbonate buffer used to make luminol solutions, but it looked pale yellow to the naked eye. **Figure 9** contains UV spectra of representative <sup>ih</sup>PBE samples after CL had ceased. Based on the literature, the absorbance maximum ( $\lambda_{\max}$ ) for 3-AP is often given as 425 nm.<sup>22, 29, 30, 33, 38</sup> Under the given reaction conditions, anionic 3-AP is capable of forming ion pairs with Na<sup>+</sup> ions. This ion pairing, along with the mixed solvent used in this case (i.e., roughly 25% ACN in water) probably explains the lower  $\lambda_{\max}$  that was observed for <sup>ih</sup>PBE samples.<sup>26, 30, 38</sup>

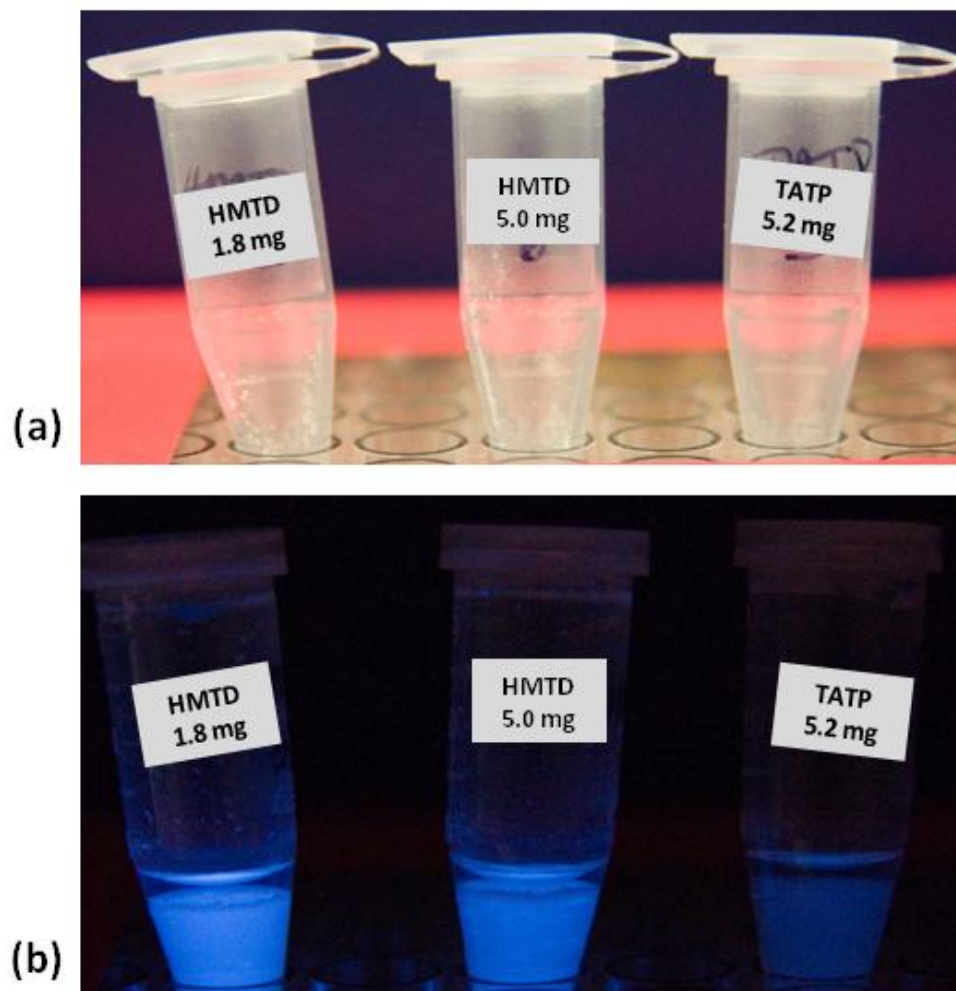


**Figure 6:** HPAL assay of (a)  $^{1h}$ PBE samples prior to addition of ACN and (b) luminescence observed after addition of ACN to  $^{1h}$ PBE samples. A 1 min acid digest time was used.

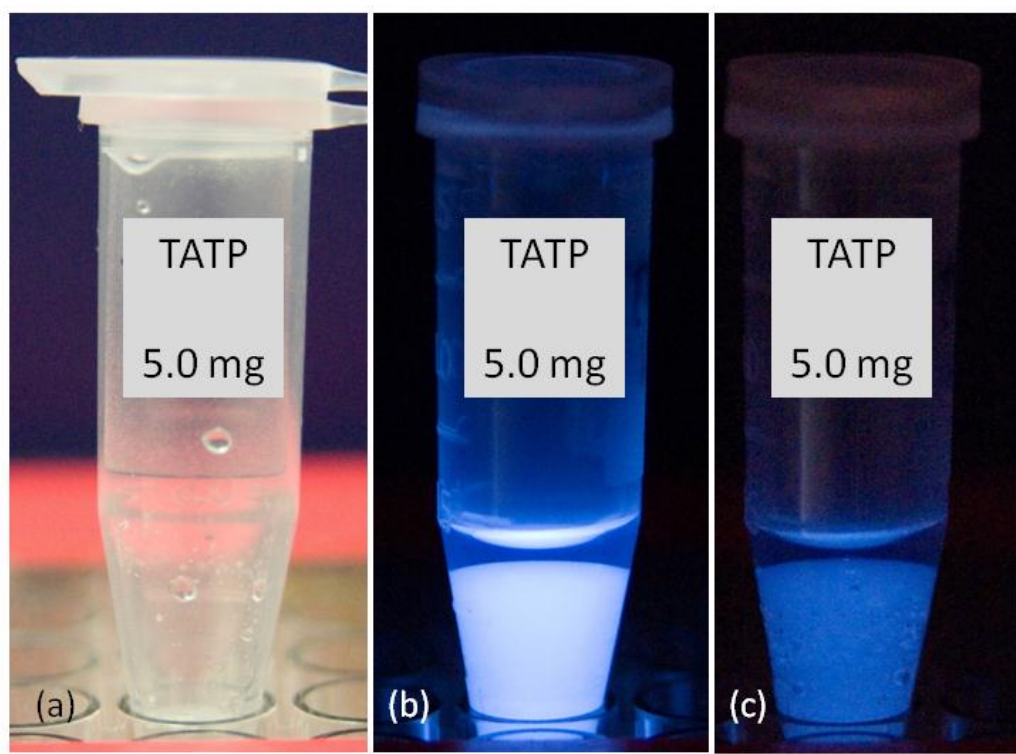


**Figure 7:** HPAL assay of  $^{14}\text{C}$ -PBE TATP sample (a) prior to addition of ACN, (b) luminescence observed after addition of ACN and (c) luminescence observed approximately 5 min after addition of ACN. A 2 min acid digest time was used.



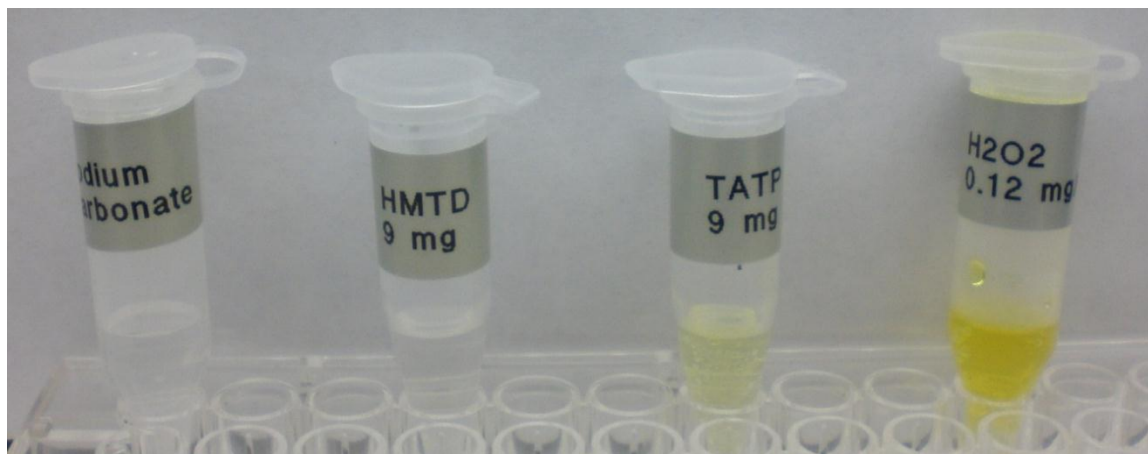


**Figure 8:** HPAL assay reaction vessels of sodium carbonate buffer used to make luminol solution (far left), <sup>ih</sup>PBE 9 mg HMTD (center left), <sup>ih</sup>PBE 9 mg TATP (center right), 0.12 mg/mL H<sub>2</sub>O<sub>2</sub> solutions after CL has ceased.

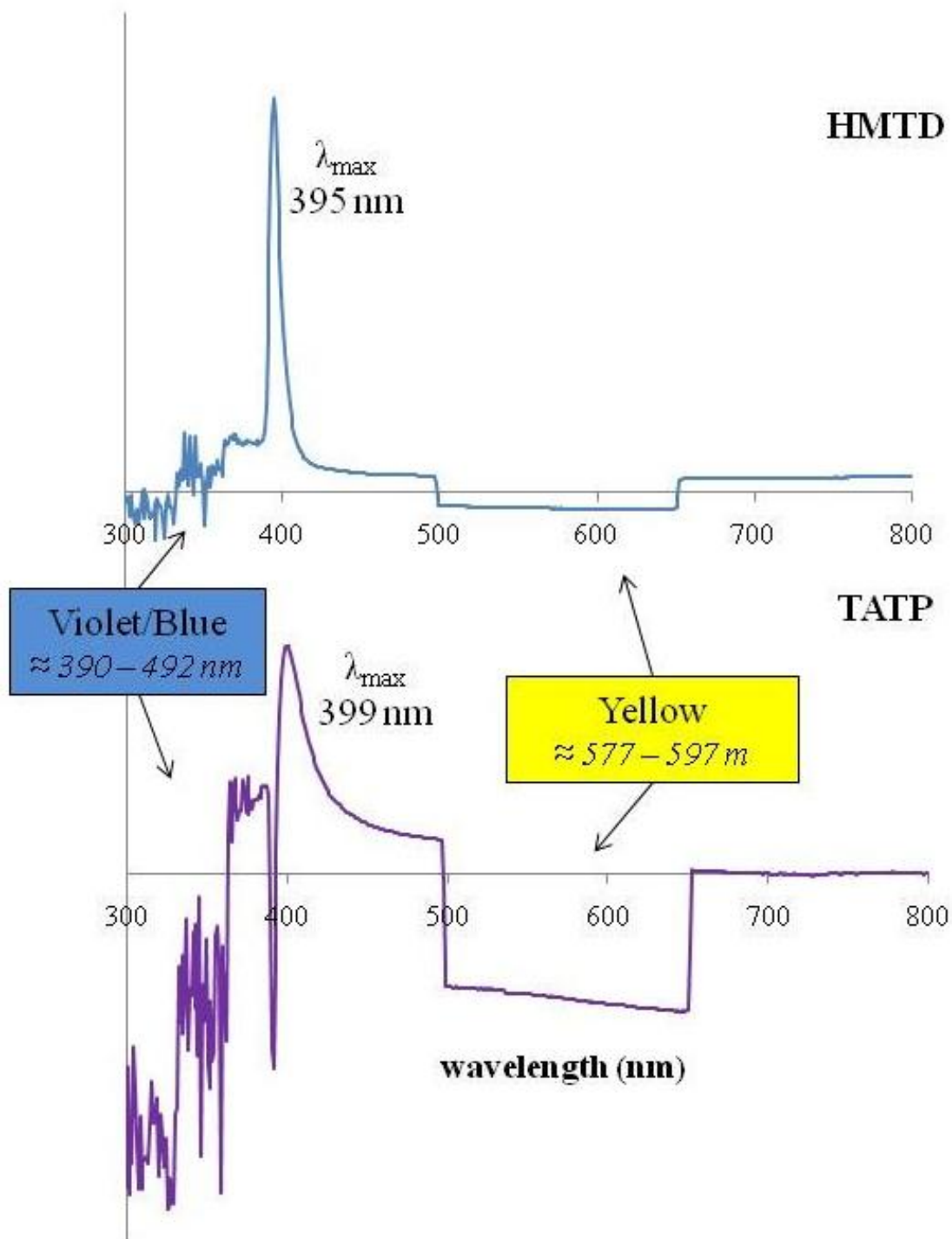


**Figure 9:** UV spectra of <sup>ih</sup>PBE samples after CL has ended for (a) HMTD (b) TATP.

The violet/blue and yellow regions of the visible light range are highlighted in these spectra for reference.

In addition to CL and color change at a suitable concentration of  $\text{H}_2\text{O}_2$ , the HPAL reaction was often marked by the visible evolution of gas. This gas was  $\text{N}_2$ , a known side product of luminol oxidation. The time required to perform our presumptive assay is 2 to 4 min, including the time needed for the acid digest.

#### ***6.4 Conclusion and Future Work***

A simple assay for the indirect detection of PBEs has been developed. Requiring just four simple reagents, this HPAL assay provides a quick response and appears suitable for integration into a field testing kit. To make this assay field ready, commonly encountered compounds that contain or decompose to  $\text{H}_2\text{O}_2$  (e.g. household cleaners, select beauty products, etc.) must be studied to identify major sources of false positive or false negative results. In addition, compounds that quench or react with singlet oxygen<sup>8</sup>,<sup>16</sup> (e.g. sodium azide, dimethylfuran, etc.) must also be examined to gauge their effect on assay response. Despite the need for further study, this initial work shows the potential of the HPAL assay as a presumptive screen for PBEs by forensic scientists, law enforcement and military personnel.

## 6.5 References

1. O'Neal, C.; Crouch, D.; Fatah, A., *Forensic Sci. Int.* **2000**, *109*, 189-201.
2. Programme, U. N. I. D. C., Rapid testing methods of drugs of abuse. United Nations: Vienna, 1995.
3. Christian, D., Forensic Chemistry. In *The Forensic Laboratory Handbook*, Mozayani, A.; Noziglia, C., Eds. Springer: New York, 2006.
4. Almog, J.; Klein, A.; Tamiri, T.; Shloosh, Y.; Abramovich-Bar, S., *J. Forensic Sci.* **2005**, *50*, 582-586.
5. Meaney, M.; McGuffin, V., *Anal. Bioanal. Chem.* **2008**, *391*, 2557-2576.
6. Crippen, J., Explosives and Arson: Boom and Flame. In *The Forensic Laboratory Handbook*, Mozayani, A.; Noziglia, C., Eds. Springer: New York, 2006.
7. Burks, R.; Hage, D., *Anal. Bioanal. Chem.* **2009**, *395*, 301-313.
8. Lu, J.; Lau, C.; Morizono, M.; Ohta, K.; Masaaki, K., *Anal. Chem.* **2001**, *73*, 5979-5983.
9. Marielle, G.; Pirjo, L., *Forensic Sci. Int.* **2001**, *121*, 37-46.
10. Mule, S.; Bastos, M.; Jukofsky, D., *Clin. Chem.* **1974**, *20*, 243-248.
11. Cormier, M.; Prichard, P., *J. Biol. Chem.* **1968**, *243*, 4706-4714.
12. Roth, J.; Cramer, C., *J. Amer. Chem. Soc.* **2008**, *130*, 7802-7803.
13. Merenyi, G.; Lind, J.; Eriksen, T., *J. Biolum. Chemilum.* **1990**, *5*, 53-56.
14. Hodgson, E.; Fridovich, I., *Photochem. Photobio.* **1973**, *18*, 451-455.
15. Merenyi, G.; Lind, J.; Eriksen, T., *Photochem. Photobio.* **1985**, *41*, 203-208.
16. Almeida, E. A.; Miyamoto, S.; Martinez, G. R.; Medeiros, M. H. G.; Di Mascio, P., *Anal. Chim. Acta* **2003**, *482* (1), 99-104.

17. McKeown, E.; Waters, W., *Nature* **1964**, *203*, 1063-1063.
18. Wiberg, K., *J. Amer. Chem. Soc.* **1953**, *75*, 3961-3964.
19. Shellum, C.; Birks, J., Photochemical reaction detection based on singlet oxygen sensitization. In *Chemiluminescence and Photochemical Reaction Detection in Chromatography*, Birks, J., Ed. VCH Publishers, Inc.: New York, 1989.
20. Bogert, M.; Jouard, F., *J. Amer. Chem. Soc.* **1909**, *31*, 483-490.
21. Matheson, I.; Lee, J., *Photochem. Photobio.* **1976**, *24*, 605-607.
22. Roswell, D.; White, E., The chemiluminescence of luminol and related hydrazides. In *Methods in Enzymology*, Fleischer, S.; Fleischer, B., Eds. Academic Press, Inc.: London, 1978; Vol. LVII, pp 409-423.
23. Company, L. P. QuickCheck Narcotic Identification Kits.  
[www.lynnpeavey.com/product\\_info.php?cPath=33&products\\_id=947](http://www.lynnpeavey.com/product_info.php?cPath=33&products_id=947).
24. Munoz, R.; Donglai, L.; Cagan, A.; Wang, J., *Analyst* **2007**, *132*, 560-565.
25. Nieman, T., Detection based on solution-phase chemiluminescence systems. In *Chemiluminescence and photochemical reaction detection in chromatography*, Birks, J., Ed. VCH Publishers, Inc.: New York, 1989.
26. Beck, M.; Joo, F., *Photochem. Photobio.* **1972**, *16*, 491-497.
27. Omote, Y.; Miyake, T.; Ohmori, S.; Sugiyama, N., *B. Chem. Soc. Jpn.* **1967**, *40*, 899-903.
28. Rose, A.; Waite, T., *Anal. Chem.* **2001**, *73*, 5909-5920.
29. White, E.; Bursey, M., *J. Amer. Chem. Soc.* **1964**, *86*, 940-86.
30. White, E.; Roswell, D.; Wildes, P., *J. Amer. Chem. Soc.* **1972**, *94*, 6223-6225.

31. Wierrani, F.; Kubin, A.; Loew, H.; Henry, M.; Spangler, B.; Bodner, K.; Grunberger, W.; Ebermann, R.; Alth, G., *Naturwissenschaften* **2002**, *89*, 466-469.
32. Yasuta, N.; Takahashi, S.; Takenaka, N.; Takemura, T., *B. Chem. Soc. Jpn.* **1999**, *72*, 1997-2003.
33. Lee, J.; Seliger, H., *Photochem. Photobio.* **1970**, *11*, 247-258.
34. White, E.; Bursey, M., *J. Amer. Chem. Soc.* **1964**, *86*, 941-942.
35. **Brauer, H.; Eilers, B.; Lange, A.**, *J. Chem. Soc., Perkin Trans. 2* **2002**, 1288–1295.
36. Oxley, J., What's special about liquid explosives. In *Detection of Liquid Explosives and Flammable Agents in Connection with Terrorism*, Schubert, H.; Kuznetson, A., Eds. Springer: Dordrecht, 2008; pp 27-38.
37. Cotte-Rodriquez, I.; Hernandez-Soto, H.; Chen, H.; Cooks, R., *Anal. Chem.* **2008**, *80*, 1512-1519.
38. Wildes, P.; White, E., *J. Amer. Chem. Soc.* **1973**, *95*, 2610-2617.